FINITE ELEMENTS FOR THE ANALYSIS OF ROTOR-DYNAMIC SYSTEMS THAT INCLUDE GYROSCOPIC EFFECTS

A thesis submitted for the degree of Doctor of Philosophy

By

Simon Jones

Department of Mechanical Engineering, Brunel University

April 2005

ABSTRACT

This thesis presents new finite element formulations for the analysis of rotor-dynamic systems that include the effects of gyroscopic influence. Euler-Bernoulli finite elements have been created for both shaft and propeller descriptions. In addition to the gyroscopic effects, centrifugal stiffening has been considered for the propeller elements. The principle of virtual work has been used to determine the equations of motion and formulate element matrices.

The proposed element matrices have been incorporated in the VIBRATIO suite of vibration analysis software in order to test the formulations. The software uses an innovative hybrid modelling technique that enables the user to analyse various dynamic problems including rotating beam elements with rigid body attachments.

A model of a ship's drive shaft has been created in VIBRATIO for comparison against a verified ANSYS model. Results for forced vibration shaft analysis show excellent correlation between VIBRATIO's Euler shaft formulation and ANSYS's Timoshenko formulation.

Incremental analyses of propeller systems using the novel gyroscopic formulation show gyroscopic effects of flexible blade attachments, and also the changing mode shapes and frequencies due to centrifugal stiffening. Results show gyroscopic and centrifugal stiffening effects must not be ignored for an accurate propeller analysis.

TABLE OF CONTENTS

NOMENCLATURE

SYMBOLS

A	cross sectional area	m^2
A_S	shear area ($A_S = A/2$)	m^2
$\mathbf{C}$	global damping matrix	N·s/m
$\mathbf{C}_e$	elemental damping matrix	N·s/m
E	Young's modulus	N/m^2
$\mathbf{F}$	global external force vector	N
$\mathbf{F}_e$	elemental external force vector	N
J		
$\mathbf{J}$	global inertia matrix	kg m^2
G	shear modulus	N/m^2
$\mathbf{G}$	global gyroscopic matrix	
$\mathbf{G}_e$	elemental gyroscopic matrix	
$\mathbf{G}_{e_p}$	elemental propeller gyroscopic matrix	
I	second moment of area	m^4
$\mathbf{K}$	global stiffness matrix	N/m
$\mathbf{K}_e$	elemental stiffness matrix	N/m
$\mathbf{K}_{e_p}$	elemental propeller stiffness matrix	N/m
$\mathbf{K}_{e_{cs}}$	elemental propeller centrifugal stiffening matrix	N/m
l	element length	m
$\mathbf{M}$	global mass matrix	kg
$\mathbf{M}_e$	elemental mass matrix	kg
$\mathbf{M}_{e_p}$	elemental propeller mass matrix	kg
$\mathbf{N} = \begin{pmatrix} 0 & -1 \\ 1 & 0 \end{pmatrix}$	*Note:* **N** *is used to introduce the gyroscopic cross-coupling terms.*	
r	radius	m
s	radial distance to elemental mass under consideration	m
u	shaft deflections of geometric centre	m
u_M	shaft deflections of the mass centre	m
u_e	shaft deflections of a beam element	m
$\mathbf{V}(x)$	matrix of element shape functions	
x, y, z	local coordinates for element	m

x_g, y_g, z_g	global coordinate axes with origin at root of beam (Fig 5.1)	m
X, Y, Z	global coordinates	m
α	rotation about the x axis	rad
β	rotation about the y axis	rad
γ	rotation about the z axis	rad
θ_P	polar mass moment of inertia per unit length	kg·m
μ	mass per unit length	kg/m
ρ	mass density	kg/m^3
Ω	shaft rotational velocity	rad/s

$$\dot{O} = \frac{\partial}{\partial t} \quad \text{and} \quad O' = \frac{\partial}{\partial x}$$

SUBSCRIPTS

G	gyroscopic
e	element
p	propeller
$magn$	magnetic

LIST OF FIGURES

FIGURES

TABLES

GRAPHS

ACKNOWLEDGEMENT

The author would like to express his indebted thanks to the following people and organisations without which this research would not have been possible:

- Prof. I. Esat, for his encouragement, supervision and advice throughout the duration of this research.
- Brunel University for sponsoring this research and providing the necessary resources.
- My family and friends who have patiently awaited the completion of this work, providing encouragement throughout.

CHAPTER 1

INTRODUCTION

Flexible mechanical systems are gaining an increasing significance as more large-scale machinery is being built. The majority of modern machines incorporate some form of flexible rotor-bearing system in order to control and distribute mechanical power and many of these include propeller attachments. Examples include wind turbines, marine propulsion systems and turbo-machinery. Current design trends for rotating equipment aim to heighten efficiency by reducing weight and increasing operating speeds. These goals are being made more attainable by a greater understanding of rotor-dynamic behaviour and improved methods for predicting system responses. The ground theory of mechanisms and machines dates back to the early twentieth century, but the dynamic analysis of flexible mechanisms is often too complex for an analytical solution. Thus it is with the increased power of modern computers that new methods of behaviour prediction are being developed for flexible mechanisms.

Vibration analysis is essential in the design and analysis of rotating machinery. The majority of vibrations are caused by rotation related sources of some description, (normally imbalance) consequently the forces are synchronous to the rotational speed. Thus, forced vibration analysis is fundamental in the design and analysis of rotating machinery. The two most commonly used methods of forced frequency analysis are the finite element, or transfer matrix method. However since certain effects (including, gyroscopic, centrifugal stiffening, and fluid bearings) are dependant on the rotational speed the methods require computational assembly and inversion of large matrices at each frequency step.

This is computationally expensive and inefficient however with the advances in modern computing speed it is rapidly becoming less of a problem.

The transfer matrix approach allows for a continuous representation of the shaft system and produces results in good agreement to experimental work. Its main advantage is the small amount of computer memory and power required to analyse systems. However, the equations of motion are not explicitly written and some experimental work is usually required in obtaining the transfer matrices. Therefore, as computers have become exponentially more powerful, finite element methods are now largely replacing those based on transfer matrices. This is especially true during initial system design stages when transfer matrices may be difficult to verify.

The finite element method provides a methodical approach for the discretization of a continuum. It can provide a solution for many types of complicated systems including fluid flows, heat exchange, static mechanical stresses, or dynamic mechanical systems, including those examined in this study. In each case the system is divided into smaller contacting regions known as elements which are described mathematically. For rotor-dynamic systems finite element models aim to describe them mathematically using a system of differential equations. As with all finite element modelling this can only ever be an approximation, although potentially a very good one. Subsequently engineers seek to simplify systems, making assumptions that reduce the mathematical complexity of models, ideally without compromising the results. Two such common simplifications are the omission of gyroscopic effects, and the disregard for the exact geometry of propeller blades, which are instead treated as attached rigid or flexible discs with the same value of inertia.

There have been analyses performed on systems that incorporate flexible blade arrays (propellers) however these are usually small blades attached to the periphery of a disc. This is because traditionally the majority of research in the field of rotor-dynamic shaft analysis is based around gas turbines. This is due to the abundant use of gas turbines in modern industry and the inherent resonance

problems associated with their design. Accordingly, there are considerable financial gains to be made from improvements in gas turbine design, especially those that increase the efficiency of large power stations. This research has resulted in most modern gas turbines operating beyond their first and second order rigid body critical speeds. Further advancements are pushing operating frequencies towards even higher speeds approaching the bending modes of the rotating group. This has been facilitated by improved balancing techniques, bearing designs and computer simulations. Moreover, designers face demands to achieve these improvements whilst reducing both the initial and operating costs. Hence, when research is performed on propeller attachments, it is mostly done on systems that best represent a gas turbine rotor. Other analyses tend to focus on the behaviour of helicopter blades. These are very lightweight and so in consideration of this researchers normally do not include gyroscopic effects of the blade, assuming them to be negligible, but are more concerned with the effects of the blade tip masses. The need for a model that takes into account the interaction between the shaft and blades is paramount to describe systems such as wind turbines or ship propellers.

With the abundant availability of fast computers it is now cost effective to apply finite element techniques to this broader range of problems, where traditionally it was perhaps more cost effective to solve them in an empirical, heuristic fashion. Producing a universal code to encompass all possible dynamical systems is arguably the ultimate goal for a dynamic finite element analysis package. However, the factors governing the behaviour of various dynamical systems are so copious and interrelated that the task might appear almost impossible. Additionally a computer program capable of considering each and every aspect of all systems no matter how small the consequence would be computationally expensive. One solution is to use modules within the code so that various types of problem can be analysed in isolation. However, all these separate analysis modules still have to be developed and written.

The aim of the present investigation is to develop a reliable computational technique for the analysis of the dynamic response of flexible shaft and propeller

systems, paying particular attention to the often-ignored subject of gyroscopic response. The modelling of shaft and shaft-propeller systems has been achieved using the finite element method (FEM). Firstly, a gyroscopic finite element capable of describing shaft systems has been derived. The derivation principles used have been further developed and extended in order to create a finite element capable of modelling and predicting the response of rotating propeller blades, including the effects of gyroscopic moments. This new approach for describing the behaviour of propeller elements using an Euler-Bernoulli finite element that incorporates gyroscopic behaviour in this manner has not previously been reported. The effect of centrifugal stiffening on propeller blades has also been considered in the analysis. This is due to the possible size and speed of some blades which could be analysed in a more universal code. Finally, the developed elements have been incorporated into a hybrid finite element model in order that they can be verified.

CHAPTER 2

LITERATURE REVIEW

2.1 INTRODUCTION

This chapter presents a survey of key research conducted in the field of the dynamics of flexible shafts and propellers with respect to finite element modelling. For dynamic shaft or propeller systems finite element code usually falls into one of two categories using either Euler-Bernoulli beam theory, which ignores the effect of shear stress, or Timoshenko theory, which includes the shear effect. Although both methods are very similar, and in some papers they are treated as almost interchangeable with shear effects being added to classical Euler beam theory, in general the Timoshenko method is considered to be superior for thick shafts. Section 2.2 presents the research work conducted on the modelling of flexible shafts, in particular that which incorporates the effects of gyroscopic behaviour. Section 2.3 reviews the research performed on the various methods of modelling propeller blades as flexible beam elements, once again focusing on work that includes any gyroscopic behaviour. This chapter concludes in section 2.4 by describing the aims and scope of the present research against the background of previous research.

2.2 FLEXIBLE SHAFT MODELLING

Much of the early research into the finite element computer analysis of rotor-dynamic systems was developed with the intent of analysing turbo-machinery in power plants. The abundant use of turbo-machinery creates considerable financial gains if benefits in both weight and performance are found, especially when this enables operation at supercritical speeds. For this section on shaft

modelling it is the gyroscopic effect that is of main concern due its tendency to be omitted from many finite element models. This is of particular interest for system types where the rotational inertia or speed is great enough that its inclusion is significant. Also of interest are various possible methods of combining finite elements into a computer code that is flexible enough to analyse different problem types.

The theory of beams and vibrations was developed in the late 1800's and early 1900's. However, the large number of equations that needed to be solved limited its application to complex programs. Therefore, research into finite element modelling of dynamic systems didn't really begin to flourish until the 1960's and 1970's, which coincided with the availability of modern computers on which to calculate results. Rankine, W.A., [1879] published the first recorded attempt to discuss the nature of a rotor-dynamic shaft. Neglecting the Coriolis acceleration for a uniform frictionless shaft, he concluded that the shaft should be stable below its first critical speed, in neutral stability, or "indifferent equilibrium" at the critical speed and unstable above it. Jeffcott, H.H., [1919] investigated the effect of unbalance on rotating shafts and, unlike Rankine, allowed for the possibility of successful operation above the first critical speed. By the early 1920's some rotors were operating above their first critical speeds, but it was yet to be understood why some rotors could operate at these speeds while other designs would fail. Over the coming years much research was performed in the study of whirling, oil whip, unbalance, shafts and bearings, whilst trying to explain observed phenomenon.

Green, R.B., [1948] was one of the first to investigate the gyroscopic effects on the critical speeds of flexible rotor-disc systems using analytical techniques. Due to the difficulties associated with calculating analytical solutions, many graphical plots to aid the design of early rotor-disc systems were created. These were for cantilever, simply supported single and dual disc systems and infinite-disc systems. The paper shows the gyroscopic effect for all degrees of freedom and possible ratios of shaft rotating frequency to whirl or precession frequency.

With the advancements in modern computing Kapur, K.K., [1966], Morton, P.G., [1968], and Ruhl, R.L., [1970] published the earliest concise methods of partial differential equations for finite element analysis. Ruhl, R.L., and Booker, J.F., [1972] took this work further, producing an Euler-Bernoulli finite element model for a turbo-rotor system with the provision for a rigid disc attachment. The finite element method developed by Ruhl was used to study rotor stability and unbalance response, but only the effects of elastic bending energy and translational kinetic energy were considered. The work by Ruhl was later improved upon by Nelson, H.D., and McVaugh, J.M., [1976], including the effects of rotary inertia, gyroscopic moments and axial load, for disc-shaft systems. Later, Zorzi, E.S., and Nelson, H.D., [1977] included the effects of internal damping to the beam elements. Zorzi, E.S., and Nelson, H.D., [1980] culminate their work by modelling the effect of constant axial torque on the model, producing a corresponding axial stiffness matrix. Although constant torque may be suitable for a gas turbine shaft, it must be noted that this is not sufficient to model an internal combustion engine shaft, for example, for which a time dependant torque will be required.

Davis, R., Henshell, R.D., and Warburton, G.B., [1972], wrote one of the first early works on Timoshenko finite beam elements for rotor-dynamic analysis. Previous to this Timoshenko beams had mostly been used to analyse vibrations in non-rotating structures. The work was performed because of the tendency for Euler-Bernoulli beam theory to overestimate the frequency of vibration. It was noted that this overestimation increased with the ratio of beam depth to vibration wavelength. The paper derives matrices for a Timoshenko beam element, sets out boundary conditions and performs convergence tests. Finally, there is some discussion over the shear coefficient K, which is often a point of contention in the analysis of Timoshenko beams. For a more detailed derivation of the Timoshenko shear coefficient in relation to various material cross sections the author refers to Cowper, G.R., [1966] and Timoshenko, S.P., [1922].

Thomas, D.L., Wilson, J.M., and Wilson R.R., [1973] also published early work on tapered Timoshenko finite beam elements. They produced an element with

three degrees of freedom at each node, comparing it to earlier elements containing only two. This allowed for translational motion, shear deformation and the rotation of the cross-section. The work concluded by suggesting that it is in fact the simplest Timoshenko beam elements (i.e. those concerned only with bending) that are most useful for a general finite element code. However, for the analysis of structures in which shear and rotary inertias are important, the presented element will render better results.

Thomas, J., and Abbas, B.A.H., [1975] presented a Timoshenko finite element that enabled the user to apply geometric, boundary, and force conditions correctly, thus giving an accurate representation of a Timoshenko beam. The author claims to produce a model that gives far superior results than those given by Kapur, K., [1966] and Davis, R., Henshell, R.D., and Warburton, G.B., [1972].

Nelson, H.D., [1980] continues the development of finite elements for rotor-dynamic analysis using Timoshenko beam theory. The paper generalizes previous works, establishing Timoshenko matrices using the shape functions proposed in Nelson, H.D., [1977]. The model includes translational and rotational inertia, gyroscopic moments, bending and shear deformation, as well as axial loads, but ignores internal damping. It is shown that accuracy improves with the number of finite elements used. The methods used can easily be incorporated into existing computer programs using Euler beam theory with negligible increases in computation time and storage requirements.

Gasch, R., [1976] presented a concise work on the modelling of vibrations in large turbo rotors using the finite element method. The aim of the work was to produce a much more accurate analysis of large turbo rotors than that provided by transfer matrix methods. Gasch uses the principle of virtual work to determine the Euler beam element matrices. His formulation includes provision for gyroscopic forces, internal damping, fluid film forces and unbalance response terms amongst others in a thorough analysis. However, it does not consider the effects of propeller blades, instead treating the rotors as rigid discs, which for

this application is acceptable. Gasch also reduces computational effort by using a banded system of matrices that allows the large number of zeros in the global system matrix to be ignored.

Rouch, K.E., and Kao, J.S. [1979] developed stiffness and mass matrices for a tapered beam finite element, additionally including gyroscopic effects by means of a skew-symmetric damping matrix. Nodal end variables were used to include the shear deflection, and rotary inertia effects were included in the energy function, effectively creating a Timoshenko beam. Finally, a reduction of the shear nodal variables was performed prior to global assembly in order to reduce computation time. The accuracy of the approach was verified through analysis of simple cantilever beams and simply supported rotating shafts.

The most common formulation for finding the critical speeds of a rotor is based on the assumption that both rotational inertia and shear deformations are negligible. However, the consequence of neglecting these effects is that the critical speeds coincide with the natural frequencies of the non-rotating shaft. Genta, G., [1985] goes further to state that because the effects of rotational inertia and shear deformations have an opposite effect on critical speeds, models which only include rotational inertia (which has a lesser effect) can be less accurate than those which ignore both. Genta also states that shear and rotational inertia effects are stronger at higher critical speeds, in particular during supercritical running. The tests performed were done for a simple uniform shaft such that an eigenvalue analysis was compared against a closed form solution. Genta also noted that the inclusion of shear deformation under axial loads was of little practical importance as it introduced very small corrections.

Kim, Y.D., and Lee, C.W., [1986] furthered the previous work on Euler finite beam elements, including the gyroscopic effects. They produced a matrix reduction technique, which they claim substantially reduces computation time. Although very significant at the time and still worth incorporating, it is perhaps becoming less important due to the exponential increase in computing speed seen over past years.

Sauer, G., and Wolf, M., [1989] worked on the gyroscopic effect of rotating disc-shaft systems. Included in their work is a method for calculating the natural eigenfrequencies of such a shaft. Using a base excited pump rotor they showed the effect of separation, whereby the natural resonant frequency of a shaft is separated into two resonant frequencies approximately equidistant above and below the original natural frequency. It was also observed that at certain excitation frequencies the response in the direction normal to the plane of excitation is higher than that parallel to it, and for a broad frequency range the response is dominated by displacements normal to the excitation. This is a well-known gyroscopic phenomenon caused by coupling of the moments. It is noted that with the gyroscopic effects omitted for the particular 'simple' problem studied there is no response normal to the plane of excitation. Sauer and Wolf continue to show how to analytically determine the frequencies at which the excitation parallel to the plane of excitation is equal to the response normal to the plane.

Chen, L.W., and Ku, D.M., [1991] developed a Timoshenko finite beam element with three nodes for the analysis of the natural whirl speeds of rotating shafts. Axial deformations are not considered, hence each node has four degrees of freedom; two translational and two rotational. The purpose of the investigation was to develop a C^0 Timoshenko beam element in place of the more usual C^1 class elements. The finite element model presented provided and accurate representation of rotating shaft systems. Interestingly, Chen and Ku noted that the shear effect has a considerable effect on shafts where the end conditions are hinged-clamped or clamped-clamped. The effect is much less significant for clamped-free or hinged-hinged conditions.

Gmür, T.C., and Rodrigues J.D., [1991] proposed linearly tapered finite elements for the modelling of rotor bearing systems. The elements include the effects of translational and rotational inertia, gyroscopic moments, internal damping, shear deformations and mass eccentricity. Changing the shape functions used created linear, quadratic and cubic elements. Results showed accuracy improving with

the order of element used. The eight degree of freedom cubic elements are published and are suitable for use analysing cylindrical or conical rotors.

Hong, S-W., and Park, J-H., [1999] proposed a new method to obtain exact solutions for multi-stepped rotor bearing systems. An exact dynamic beam element matrix in Laplace domain for a Timoshenko shaft was derived. The most important advantage of the method was to reduce the system matrix size. This was achieved because the method allows a uniform shaft segment, regardless of length, to be modelled by a single element without loss of accuracy or incursion of error.

Mohiuddin, M.A., and Khulief, Y.A., [1999] presented a finite element formulation for a rotor-bearing system. The model accounts for gyroscopic effects and the inertial coupling between bending and torsional deformations. This appears to be the first work where inertial coupling has been included in this manner. The work also presents a truncation method to reduce the order of the model. The reduced order matrices are shown to preserve the selected lower modes of the system, while significantly reducing computation time.

Łuczko, J., [2002] developed a geometrically non-linear model for rotating shafts, with internal resonance and self excited vibration. He states that in order to analyse the physical phenomenon of shafts rotating close to critical speeds, it is necessary to use non-linear models. This is due to the large vibration amplitudes that occur at critical speeds and accordingly, geometrical non-linearities need to be considered. Another factor in the non-linearity noted is the influence of axial forces on the transverse vibrations. In the analysis it is an Euler type model of a slender shaft that is considered. The solution is based on the Galerkin method. The model allows investigation of coupled torsional, longitudinal and transverse vibrations. Results demonstrate torque has an important effect on stability regions and in general reduces a systems critical speed. Some dynamical characteristics showing the effects of internal resonance and self excited vibrations were obtained. Results also showed that at critical

speeds there could be vast differences with results obtained using a standard Euler model.

Zou, C-P., Hua, H-X., and Chen, D-S., [2002] proposed a modal synthesis method for the analysis of rotor-bearing systems with multi-branched shafting. The method was specifically developed to tackle internal combustion engines, where the number of connected shafts makes them difficult to model by conventional means. Although modelling could be achieved using existing techniques, very large matrices are needed for the models and as such, computers of great capacity are required. The final model is a shafting system whereby rigid couplings and flexible connections are combined. As such, the method is similar to the hybrid modelling technique used here. Additionally, the higher order modes were neglected to further reduce computation requirements. The proposed method gives results with good agreement to those found by the transfer matrix method and full FEM for the lower order frequencies.

Xiong, G.L., Yi, J.M., Zeng, C., Guo, H.K., and Li, L.X., [2003] studied the gyroscopic effects of the spindle on the characteristics of a milling system. The method used was finite elements based on Timoshenko beams. This is not the first time Timoshenko elements have included gyroscopic moments. In fact, the method uses matrices originally developed by Nelson, H.D., [1980], but it is considered to be the first analysis of a milling machine in this manner and full matrices are provided.

During the evolution of rotor-dynamic knowledge many insightful books have been written on the subject, with authors attempting to encapsulate all of the most relevant work that is commonly used. Although most of these works omit finer points such as the gyroscopic effect or influences of fluid film bearings, many proffer the reader a good insight into computer modelling and finite elements for rotor-dynamic applications. Some of the more concise works include Zienkiewicz, O.C., [1971], Thomson, W.T., [1993] originally published in 1972, Lee, C-W., [1993], and Zienkiewicz, O.C., and Taylor, R.L., [2000].

These publications prove a valuable source of reference during rotor-dynamic research.

2.3 FLEXIBLE PROPELLER BLADE & DISC MODELLING

Flexible blade modelling is typically performed using one of two common methods; either the blades are individually ignored and a rigid or flexible disc attachment of the same inertia is used (disc models), or the blades are considered to be short and attached to a rigid or flexible disc (bladed disc models). This is because these methods best describe gas turbines, which are probably the most common problem analysed by the rotor-dynamic finite element method. Consequently, many of the modelling techniques are not applicable for a flexible blade attached to a rotating shaft with no disc. Nevertheless, there is some research in this area; normally regarding wind turbines, ship propellers, or helicopter rotors (which usually include a tip mass in the model). However, at present these works tend to ignore the gyroscopic effects due to blade bending in order to simplify the problems.

The first attempt to analyse the vibrations of shaft-disc assemblies was probably made by Lamb, F.R.S., and Southwell, R.V., [1921], who investigated the vibrations of a flexible disc while studying the failure of turbine discs. The analytical formulation proposed was aimed at finding the first critical speed and it included both centrifugal stiffening and the effects of bending. The work was a joint production but the important formulation was credited to Southwell. The study of vibrations of rotating cantilever beams also originated from work by Southwell, but he worked with Gough (Southwell, and Gough., [1921]) on this. Based on the Rayleigh energy theorem they suggested a simple equation to estimate the natural frequencies of rotating cantilever beams. This is now known as the Southwell equation.

Handelman, G., Boyce, W., and Cohen, H., [1958], analytically investigated the effect of a tip mass on the transverse vibrations of a uniform cantilever beam. The work was specifically done to understand the behaviour of helicopter blades,

considering both the increase in centrifugal force, which stiffens the blade, and the increase in kinetic energy. They were probably the first to observe that the centrifugal stiffening effect largely governs the first mode of vibration, whilst for the higher modes it is the elastic behaviour of the material that is the dominant factor. They were unable to determine at which mode the interchange between the two mechanisms occurs.

Carnegie, W., [1959] derived an early expression based on energy methods for the work done due to centrifugal effects when a rotating cantilever blade executes small vibrations. The formulation included the total potential and kinetic energy for vibration purposes. Being formulated when almost all rotor-dynamic analysis was centred on the analysis of gas turbines, the blades were treated as being attached to a rotating disc. By determining the potential energy due to centrifugal force and previously derived expressions for stationary beams, Carnegie was able to use Rayleigh's method to formulate an approximate expression for the first critical frequency. Carnegie, W., [1964] then derived an expression that allowed for the inclusion of rotary inertia and shear deflections. Carnegie, W., Stirling, C., and Fleming, J., [1965-66] investigated the centrifugal stiffening effect further by comparing theoretical results with experimental ones from a high speed test rig using the finite difference method. Results were deemed 'satisfactory', noting that in practice the blade root was less than rigid leading to lower frequency values than the theoretical predictions. There was an obvious agreement for a relative rise in frequency with speed above the 'standstill' value for any given shaft. Furthermore, it was observed that the assumption of $(\text{frequency})^2 - (\text{speed})^2$ being linear seemed to be a satisfactory approximation for theoretical and experimental results over modes one to four for the various blades examined. Finally, it was noted that theoretical inaccuracies could be reduced for the higher order modes to that of the first, but only at the expense of a considerable increase in work. Rao, J.S., and Carnegie, W., [1969] then continued to study the vibrations of rotating cantilever beams, this time using a non-linear approach for a bladed disc model. Magari, P.J., and Shultz, L.A., [1987] also used the potential energy theorem to produce a rotating

twisted blade finite element for the analysis of helicopter blades, but matrices were not given.

Dokainish, M.A., and Rawtani, S., [1971] investigated the vibration response of rotating cantilever plates using finite elements. The plates were mounted on the periphery of a rotating disc and although centrifugal forces were considered, gyroscopic moments were ignored. Because of the rectangular geometry of the plate, flat triangular elements of constant thickness were chosen to describe it. The increase in bending stiffness due to the centrifugal force was calculated from the in plane stresses induced in the plate. The natural frequencies of the blades were shown to be significantly higher than those of non-rotating blades.

Peters, D.A., [1973] produced extensive analytical work on the free vibrations of rotating uniform cantilever beams. He did this in order to simplify results from previous models so that approximate solutions for the main modes of vibration were easily obtainable. Although finite element eigenvalues were obtainable at the time, the large number of modes produced by an eigenvalue analysis of a system containing a number of elements makes results very difficult to interpret. Although the analysis is very detailed, it only considers the natural frequencies of various blade types and does not consider gyroscopic influences on vibrations.

Kumar, R., [1974] investigated the vibrations of space booms under a centrifugal force field, using the Myklestad method. Analysis showed that the difference in natural frequency caused by centrifugal stiffening was highest for the first mode and becomes insignificant for higher modes. This is in agreement with results produced by Handelman, G., Boyce, W., and Cohen, H., [1958]. These centrifugal variations are larger for out of plane vibrations than in plane vibrations. Otherwise, this paper produces results that despite being applicable to the sizing of a space boom, are largely irrelevant to the research here.

Stafford, R.O., and Giurgiutiu, V., [1975] developed a number of semi-analytic methods for rotating Timoshenko beams acting as propellers. The analysis included centrifugal force, shear and rotary inertia, but ignored axial motion and

eliminated the Coriolis forces. The majority of analysis was based around the transfer matrix method. The usual Euler beam theory assumptions are used, but first order corrections were used in order to account for shear and rotary inertia. They noted that at a frequency of 50 rad/s the total correction due to shear and rotary inertia only changed the vibration frequency by approximately 3%. Of this correction, the largest change (68% of total correction) was due to shear effects, so it was concluded for many applications it would be sufficient to only include the shear corrections.

Jones, L.H., [1975] presented the method of integral equations for determination of the eigenvalues of a rotating beam with tip mass. The work was performed because of the difficulties of finding the closed form solution to the eigenvalue problem. The primary aim was to compute improvable lower bounds for the eigenvalues of the reduced problem, as finding the exact solution was still proving to be problematic. The work concluded finding improved lower bounds for the second eigenvalue. The lower bounds agreed with approximate results obtained previously by methods including Rayleigh-Ritz. Furthermore, the Volterra equation method used offered substantial computational advantages over the Fredholm equation method. At the time of publication these computational advantages were highly significant.

Hoa, S.V., [1978] uses the energy method to develop a finite element model for a flexible curved blade with a weighted edge. This model is primarily aimed at the analysis of auto cooling fans. However, Hoa, S.V., [1979] then extends this method using work by Wang, J.T.S., Mahrenholtz, O., and Böhm, J., [1976] to create a more universal finite element code utilising Euler beam theory for the analysis of flexible blades with tip masses. Although gyroscopic bending effects are ignored, centrifugal stiffening is considered and a corresponding matrix developed. This accounts for the effect of the propeller element's own mass putting itself and any other connected elements towards the root of the blade under tension as the system rotates. Although the centrifugal stiffening formulation is well presented, discrepancies have been found in the final matrix.

Putter, S., and Manor, H., [1978] investigated the natural frequencies of radial rotating beams mounted on a rotating disc. The centrifugal force for a uniform tapered beam is considered in the work, the derivation being very similar to that proposed by Hoa, S.V., [1979]. Unlike Hoa who uses axial stress to produce a stiffening matrix in addition to the standard stiffness matrix for bending, Putter and Manor derive an energy matrix from the centrifugal effect. They then use this to calculate stress at the root of the beam (where it is greatest) in order to produce an expression for an approximate maximum permissible speed of a radial rotating beam, dependant on the material's strength. Detailed aspects of working designs will influence maximum permissible speeds in ways not accountable by a formulation such as this.

Hodges, D.H., [1979] developed a finite element method for non-uniform rotating propeller beams, which he coined the Ritz Finite Element Method, due to its similarities to the Ritz analytical method. Although effective at converging to the correct solution for the first natural frequency, there was no attempt to include either centrifugal stiffening or gyroscopic effects. It was suggested the method be used as a method of analysing non-linear and non-conservative systems.

Wright, A.D., et al [1982] also considered centrifugally stiffened beams, taking into account previous works by Hoa, S.V., [1979], Peters, D.A., [1973] and Hodges, D.H., [1979]. Wright et al used the Frobenius method to calculate exact frequencies and mode shapes for centrifugally stiffened beams where both flexural rigidity and mass distribution varied linearly. The results were tabulated and compared with other solutions including a conventional finite element code. Where zero root offset and zero tip mass are used for ease of comparison, it can be seen that results correspond almost exactly to both Hoa's and Hodges' methods. Also published is a wide variety of results for other test geometries for the verification of future codes. Furthermore, the authors observe that centrifugal stiffening has a decreasing influence with increasing mode numbers. The mathematics of centrifugal stiffening and corresponding effects has been further investigated in Chapter 6.

Stephen, N.G., and Wang, P.J., [1986] continued along the lines of earlier boundary value solutions to tackle problems where the material cross sections did not posses two axes of symmetry. They did this in order to find the deformed shape of loaded turbine blades before performing vibration analysis. Three-dimensional problems were reduced to two-dimensional boundary value problems in order to predict the curvature of the blade centreline, taking into account the centrifugal forces on these rotating cantilevers. Yet since finite element modelling was beginning to become commonplace, the value at the stage is difficult to quantify. As the author himself states, "Apart from classical interest, the solution should provide a test for approximate methods of analysis".

Bauer, H.F., and Eidel, W., [1988] investigated the vibrational behaviour of a uniform beam orientated perpendicular to the axis of rotation. The fundamental frequency for beams was determined by using approximated mode shape functions and solved using the Ritz-Galerkin method. The analysis was performed for all possible combinations of free, clamped, hinged, and guided boundary end conditions, in order to investigate the effects of spin speed, hub radius and aspect ratio on the various geometries. Centrifugal and Coriolis effects were considered. The most important conclusion was that the spin speed has a pronounced influence on the natural frequency of a rotating beam. Depending on boundary conditions the natural frequency may increase or decrease with an increase in spin speed.

Yigit, Scott and Galip-Ulsoy [1988] investigated the flexural motion of a radial rotating beam attached to a rigid body. Deriving fully coupled non-linear equations using Hamilton's principle and Euler beams. Note that the term 'coupled' is used to denote a system in which elastic and rigid body motions are interdependent. As with previous investigations, centrifugal forces were included and deemed a necessity, but gyroscopic effects were not. A torque profile was used to drive the body so that the rigid body motion was an unknown prior to the solution. Using both linearised analysis and numerical solution of differential

equations, it was found that uncoupled equations could lead to substantially incorrect results, particularly with regard to frequencies.

Sakata, M., et al [1989] investigated the vibration of a bladed flexible rotor due to gyroscopic moment. The work was principally aimed at describing a jet engine's response to a change in angular velocity produced by the aircraft changing direction. Experimental and finite element work was performed using flexible blades, disc and shaft. The model has been simplified such that only eight degrees of freedom are used and full finite element derivations and results are not given. However, results show reasonable agreement between experimental and computational results.

Naguleswaran, S., [1994] studied the vibrations of uniform Euler-Bernoulli beams under centrifugally induced tension. Results have been tabulated in order to serve as data for the development of problems with more complicated flexural rigidity and/or mass distributions. In and out of plane vibrations are considered to be uncoupled, due to a principle axis of the blade cross-section being assumed parallel to the axis of rotation, and torsional motion is not considered. The mode shape equation was solved using Frobenius' method, with the general solution being expressed by four linearly independent shape function polynomials. Natural frequencies are shown to increase with blade offset (from the axis of rotation) and/or rotational speed.

Genta, G., and Tonoli, A., [1996] developed a disc finite element for the analysis of rotor-dynamic behaviour. The disc is treated as being thin (two-dimensional) and flexible, taking account of centrifugal forces, gyroscopic effects, and thermo-elastic effects. The element is developed in a complex co-ordinate formulation. However, there should be no problems obtaining the relevant matrices in real co-ordinate form. It is shown that although linear shape functions are suitable for the analysis of a disc, in the case of blade arrays, cubic functions must be used. With a low number of degrees of freedom the element model is said to be very useful for complex rotor-dynamic computations. Genta,

G., and Tonoli, A., [1997] then expanded the model to accommodate bladed-discs.

Jacquet-Richardet, G., Ferraris, G., and Rieutord, P., [1996] were also concerned with the reduction of computation time. They investigated the vibration modes of flexible bladed disc-shaft systems. To reduce computation time global non-rotating mode shapes are used in a modal analysis to evaluate the dynamic response. Gyroscopic and centrifugal stiffening effects are accounted for and all possible couplings are allowed. Very good agreement was shown between this and a full mathematical model, with the intended advantages in computation time being achieved.

Al-Ansary, M.D., [1998] investigated the effects of rotary inertia on the flexural vibrations of rotating cantilever beams, taking into account longitudinal elasticity. Galerkin's method was used to create a simple formulation demonstrating that for a typical helicopter blade the extensional force may increase by up to 10% if the rotary inertia contribution is retained in the analysis. This relationship may be used in the initial design stages of rotating beams.

Yoo, H.H., and Shin, S.H., [1998] investigated the vibrations of rotating cantilever beams. They developed linear equations of motion based on a new dynamic modelling method which employs a hybrid set of deformation variables. The Rayleigh-Ritz assumed mode method is used to approximate the hybrid variables. Stretching and bending terms were coupled gyroscopically. Natural frequencies were shown to increase as angular speed and hub radius increased. The chord-wise bending proved to be coupled with the stretching motion of the beams, with different natural frequencies being exhibited, especially for high angular velocities. This coupling effect was proved to become negligible as the beam's slenderness ratio increased. Since the gyroscopic effects are closely related to centrifugal stiffening this is to be expected. Beam element matrices were not published and results were not compared against other data due to a lack of published material.

Bir, G., and Stol, K., [1999] investigated the operating modes of a teetered-rotor wind turbine. They examined a two-bladed wind turbine because the gyroscopic asymmetry can make the dynamics quite distinct from a turbine with three or more blades. Traditional modelling of wind turbines analyses the modes of vibration with the blades not rotating. This is because of the difficulty associated with modelling coupled stationary and rotating components. However, this method ignores the centrifugal and gyroscopic effects. The system was modelled as having four degrees of freedom and it was shown that centrifugal stiffening dictates rotor flap modes, whilst gyroscopic effects control yaw and teeter modes. Blade flexibility and aerodynamic effects were ignored.

Aleyaasin, M., Ebrahimi, M., and Whalley, R., [2000] presented a paper on vibrations of rotating shafts by frequency domain hybrid modelling. The problem analysed was that of a cantilevered rotating marine propeller. The distributed-lumped model for the system was derived from the transfer matrices. Gyroscopic effects were considered and results showed this reduced order model accurately represented the system. The modelling technique was essentially a simplified version of that used in this study because the system is derived from transfer matrices instead of being modelled.

Huang, B.W., and Huang, J.H., [2001] investigated the effects of centrifugal and Coriolis forces on a mistuned bladed disc. The blades were approximated as cantilever beams, with ten modal co-ordinates considered for each blade. Results were a little inconclusive but showed that the Coriolis forces might enhance the localization vibration. This phenomenon is seen in mistuned systems where the vibration amplitude of individual defected blades may be seriously affected by the local irregularities.

Yoo, H.H., Park, J.H., and Park, J., [2001] derived the equations of motion for a pre-twisted cantilever blade, using a method that employs hybrid deformation variables. The method uses Rayleigh Ritz theory to approximate the deformation within the system. Shear, rotary inertia and gyroscopic effects were considered negligible. Results are expressed in dimensionless form, showing the gap

between natural frequency loci increasing with pre-twist angle and also that the hub radius significantly affects natural frequencies.

Chen, C.L., and Chen, L.W., [2002] investigated the random vibrations of a rotating cantilever blade with external and internal damping using the finite element method. Euler thin beam elements were used to describe the system, with base excitation (earthquake simulation) and white noise being the main methods of excitation. There was however, no attempt to describe the gyroscopic moments induced by such a system.

Yang, J.B., Jiang, L.J., and Chen, D.CH., [2004] investigated the dynamic modelling and control of a rotating Euler-Bernoulli beam. A finite element model is produced containing the effects of centrifugal stiffening as derived by Hoa, S.V., [1979]. Gyroscopic effects are however ignored as the study focuses on the active vibration control of rotating beams. It is indicated that the scheme can produce excellent results in the suppression of vibrations.

Chatelet, E., D'Ambrosio, F., and Jacquet-Richardet, G., [2005] investigated a global modelling approach to the analysis of flexible bladed systems. The study focuses on the interaction between shafts and propellers and as such uses a fine finite element mesh which is of course very computationally expensive. Gyroscopic and centrifugal stiffening effects are accounted for in the analysis. The model's complexity drives the work towards reduction techniques to improve computation time. The results show that the behaviour of complex systems may be poorly modelled using traditional modelling techniques based on one-dimensional beam approaches. However these one dimensional approaches have not used the gyroscopic formulations developed here.

2.4 THE AIMS OF CURRENT RESEARCH

The main objectives of this research are:

- To develop and/or validate a finite beam element that can be used to analyse forced shaft vibrations of shaft systems with complex geometry, including gyroscopic effects.

- To develop a finite beam element that can be used to analyse forced propeller vibrations. The element must include the gyroscopic effect, as for a propeller it can be quite large. The technique should be effective in allowing the modelling of propellers to be easily achieved in place of the current trend to model them as discs where a gyroscopic effect is expected.

- To investigate and validate the effect of centrifugal stiffening on propeller blades. Specifically, the perceived effect of a propeller blades' stiffening as it experiences an axial tension due to the forces imposed on it under rotation. Including the effect in the model.

- To perform simulations of dynamic behaviour of mechanical shaft and propeller systems in order to demonstrate the capability of the proposed finite elements.

CHAPTER 3

FINITE ELEMENT HYBRID MODELLING OF FLEXIBLE SHAFTING SYSTEMS

3.1 INTRODUCTION

This chapter presents the Euler Newton formulation of the vibrational behaviour of a multi-body system interconnected by discrete stiffness elements. The formulation is extended to incorporate flexible shafting systems. It is assumed that flexible shafts are connected to rigid bodies and the connection can be either built-in or pin jointed. The described methods are used in the VIBRATIO suite of vibration analysis software which has been used to incorporate elements developed in Chapters 4 to 6. A typical multi-rigid-body system supported or interconnected by discrete spring elements and beams is shown in Figure 3.1

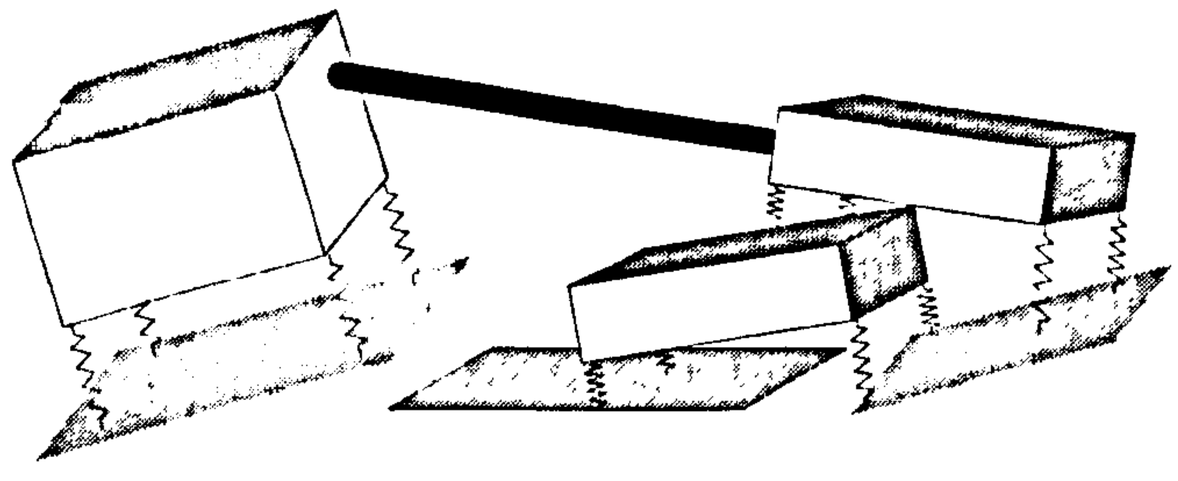

Figure 3.1: Schematic Representation of a Multi-Body System

3.2 THE FINITE ELEMENT METHOD

The finite element method provides a systematic approach for the discretization of a continuum. It can provide a solution for many different types of complicated systems including fluid flows, heat exchange, static mechanical stresses, or dynamic mechanical systems, and the rotor-dynamic systems examined here.

These problem types are very complex and would be difficult to analyse by other techniques (classical methods).

In each case the system is divided into small contacting regions known as elements. Described mathematically, adjacent elements are effectively allowed to touch each other without overlapping. Usually the element shapes are chosen to be as simple as possible, but when grouped together they can still be used to describe a complex geometry. In the case of dynamic rotor-bearing systems, the system is approximated by finite degree of freedom beam elements whose motions are described by ordinary differential equations. This method of describing a complex system as a group of small attached elements is more straightforward to analyse than if it were treated as a single unit. This is because each element is mathematically more easily expressed than the whole system. Numerically, combining a number of elements to model the whole system and solving them by computer is a routine task that can be performed very easily compared to a classical analysis.

For each element the governing equations (usually in differential form) are transformed into algebraic equations called the element equations. For simplicity these are often expressed in matrix form and thus tend to be referred to as the element matrices. When fully assembled these element matrices represent an approximation of the physical system, with the equations expressing a balance of some physical property. For the rotor-dynamic analysis performed here, the expressed property is energy. The ease of use of the finite element method revolves around the fact that the element equations are identical for each element of the same type. Consequently, element equations need only be derived for each typical element type, not for every element. It is normally possible to describe even a complex system with only a limited number of element types, perhaps only one or two. Thus the entire problem of solving a set of algebraic equations is reduced to finding an adequate set of equations for the simple elements used; combining them into the appropriate system equations and solving them as a system. The approach used produces large system matrices that would be very

difficult to solve by hand, however the assembly and solution of these matrices is a routine task that is ideally suited to the modern computer.

3.3 RIGID BODY THEORY

3.3.1 Definitions and Assumptions

- The model is geometrically linear: i.e. the geometry of the system does not change during vibration, thus the vibration amplitudes are assumed to be small.
- Gyroscopic effects are assumed to be small and negligible for the rigid bodies, but significant for shafting systems.
- For FEA of shafting systems all the assumptions relating to linear elasticity are assumed.
- The time dependent effects of hyper-elastic materials are excluded.
- It is generally assumed that the mounting (or spring) has zero length.
- Throughout the analysis it is assumed that the stiffness of springs in their principal axes of deflection are uncoupled.

These assumptions are acceptable for most of the engineering vibration problems where the vibration amplitude is small, as is the case with most systems.

3.3.2 Equations of Motion

In order to set up the equations of motion for a dynamic system the following are required:

- Generalisation of the equations of external forces and internal reactions. (Internal reactions due to damping and stiffness elements)
- Generalisation of the equations of linear momentum. (Force - acceleration equations)
- Generalisation of the equations of angular momentum. (Turning moment equations)

3.3.3 Stiffness and Damping Systems

The presented stiffness matrix formulations apply equally to the damping matrix. This is achieved by replacing the stiffness parameters with the corresponding damping parameters.

Assuming the stiffnesses are described in a Cartesian local axis system that coincides with the principal axes system, then the force **f** acting on the spring may be expressed as:

$$\mathbf{f} = \mathbf{kx} \tag{3.1}$$

Where **k** is the stiffness matrix and **x** is the displacement vector.

Generally it is most convenient to describe the behaviour of a system in the global axis system OXYZ. However this is not a prerequisite as it is equally possible to set equations of each body in its own frame, in this study all stiffness matrices are expressed in a common global axes frame. Therefore the individual matrices have been transformed accordingly. Since the principal axes of the local and global axes are orthogonal, an orthogonal transformation exists between the two frames. Thus a displacement vector **x** in local axes coordinates can be expressed as vector **X** in the global axes system using **T**, a transformation matrix which may be described by three Euler rotations.

Giving:

$$\mathbf{X} = \mathbf{Tx} \tag{3.2}$$

Therefore, the reaction force **F** in the global system, by pre multiplying Equation 3.1 by **T**, can be expressed as:

$$\mathbf{F} = \mathbf{Tkx} \tag{3.3}$$

Now since:

$$\mathbf{x} = \mathbf{T}^T\mathbf{X} \tag{3.4}$$

$$\mathbf{F} = \mathbf{T}\mathbf{k}\mathbf{T}^T\mathbf{X} \tag{3.5}$$

Introducing a new matrix notation **K**, to represents the global stiffness matrix:

$$\mathbf{K}=\mathbf{T}\mathbf{k}\mathbf{T}^T \tag{3.6}$$

It can be seen that:

$$\mathbf{F} = \mathbf{K}\mathbf{X} \tag{3.7}$$

3.3.4 Generalisation of the Equations of Linear Momentum

If the mass matrix in the Euler Newton formulation is obtained relative to the axis passing through its centre of mass, then the subsection of the mass matrix corresponding to linear momentum is a diagonal matrix containing the mass elements.

Then it can be stated that:

$$\mathbf{h}_l = \mathbf{m}\dot{\mathbf{x}} \tag{3.8}$$

Where $\mathbf{h}_l$ is linear momentum, **m** is a diagonal mass matrix, and $\dot{\mathbf{x}}$ is the velocity vector of the body.

Using the transformation expressed previously, the global matrix $\mathbf{H}_l$ can be expressed as:

$$\mathbf{H}_l = \mathbf{T}\mathbf{m}\mathbf{T}^T\dot{\mathbf{X}} \tag{3.9}$$

Since:

$$\mathbf{M} = \mathbf{T}\mathbf{m}\mathbf{T}^T \tag{3.10}$$

The force acting on a body *i*, which can be described as the rate of change of momentum is:

$$Force_i = \dot{\mathbf{H}}_i = \frac{\partial \mathbf{H}_i}{\partial t} = \mathbf{m}_i \ddot{\mathbf{x}}_i \tag{3.11}$$

3.3.5 Generalisation of the Equations of Angular Momentum

Similarly, the equations of moment of momentum may be expressed as:

$$\mathbf{h}_a = \mathbf{j}\dot{\alpha} \tag{3.12}$$

Here $\mathbf{h}_a$ is the angular momentum, and $\mathbf{j}$ may or may not be a diagonal matrix.

Once again this can be transformed into the global axes system giving:

$$\mathbf{H}_a = \mathbf{T}\mathbf{j}\mathbf{T}^T \dot{\mathrm{A}} \tag{3.13}$$

Introducing a new matrix notation **J**:

$$\mathbf{J}=\mathbf{T}\mathbf{j}\mathbf{T}^T \tag{3.14}$$

It can be seen that:

$$\mathbf{H}_a = \mathbf{J}\dot{\mathrm{A}} \tag{3.15}$$

The vector differentiation of $\mathbf{H}_a$ with respect to time gives the moment vector in the global axes system:

$$Moment_a = \dot{\mathbf{H}}_a = \frac{\partial \mathbf{H}_a}{\partial t} + \dot{\mathrm{A}} \times \mathbf{H}_a \tag{3.16}$$

The term $\dot{\mathrm{A}} \times \mathbf{H}_a$ contains the product of angular velocity (usually referred to as the gyroscopic effect). For most vibration problems this is small and may be

ignored. However, in this work the effect has been included for both shaft and propeller finite elements.

3.4 ASSEMBLY OF EQUATIONS

3.4.1 Force – Acceleration Equations

In order to assemble the equations of motion, the internal forces acting on the individual bodies due to their motion relative to each other are required. Figure 3.2 shows two bodies (*i* and *j*) in motion.

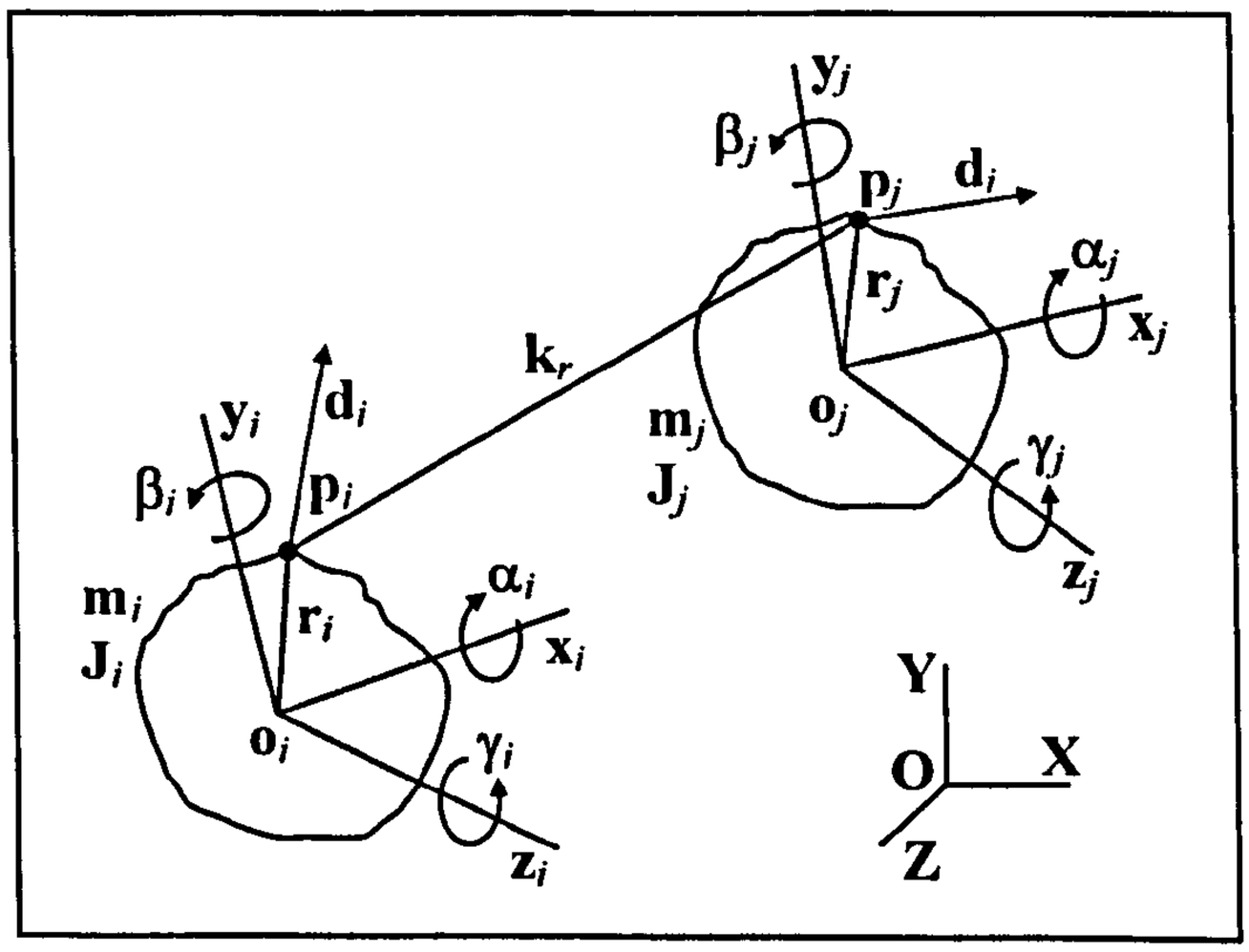

Figure 3.2: Bodies *i* and *j* Connected by Spring k_r

The motion of the axis system belonging to body *i* is given by the vector x_i and the angular rotation of the axes by vector α_i. Similarly, the motion of body *j* is described by x_j and α_j.

For small motions, displacements of the end points of springs on each body described in the axes frame of each body, are given by:

$$\mathbf{d}_i = \boldsymbol{x}_i + \boldsymbol{\alpha}_i \times \mathbf{r}_{pi} \tag{3.17}$$

$$\mathbf{d}_j = \boldsymbol{x}_j + \boldsymbol{\alpha}_j \times \mathbf{r}_{pj} \tag{3.18}$$

Where $\mathbf{r}_{pi}$ and $\mathbf{r}_{pj}$ are the coordinates of the spring attachment relative to bodies *i* and *j* respectively.

$\mathbf{d}_i$ can be expressed in matrix form including the cross product term as:

$$\begin{Bmatrix} d_{xi} \\ d_{yi} \\ d_{zi} \end{Bmatrix} = \begin{Bmatrix} x_i \\ y_i \\ z_i \end{Bmatrix} + \begin{bmatrix} 0 & z_{pi} & -y_{pi} \\ -z_{pi} & 0 & x_{pi} \\ y_{pi} & -x_{pi} & 0 \end{bmatrix} \begin{Bmatrix} \alpha_i \\ \beta_i \\ \gamma_i \end{Bmatrix} \tag{3.19}$$

Or in short using new notation as:

$$\mathbf{d}_i = \mathbf{x}_i + \mathbf{R}_{pi}\boldsymbol{\alpha}_i \tag{3.20}$$

And $\mathbf{d}_j$ can be written in matrix form including its cross product term as:

$$\begin{Bmatrix} d_{xj} \\ d_{yj} \\ d_{zj} \end{Bmatrix} = \begin{Bmatrix} x_j \\ y_j \\ z_j \end{Bmatrix} + \begin{bmatrix} 0 & z_{pj} & -y_{pj} \\ -z_{pj} & 0 & x_{pj} \\ y_{pj} & -x_{pj} & 0 \end{bmatrix} \begin{Bmatrix} \alpha_j \\ \beta_j \\ \gamma_j \end{Bmatrix} \tag{3.21}$$

Which in short hand becomes:

$$\mathbf{d}_j = \mathbf{x}_j + \mathbf{R}_{pj}\boldsymbol{\alpha}_j \tag{3.22}$$

The relative displacement of the bodies is given by:

$$\mathbf{d} = \mathbf{d}_j - \mathbf{d}_i \tag{3.23}$$

Reaction forces due to the relative displacements on each body are respectively given by:

$$\mathbf{F}_i = \mathbf{k}_r\,\mathbf{d} \qquad \mathbf{F}_j = -\mathbf{k}_r\,\mathbf{d} \tag{3.24}$$

And moments by:

$$\text{Moment}_i = \mathbf{r}_i \times \mathbf{F}_i \quad \text{and} \quad \text{Moment}_j = \mathbf{r}_j \times \mathbf{F}_j \tag{3.25}$$

The cross products can be expressed in matrix form so that:

$$\begin{Bmatrix} Moment_{\alpha i} \\ Moment_{\beta i} \\ Moment_{\gamma i} \end{Bmatrix} = \begin{bmatrix} 0 & -z_{pi} & y_{pi} \\ z_{pi} & 0 & -x_{pi} \\ -y_{pi} & x_{pi} & 0 \end{bmatrix} \begin{Bmatrix} F_{xi} \\ F_{yi} \\ F_{zi} \end{Bmatrix} \tag{3.26}$$

Noting that the matrix in Equation 3.26 is the transpose of the matrix in Equation 3.19 it can be stated that:

$$Moment_i = \mathbf{R}_{pi}^T \mathbf{F}_i \tag{3.27}$$

Again for Moment$_j$ the cross products can be expressed in matrix form so that:

$$\begin{Bmatrix} Moment_{\alpha j} \\ Moment_{\beta j} \\ Moment_{\gamma j} \end{Bmatrix} = \begin{bmatrix} 0 & -z_{pj} & y_{pj} \\ z_{pj} & 0 & -x_{pj} \\ -y_{pj} & x_{pj} & 0 \end{bmatrix} \begin{Bmatrix} F_{xj} \\ F_{yj} \\ F_{zj} \end{Bmatrix} \tag{3.28}$$

Noting also that the matrix in Equation 3.28 is the transpose of the matrix in Equation 3.21 it can be stated that:

$$Moment_j = \mathbf{R}_{pj}^T \mathbf{F}_j \tag{3.29}$$

Now the equations of motion can be compiled as:

$$\mathbf{m}_i \ddot{x}_i + (\mathbf{k}_r \mathbf{d}_i - \mathbf{k}_r \mathbf{d}_j) = \mathbf{F}_i \tag{3.30}$$

Here $\mathbf{F}_i$ is the vector of external forces acting on body *i*.

And:

$$\mathbf{m}_j \ddot{x}_j - (\mathbf{k}_r \mathbf{d}_i - \mathbf{k}_r \mathbf{d}_j) = \mathbf{F}_j \tag{3.31}$$

Then substituting $\mathbf{d}_j$ and $\mathbf{d}_i$ from Equations 3.20 and 3.22 then $\mathbf{F}_i$ can be expressed as:

$$\mathbf{m}_i \ddot{x}_i + \mathbf{k}_r (x_i + \mathbf{R}_{pi} \alpha_i) - \mathbf{k}_r (x_j + \mathbf{R}_{pj} \alpha_j) = \mathbf{F}_i \tag{3.32}$$

Similarly:

$$\mathbf{m}_j \ddot{x}_j + \mathbf{k}_r (x_j + \mathbf{R}_{pj}\, \alpha_j) - \mathbf{k}_r (x_i + \mathbf{R}_{pi}\, \alpha_i) = \mathbf{F}_j \qquad (3.33)$$

Expanding gives:

$$\mathbf{m}_i \ddot{x}_i + \mathbf{k}_r x_i + \mathbf{k}_r \mathbf{R}_{pi}\, \alpha_i - \mathbf{k}_r x_j - \mathbf{k}_r \mathbf{R}_{pj}\, \alpha_j = \mathbf{F}_i \qquad (3.34)$$

$$\mathbf{m}_j \ddot{x}_j - \mathbf{k}_r x_i - \mathbf{k}_r \mathbf{R}_{pi}\, \alpha_i + \mathbf{k}_r x_j + \mathbf{k}_r \mathbf{R}_{pj}\, \alpha_j = \mathbf{F}_j \qquad (3.35)$$

Equations 3.34 and 3.35 are the Force – Acceleration equations.

3.4.2 Moment Equations

Writing the moment equation for body *i*, where it is the external moment acting on body *i*:

$$\mathbf{J}_i \ddot{\alpha}_i + \mathbf{R}_{pi}^T (\mathbf{k}_r \mathbf{d}_i - \mathbf{k}_r \mathbf{d}_j) = \text{Moment}_i \qquad (3.36)$$

Similarly :

$$\mathbf{J}_j \ddot{\alpha}_j - \mathbf{R}_{pj}^T (\mathbf{k}_r \mathbf{d}_i - \mathbf{k}_r \mathbf{d}_j) = \text{Moment}_i \qquad (3.37)$$

Substituting $\mathbf{d}_i$ & $\mathbf{d}_j$ as before and expanding gives:

$$\mathbf{J}_i \ddot{\alpha}_i + \mathbf{R}_{pi}^T \mathbf{k}_r \mathbf{x}_i + \mathbf{R}_{pi}^T \mathbf{k}_r \mathbf{R}_{pi}\, \alpha_i - \mathbf{R}_{pi}^T \mathbf{k}_r \mathbf{x}_j - \mathbf{R}_{pi}^T \mathbf{k}_r \mathbf{R}_{pj}\, \alpha_j = \text{Moment}_i \qquad (3.38)$$

$$\mathbf{J}_j \ddot{\alpha}_j - \mathbf{R}_{pj}^T \mathbf{k}_r \mathbf{x}_i - \mathbf{R}_{pj}^T \mathbf{k}_r \mathbf{R}_{pi}\, \alpha_i + \mathbf{R}_{pj}^T \mathbf{k}_r \mathbf{x}_j + \mathbf{R}_{pj}^T \mathbf{k}_r \mathbf{R}_{pj}\, \alpha_j = \text{Moment}_j \qquad (3.39)$$

Equations 3.38 and 3.39 are the moment equations.

Expressing Equations 3.34 and 3.38 in matrix form gives:

$$\begin{bmatrix} \mathbf{m}_i & 0 \\ 0 & \mathbf{J}_i \end{bmatrix} \begin{Bmatrix} \ddot{\mathbf{x}}_i \\ \ddot{\boldsymbol{\alpha}}_i \end{Bmatrix} + \begin{bmatrix} \mathbf{k}_r & \mathbf{k}_r\mathbf{R}_{pi} \\ \mathbf{R}_{pi}^T\mathbf{k}_r & \mathbf{r}_i\mathbf{k}_r\mathbf{R}_{pi} \end{bmatrix} \begin{Bmatrix} \mathbf{x}_i \\ \boldsymbol{\alpha}_i \end{Bmatrix} - \begin{bmatrix} \mathbf{k}_r & \mathbf{k}_r\mathbf{R}_{pj} \\ \mathbf{R}_{pj}^T\mathbf{k}_r & \mathbf{R}_{pj}^T\mathbf{k}_r\mathbf{R}_{pj} \end{bmatrix} \begin{Bmatrix} \mathbf{x}_j \\ \boldsymbol{\alpha}_j \end{Bmatrix} = \begin{Bmatrix} Force_i \\ Moment_i \end{Bmatrix} \tag{3.40}$$

Similarly Equations 3.35 and 3.39 are expressed as:

$$\begin{bmatrix} \mathbf{m}_j & 0 \\ 0 & \mathbf{J}_j \end{bmatrix} \begin{Bmatrix} \ddot{\mathbf{x}}_j \\ \ddot{\boldsymbol{\alpha}}_j \end{Bmatrix} - \begin{bmatrix} \mathbf{k}_r & \mathbf{k}_r\mathbf{R}_{pi} \\ \mathbf{R}_{pi}^T\mathbf{k}_r & \mathbf{r}_i\mathbf{k}_r\mathbf{R}_{pi} \end{bmatrix} \begin{Bmatrix} \mathbf{x}_i \\ \boldsymbol{\alpha}_i \end{Bmatrix} + \begin{bmatrix} \mathbf{k}_r & \mathbf{k}_r\mathbf{R}_{pj} \\ \mathbf{R}_{pj}^T\mathbf{k}_r & \mathbf{R}_{pj}^T\mathbf{k}_r\mathbf{R}_{pj} \end{bmatrix} \begin{Bmatrix} \mathbf{x}_j \\ \boldsymbol{\alpha}_j \end{Bmatrix} = \begin{Bmatrix} Force_j \\ Moment_j \end{Bmatrix} \tag{3.41}$$

The overall equations of motion are now complete. It is worth noting that the stiffness and damping matrices are identical in structure. Thus in order to obtain the damping matrix, one simply replaces stiffness coefficients with the corresponding damping coefficients.

3.5 THE FEA FORMULATION FOR BEAMS

The FEA formulations for standard Euler or Timoshenko beams are both widely available in the literature. These formulations will therefore only be stated for Euler beams. The full matrices used are given in Appendix A.

3.5.1 Stiffness Matrices

Assuming suffixes 1 and 2 represent each endpoint of a beam, u and θ represent unit displacements, then the bending and lateral motion for the coupled y and gamma axes are given by:

$$\begin{Bmatrix} F_{y1} \\ M_{y1} \\ F_{y2} \\ M_{y2} \end{Bmatrix} = \frac{EI}{l^3} \begin{bmatrix} 12 & 6l & -12 & 6l \\ 6l & 4l^2 & -6l & 2l^2 \\ -12 & -6l & 12 & -6l \\ 6l & 2l^2 & -6l & 4l^2 \end{bmatrix} \begin{Bmatrix} u_{y1} \\ \theta_{y1} \\ u_{y2} \\ \theta_{y2} \end{Bmatrix} \tag{3.42}$$

The same matrix can be rotated and used to represent bending in the second lateral axis (in this case the z and beta).

The axial deformation is given by:

$$\begin{Bmatrix} F_{x1} \\ F_{x2} \end{Bmatrix} = \frac{EA}{l}\begin{bmatrix} 1 & -1 \\ -1 & 1 \end{bmatrix}\begin{Bmatrix} u_{x1} \\ u_{x2} \end{Bmatrix} \tag{3.43}$$

Torsional deformation is given by:

$$\begin{Bmatrix} M_{a1} \\ M_{a2} \end{Bmatrix} = GJ\begin{bmatrix} 1 & -1 \\ -1 & 1 \end{bmatrix}\begin{Bmatrix} \theta_{a1} \\ \theta_{a2} \end{Bmatrix} \tag{3.44}$$

3.5.2 Mass Matrices

The mass matrix corresponding to the above stiffness matrix, where μ is the mass per unit length, is given as:

$$\begin{Bmatrix} F_{y1} \\ M_{y1} \\ F_{y2} \\ M_{y2} \end{Bmatrix} = \frac{\mu l}{420}\begin{bmatrix} 156 & 22l & 54 & -13l \\ 22l & 4l^2 & 13l & -3l^2 \\ 54 & 13l & 156 & -22l \\ -13l & -3l^2 & -22l & 4l^2 \end{bmatrix}\begin{Bmatrix} \ddot{u}_{y1} \\ \ddot{\theta}_{y1} \\ \ddot{u}_{y2} \\ \ddot{\theta}_{y2} \end{Bmatrix} \tag{3.45}$$

For axial motion:

$$\begin{Bmatrix} F_{x1} \\ F_{x2} \end{Bmatrix} = \frac{\mu l}{6}\begin{bmatrix} 2 & 1 \\ 1 & 2 \end{bmatrix}\begin{Bmatrix} \ddot{u}_{x1} \\ \ddot{u}_{x2} \end{Bmatrix} \tag{3.46}$$

And for the axial rotation:

$$\begin{Bmatrix} M_{a1} \\ M_{a2} \end{Bmatrix} = \frac{j'l}{6}\begin{bmatrix} 2 & 1 \\ 1 & 2 \end{bmatrix}\begin{Bmatrix} \ddot{\theta}_{a1} \\ \ddot{\theta}_{a2} \end{Bmatrix} \tag{3.47}$$

Where j' is the rotational inertial per unit length. This can be expressed as μr^2 for cylindrical beam elements.

The equations of motion for beams (or shafts) are described in their local axes frames. In order to assemble the shaft equations with the rigid body formulations given earlier, a set of co-ordinate transformations are necessary. In the Cartesian co-ordinate system there are three possible displacements and three rotations at each end of a beam element. Thus twelve co-ordinates are used to represent the end deflections of each beam element.

$$\left(u_{x1} \quad u_{y1} \quad u_{z1} \quad \theta_{\alpha 1} \quad \theta_{\beta 1} \quad \theta_{\gamma 1} \quad u_{x2} \quad u_{y2} \quad u_{z2} \quad \theta_{\alpha 2} \quad \theta_{\beta 2} \quad \theta_{\gamma 2}\right)^T \tag{3.48}$$

Writing this in short hand gives:

$$\left(u_1 \quad \theta_1 \quad u_2 \quad \theta_2\right)^T \tag{3.49}$$

To start the assembly process and find the overall equations of motion, it is convenient to convert the beam deformations into the global axis co-ordinate system for all the matrices. The transformation matrix for this operation is given by:

$$\mathbf{T} = \begin{bmatrix} \mathbf{T}_S & & & \\ & \mathbf{T}_S & & \\ & & \mathbf{T}_S & \\ & & & \mathbf{T}_S \end{bmatrix} \tag{3.50}$$

Each sub matrix $\mathbf{T}_S$ contains the direction cosines between the beams co-ordinate system and the global co-ordinate system.

After the transformation the deflection vector is expressed as:

$$\left(u_{l1} \quad \theta_{l1} \quad u_{l2} \quad \theta_{l2}\right)^T \tag{3.51}$$

The elemental mass and stiffness matrices are transformed into the global axis frame by the following operations:

$$\mathbf{K} = \mathbf{T}^T \mathbf{K}_e \mathbf{T} \tag{3.52}$$

$$\mathbf{M} = \mathbf{T}^T \mathbf{M}_e \mathbf{T} \tag{3.53}$$

Assuming the assembly of all the elemental stiffness and mass matrices gives the stiffness and mass matrices ($\mathbf{K}_{shaft}$, $\mathbf{M}_{shaft}$) for the overall shaft, then to attach a beam to a rigid body, the deformation vector at the point of attachment (Vector 3.51) has to be transformed to the motion of the mass centre of the rigid body. The following sections give the formulations for the co-ordinate transformations.

3.5.3 Co-ordinate Transformation for the Built-In Condition

Two equations are needed to relate the motion of the beam to the rigid body attachment. The first relates the movement at the point of attachment expressed in terms of rigid body motion, to the motion of the beam at the point of attachment, expressed in terms of the FEA formulation. The second equation relates the angular motion of the rigid body and the angular motion of the beam at the attached node.

Assuming $\mathbf{u}$ and $\mathbf{0}$ to be the beam node displacements and rotations respectively, $\mathbf{x}$ and $\boldsymbol{\alpha}$ to be the rigid body displacements and rotations respectively, and $\mathbf{r}_s$ the vector from rigid body's centre of origin to the point of shaft connection, then connecting beam *i* to body *j* the first equation is:

$$\mathbf{u}_i = \mathbf{x}_j + \boldsymbol{\alpha}_j \times \mathbf{r}_s \tag{3.54}$$

Where the vector $\mathbf{r}_s$ is:

$$\mathbf{r}_s = \{a \quad b \quad c\} \tag{3.55}$$

The second equation relates the angular motions of the rigid body and the shaft end. Assuming both the rigid body and beam element are expressed in the same co-ordinate system then:

$$\mathbf{0}_i = \boldsymbol{\alpha}_j \tag{3.56}$$

Thus the transformation may be written in matrix form as:

$$\begin{Bmatrix} u_{xi} \\ u_{yi} \\ u_{zi} \\ \theta_{\alpha i} \\ \theta_{\beta i} \\ \theta_{\gamma i} \end{Bmatrix} = \begin{bmatrix} 1 & 0 & 0 & 0 & c & -b \\ 0 & 1 & 0 & -c & 0 & a \\ 0 & 0 & 1 & b & -a & 0 \\ 0 & 0 & 0 & 1 & 0 & 0 \\ 0 & 0 & 0 & 0 & 1 & 0 \\ 0 & 0 & 0 & 0 & 0 & 1 \end{bmatrix} \begin{Bmatrix} x_j \\ y_j \\ z_j \\ \alpha_j \\ \beta_j \\ \gamma_j \end{Bmatrix} \tag{3.57}$$

Which may be expressed in shorthand as:

$$\begin{Bmatrix} u_i \\ \theta_i \end{Bmatrix} = [\mathbf{S}] \begin{Bmatrix} x_j \\ \alpha_j \end{Bmatrix} \tag{3.58}$$

If the local reactions at the point of attachment are expressed about the centre of mass, then the following relationship may be written:

$$\begin{Bmatrix} F_{xi} \\ F_{yi} \\ F_{zi} \\ T_{\alpha i} \\ T_{\beta i} \\ T_{\gamma i} \end{Bmatrix} = \begin{bmatrix} 1 & 0 & 0 & 0 & 0 & 0 \\ 0 & 1 & 0 & 0 & 0 & 0 \\ 0 & 0 & 1 & 0 & 0 & 0 \\ 0 & -c & b & 1 & 0 & 0 \\ c & 0 & -a & 0 & 1 & 0 \\ -b & a & 0 & 0 & 0 & 1 \end{bmatrix} \begin{Bmatrix} f_{xj} \\ f_{yj} \\ f_{zj} \\ t_{\alpha j} \\ t_{\beta j} \\ t_{\gamma j} \end{Bmatrix} \tag{3.59}$$

Or once again in short as:

$$\begin{Bmatrix} F_j \\ T_j \end{Bmatrix} = [\mathrm{S}]^T \begin{Bmatrix} f_i \\ t_i \end{Bmatrix} \tag{3.60}$$

Where the vector on the right hand side of the equation is the reaction forces at the point of attachment and the vector on the left-hand side of the equation represents these reactions in relation to the rigid body axis system.

Now extending the principle it can be seen that if both ends of the shaft were connected to rigid bodies, then the relevant transformation would be:

$$\begin{Bmatrix} u_{1i} \\ \theta_{1i} \\ u_{2i} \\ \theta_{2i} \end{Bmatrix} = \begin{bmatrix} \mathbf{S}_j & \\ & \mathbf{S}_k \end{bmatrix} \begin{Bmatrix} x_j \\ \alpha_j \\ x_k \\ \alpha_k \end{Bmatrix} \tag{3.61}$$

Here the first end of beam *i* is connected to body *j* and the second end of beam *i* is connected to body *k*.

Thus if the beam connecting the two rigid bodies is made of a number of finite elements, then the transformation matrix can be written as:

$$\begin{Bmatrix} u_{1i} \\ \theta_{1i} \\ .. \\ .. \\ u_m \\ \theta_m \end{Bmatrix} = \begin{bmatrix} \mathbf{S}_j & & & \\ & \mathbf{I} & & \\ & & \mathbf{I} & \\ & & & \mathbf{S}_k \end{bmatrix} \begin{Bmatrix} x_j \\ \alpha_j \\ .. \\ .. \\ x_k \\ \alpha_k \end{Bmatrix} \tag{3.62}$$

This is the final transformation matrix, obtained in order to provide a co-ordinate system consistent with the rigid body axis system.

If the transformation matrix is called **R**, then the stiffness matrix in this co-ordinate system could be expressed as:

$$\mathbf{K}_{Global.Shaft} = \mathbf{R}^T \mathbf{K}_{Shaft} \mathbf{R} \tag{3.63}$$

Similarly, the mass matrix would be expressed:

$$\mathbf{M}_{Global.Shaft} = \mathbf{R}^T \mathbf{M}_{Shaft} \mathbf{R} \tag{3.64}$$

These matrices can now be assembled into the system global mass and stiffness matrices. It is important to note that the first and last six variables relate to the existing rigid body motions. The other variables are 'new' variables. Therefore, the assembly operation has to be carried out with great care.

3.5.4 Co-ordinate Transformation for a Pin-Jointed Connection

Here the connection is treated as being pin-jointed for lateral rotations, but axial shaft rotation is still coupled with that of the rigid body. This can be used in the modelling of a system containing a mechanical connection akin to a universal joint, or with minor modifications could be converted to a truly pin-jointed connection. Again connecting beam *i* to body *j* the motion at the point of the attachment is:

$$\mathbf{u}_i = \mathbf{x}_j + \boldsymbol{\alpha}_j \times \mathbf{r}_s \tag{3.65}$$

However, now the second equation does not exist for lateral rotations, since there is no relationship between the rigid body and rotations of shaft end nodes:

$$\boldsymbol{\theta}_i \neq \boldsymbol{\alpha}_j \tag{3.66}$$

This means that the transformation matrix relevant to this case is the top three rows and six columns of the transformation matrix **S**, used for the built in condition. If the bending of the ends of the shaft is not coupled with the rigid body, a rigid body motion will result for the beam and the resulting stiffness matrix will be ill conditioned. This is due to the rotational rigid body motion under torsion. In order to eliminate the rigid body motion in torsion, it may be

assumed that the torsion of the shaft is equal to the component of the rigid body rotational motion along the beam. This can be expressed in terms of the dot product between the direction cosines of the beam axis, and the angular rotation α, of the rigid body.

Thus:

$$\mathbf{0}_{\alpha i} = \mathbf{u} \cdot \boldsymbol{\alpha} \tag{3.67}$$

Where $\mathbf{u} = \{u_1\ u_2\ u_3\}$ and $\boldsymbol{\alpha} = \{\alpha_j\ \beta_j\ \gamma_j\}$. Here **u** contains the direction cosines of the beam along its length.

The transformation may thus be written in matrix form as:

$$\begin{Bmatrix} u_{xi} \\ u_{yi} \\ u_{zi} \\ \theta_{\alpha i} \\ \theta_{\beta i} \\ \theta_{\gamma i} \end{Bmatrix} = \begin{bmatrix} 1 & 0 & 0 & 0 & c & -b & 0 & 0 \\ 0 & 1 & 0 & -c & 0 & a & 0 & 0 \\ 0 & 0 & 1 & b & -a & 0 & 0 & 0 \\ 0 & 0 & 0 & u_1 & u_2 & u_3 & 0 & 0 \\ 0 & 0 & 0 & 0 & 0 & 0 & 1 & 0 \\ 0 & 0 & 0 & 0 & 0 & 0 & 0 & 1 \end{bmatrix} \begin{Bmatrix} x_j \\ y_j \\ z_j \\ \alpha_j \\ \beta_j \\ \gamma_j \\ \theta_{\beta i} \\ \theta_{\gamma i} \end{Bmatrix} \tag{3.68}$$

It can be seen that at the point of connection there are now eight degrees of freedom. This is due to the fact that six belong to the rigid body and six to the shaft node, giving a total of twelve degrees of freedom. However, three displacements of the shaft node and rigid body are identical (and coupled) as is the axial rotation, so four degrees of freedom cancel. The rest of the formulation to transform the mass and stiffness matrices into the global axis system is the same as that of the built-in condition (Equations 3.60 - 3.64).

3.6 PROGRAMMING CONSIDERATIONS

The equations developed in this chapter have been formulated and structured such that they can be used for developing general vibration analysis software. As

the equations given for the rigid body motion refer to bodies *i* and *j*, they can be placed in the global axis system accordingly.

The solution of equations 3.40 and 3.41 requires four (6x6) sub matrices to be placed in the correct positions in the global system matrix as follows:

$$\begin{bmatrix} \mathbf{k}_r & \mathbf{k}_r\mathbf{R}_{pi} \\ \mathbf{R}_{pi}^T\mathbf{k}_r & \mathbf{r}_i\mathbf{k}_r\mathbf{R}_{pi} \end{bmatrix}$$ placed starting from position (6(*i*-1)+1, 6(*i*-1)+1)

$$-\begin{bmatrix} \mathbf{k}_r & \mathbf{k}_r\mathbf{R}_{pj} \\ \mathbf{R}_{pj}^T\mathbf{k}_r & \mathbf{R}_{pj}^T\mathbf{k}_r\mathbf{R}_{pj} \end{bmatrix}$$ placed starting from position (6(*i*-1)+1, 6(*j*-1)+1)

$$-\begin{bmatrix} \mathbf{k}_r & \mathbf{k}_r\mathbf{R}_{pi} \\ \mathbf{R}_{pi}^T\mathbf{k}_r & \mathbf{r}_i\mathbf{k}_r\mathbf{R}_{pi} \end{bmatrix}$$ placed starting from position (6(*j*-1)+1, 6(*i*-1)+1)

$$\begin{bmatrix} \mathbf{k}_r & \mathbf{k}_r\mathbf{R}_{pj} \\ \mathbf{R}_{pj}^T\mathbf{k}_r & \mathbf{R}_{pj}^T\mathbf{k}_r\mathbf{R}_{pj} \end{bmatrix}$$ placed starting from position (6(*j*-1)+1, 6(*j*-1)+1)

It is necessary that the entries into the global stiffness matrix are additive (i.e. each new entry is added to what has previously been recorded in order to account for the contributions of different springs/shafts). Thus it is easiest to construct the global stiffness matrix using a counting loop. The data structure for each spring needs to refer the spring to the attached mass number. In this way, a spring stiffness sub matrix can be located in the global matrix according to the mass numbers the spring ends are attached to. These principles apply equally to the damping and inertia matrices, which also need to be expressed in the global axis frame using a matrix transformation before they are located in the global matrices.

3.7 SUMMARY

This chapter presents a method of analysing general multi-rigid body systems inter connected by linear springs and shafts (beams). The mathematical modelling is for small vibrations where non-linear geometry effects and

gyroscopic couplings (between rigid body masses) are assumed to be small. Also, the deflection characteristics of mountings are assumed to be linear. There is a shortage of published material on general mathematical modelling of flexibly supported multi-rigid-body systems for vibration analysis. Additionally, little published material has been found on hybrid modelling where rigid bodies of finite size (not point masses) are modelled together with FEA representations of flexible beam elements. This chapter gives a precise formulation suitable for computational implementation; the formulation forms the core of the vibration analysis suite VIBRATIO which has been used to incorporate elements derived in Chapters 4, 5 and 6. Although rigid bodies are not mandatory for the verification of beam elements, the inclusion in the software creates a more universal modelling technique, making it easier to analyse different system types.

CHAPTER 4

SHAFT GYROSCOPIC BEAM ELEMENT MATRIX DERIVATION

4.1 INTRODUCTION

Euler beam elements are often used in finite element analysis but rarely include the relatively minor gyroscopic coupling effects. Although there are a number of papers that publish a gyroscopic beam element matrix for an Euler beam (examples include Nelson, H.D., and McVaugh, J.M., [1976], Kim, Y.D., and Lee, C.W., [1986], and also Zorzi, E.S., and Nelson, H.D., [1977]) there are none showing the full derivation. Here, the full derivation is given in order to provide the reader with a comprehensive understanding of a gyroscopic beam element, before further progressing the work to develop a gyroscopic propeller element in the following chapter. In this case the matrix has been derived using the energy methods explained by Gasch, R., [1976].

In practice it can be extremely difficult to determine the exact solution of the differential equations that describe a complex system. Hence the finite element method is an approximate solution. In the theory of finite element beams this approximation derives mainly from the fact that the element positions are determined by predefined shape functions that only approximately satisfy the differential equations and relevant boundary conditions. The higher the order of shape function that is used, the better the approximation that will be achieved. Other approximations often arise due to the omission of various effects because of the complexity of creating an all encompassing element that accounts for

everything. One good example of a simplification omission is the gyroscopic effect, which is investigated and included here.

4.2 THEORY

4.2.1 Beam Elements (Three Dimensional)

The general three dimensional beam element can be thought of as being described by four lower order displacements or elements combined. Assuming the element to lie along the X axis, then the four components can be described as follows:

- Bar element, which describes axial deformation.
- Torsional element, which describes torsional deformation.
- X-Y beam element, which describes bending in the X-Y plane.
- X-Z beam element, which describes bending in the X-Z plane.

In this analysis the beam elements are assumed to be straight bars with uniform cross-section and two nodes (one at each end). There are twelve degrees of freedom per element, six at each node (three displacements and three rotations). The shape functions are required to define the longitudinal position of the beam elements for given rotations and deflections of nodes, while the node coordinates are functions of time. Many papers ignore axial and torsional deformations in their derivations, producing element matrices that show only the eight degrees of freedom, which are those associated with bending. These bending matrices are still identical to the bending parts of twelve degree of freedom systems, but care must be taken with axis systems when making comparison.

The X-Y and X-Z bending beam elements have been constructed using Euler-Bernoulli beam theory. Euler-Bernoulli theory assumes the normal stresses (σ_y and σ_z) are zero along the longitudinal surfaces of the beam. This assumption is generally considered reasonable for slender beams, which have one predominant dimension. Furthermore, the theory assumes that under

deformation the transverse cross-section remains perpendicular to the deformed central line, meaning that there is neither shear deformation nor shear stress.

4.2.2 Equations of Motion

Gasch, R., [1976] states: "The equations of motion can be found by the principle of virtual work, which states that the work done by external forces acting on our system and the work done by the internal forces must vanish for any virtual displacement."

Therefore:

$$\partial W = 0 \tag{4.1}$$

The virtual work ∂W is summed up as follows:

$$\partial \mathbf{W} = \sum_{1}^{n} \left\{ \int_{0}^{l} \partial \mathbf{u}''^{T} EI \mathbf{u}'' dx + \int \partial \mathbf{u}''^{T} d_i EI \left(\dot{\mathbf{u}}'' - \Omega \mathbf{N} \mathbf{u}'' \right) dx + \int \partial \mathbf{u}^{T} \mu \ddot{\mathbf{u}} dx \right.$$

$$+ \int \partial \mathbf{u}^{T} d_e \dot{\mathbf{u}} dx - \int \partial \mathbf{u}^{T} k_s \mathbf{N} \mathbf{u} dx - \int \partial \mathbf{u}^{T} c_{magn} \mathbf{u} dx$$

$$\left. + [\partial \mathbf{u}^{T} m \ddot{\mathbf{u}} + \partial \mathbf{u}'^{T} \theta_a \ddot{\mathbf{u}}' - \partial \mathbf{u}'^{T} \Omega \theta_p \mathbf{N} \dot{\mathbf{u}}']_l \right\}$$

$$+ \sum_{1}^{L} \partial \mathbf{u}^{T} \left(\mathbf{C} \Omega \mathbf{u} + \mathbf{B} \Omega \dot{\mathbf{u}} \right) + \sum_{1}^{n} \left\{ -\Omega^2 \int \partial \mathbf{u}^{T} \mu \varepsilon_c dx \cos \Omega t \right.$$

$$\left. - \Omega^2 \int \partial \mathbf{u}^{T} \mu \varepsilon_s dx \sin \Omega t + \left[-\Omega^2 \partial \mathbf{u}^{T} m \varepsilon_c \cos \Omega t - \Omega^2 \partial \mathbf{u}^{T} m \varepsilon_s \sin \Omega t \right]_l \right\} \tag{4.2}$$

From which the gyroscopic virtual work is defined as:

$$\partial \mathbf{W}_G = - \int [\partial \mathbf{u}'^{T} \Omega \theta_p \mathbf{N} \dot{\mathbf{u}}']_l \tag{4.3}$$

Since the gyroscopic bending moments are dependant on the angular velocity of the beam elements, the resultant element matrix will be added to the damping matrix in the global system. For this reason, the gyroscopic coupling matrix is often referred to as the gyroscopic damping matrix.

4.2.3 Gyroscopic Beam Element Matrix Derivation

For the purposes of this analysis the following element shape functions have been used:

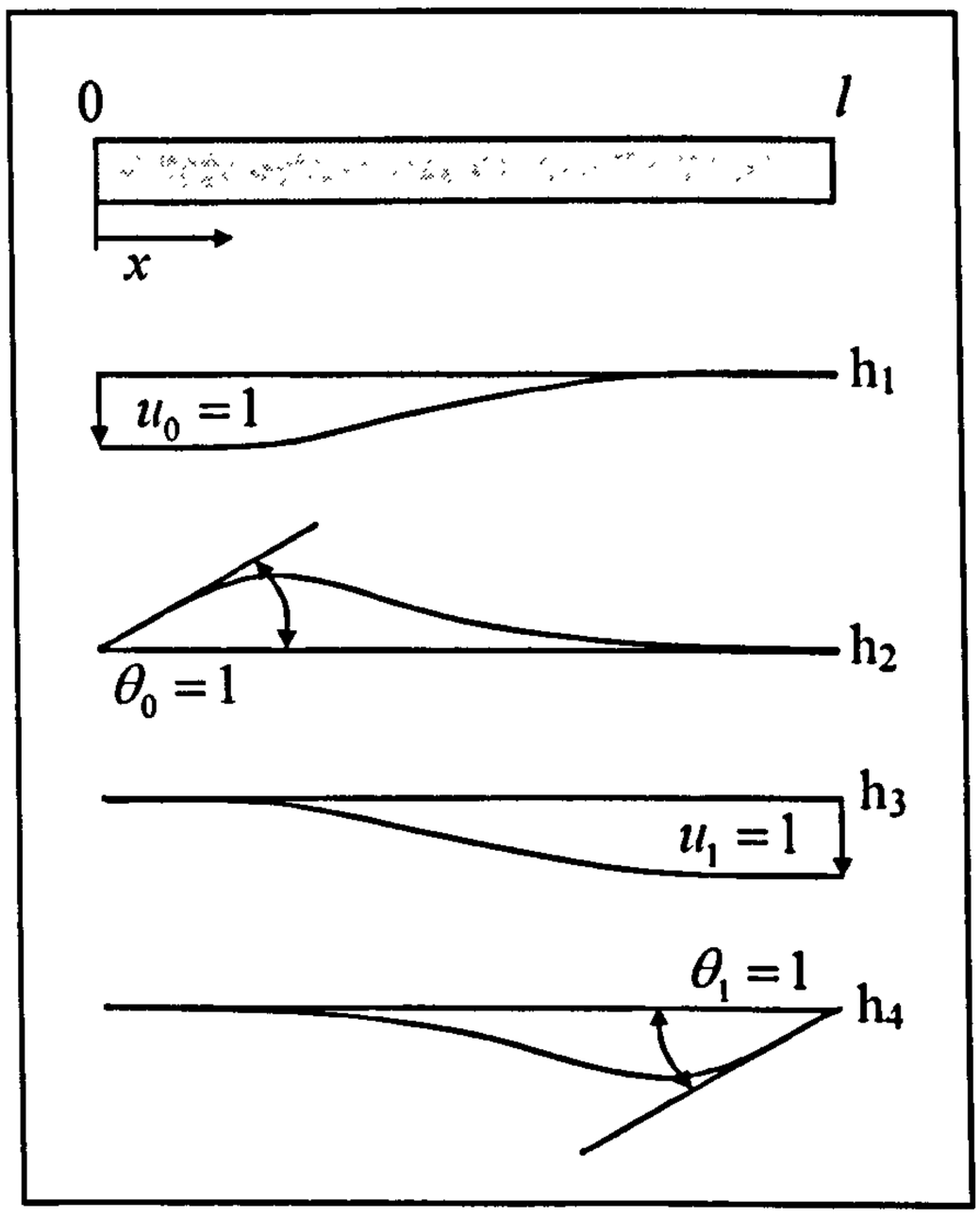

Figure 4.1: Shape Functions

Where:

$$\xi = \frac{x}{l} \tag{4.4}$$

$$h_1 = 1 - 3\xi^2 + 2\xi^3 \tag{4.5}$$

$$h_2 = -l\left(\xi - 2\xi^2 + \xi^3\right) \tag{4.6}$$

$$h_3 = 3\xi^2 - 2\xi^3 \tag{4.7}$$

$$h_4 = l\left(\xi^2 - \xi^3\right) \tag{4.8}$$

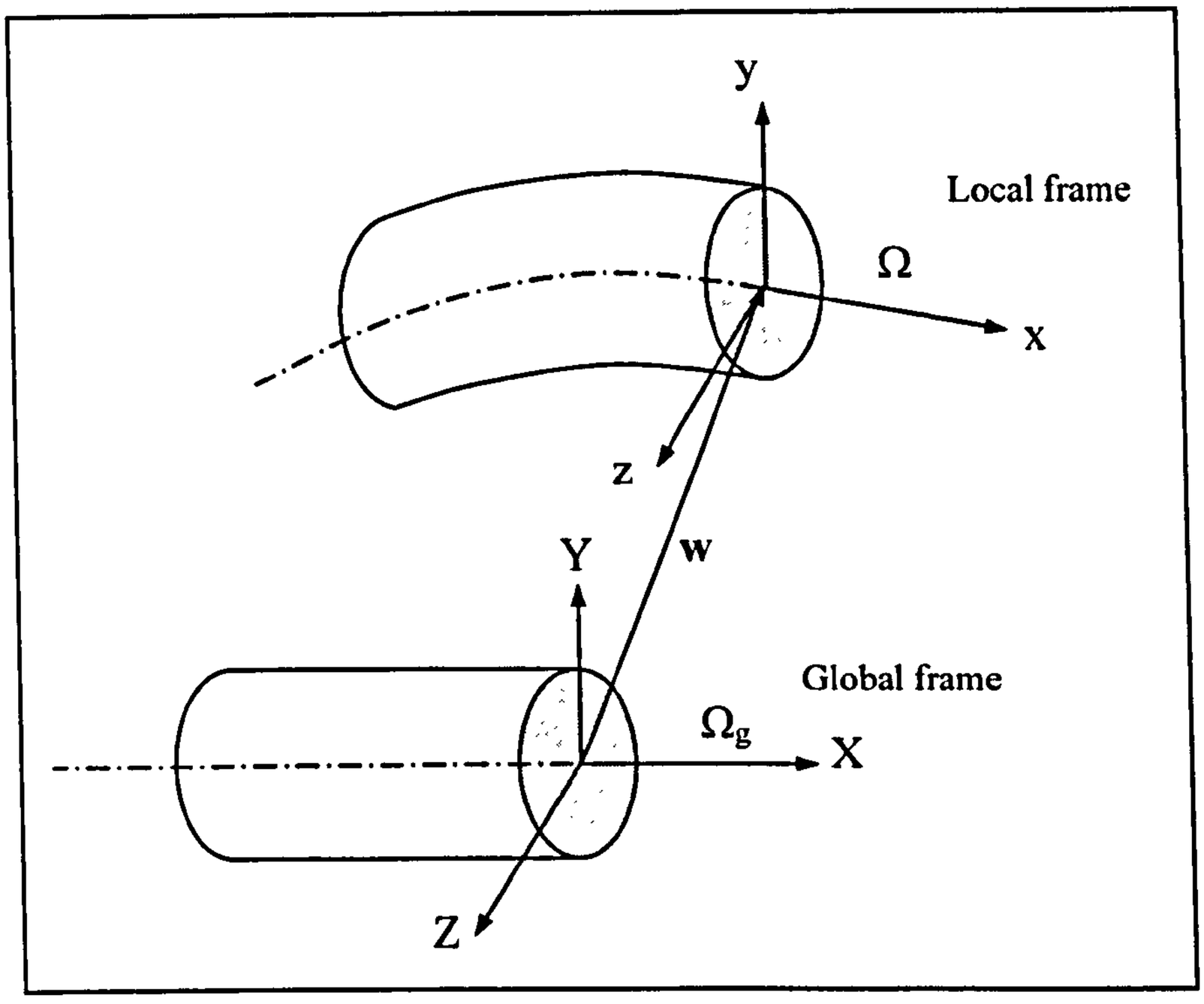

Figure 4.2: Shaft Definitions

By introducing a body frame such as Figure 4.2, the description of motion is reduced to the analysis of the motion of a coordinate system, the position of which is given at any time by the displacement vector **w** and its corresponding rotation matrix. Thus the element derivation can now be completed with the element lying in its own local axis system. Furthermore, the axis of rotation can be assumed to lie along the beam's axis of symmetry for simplicity. This is now much simpler to describe mathematically and the element can be placed into the global axis system by using a transformation matrix as part of the software assembly process.

The equations of motion for the gyroscopic effect can now be derived for a single element using the virtual work principle defined earlier:

$$\partial \mathbf{W}_G = -\int [\partial \mathbf{u}'^T \Omega \theta_p \mathbf{N} \dot{\mathbf{u}}']_l dx \tag{4.9}$$

Since:

$$\partial \mathbf{u}'(x,t) = \mathbf{V}'^{T}(x) \cdot \partial \mathbf{u}_e(t) \tag{4.10}$$

Then the gyroscopic virtual work can be described as:

$$\partial \mathbf{W}_G = -\partial \mathbf{u}_e^T \int [\mathbf{V}' \Omega \theta_P \mathbf{N} \dot{\mathbf{u}}']_l dx \tag{4.11}$$

Also:

$$\dot{\mathbf{u}}(x,t) = \mathbf{V}^T(x) \cdot \dot{\mathbf{u}}_e(t) \tag{4.12}$$

Thus the gyroscopic virtual work for an element can be expressed as:

$$\partial \mathbf{W}_{G_e} = -\partial \mathbf{u}_e^T \int_0^l [\mathbf{V}' \Omega \theta_P \mathbf{N} \mathbf{V}'^T] \, dx \cdot \dot{\mathbf{u}}_e \tag{4.13}$$

Since the rotational speed of the shaft and polar moment of inertia per unit length are constants within the integration, this can be expressed as:

$$\partial \mathbf{W}_{G_e} = -\partial \mathbf{u}_e^T \Omega \theta_P \int_0^l [\mathbf{V}' \mathbf{N} \mathbf{V}'^T] \, dx \cdot \dot{\mathbf{u}}_e \tag{4.14}$$

Expressing $\mathbf{G}_e$ as follows:

$$\mathbf{G}_e = \Omega \theta_P \int_0^l [\mathbf{V}' \mathbf{N} \mathbf{V}'^T] \, dx \tag{4.15}$$

Then:

$$\partial \mathbf{W}_{G_e} = -\partial \mathbf{u}_e^T \cdot \mathbf{G}_e \cdot \dot{\mathbf{u}}_e \tag{4.16}$$

Where $\mathbf{G}_e$ is now defined as the gyroscopic beam element matrix.

For a flexible cylindrical beam element whose axis of symmetry coincides with that of rotation, a twelve degree of freedom system is used. If x is the axis of symmetry then by the geometric displacement principles shown in Figure 4.3, $\mathbf{V}^T$ becomes:

$$\mathbf{V}^T = \begin{pmatrix} 0 & 0 & h_1 & 0 & h_2 & 0 & 0 & 0 & h_3 & 0 & h_4 & 0 \\ 0 & h_1 & 0 & 0 & 0 & -h_2 & 0 & h_3 & 0 & 0 & 0 & -h_4 \end{pmatrix} \tag{4.17}$$

The displacement and velocity components are defined as follows:

$$\mathbf{u}_e^T = \begin{pmatrix} x_0 & y_0 & z_0 & \alpha_0 & \beta_0 & \gamma_0 & x_1 & y_1 & z_1 & \alpha_1 & \beta_1 & \gamma_1 \end{pmatrix} \tag{4.18}$$

$$\dot{\mathbf{u}}_e^T = \begin{pmatrix} \dot{x}_0 & \dot{y}_0 & \dot{z}_0 & \dot{\alpha}_0 & \dot{\beta}_0 & \dot{\gamma}_0 & \dot{x}_1 & \dot{y}_1 & \dot{z}_1 & \dot{\alpha}_1 & \dot{\beta}_1 & \dot{\gamma}_1 \end{pmatrix} \tag{4.19}$$

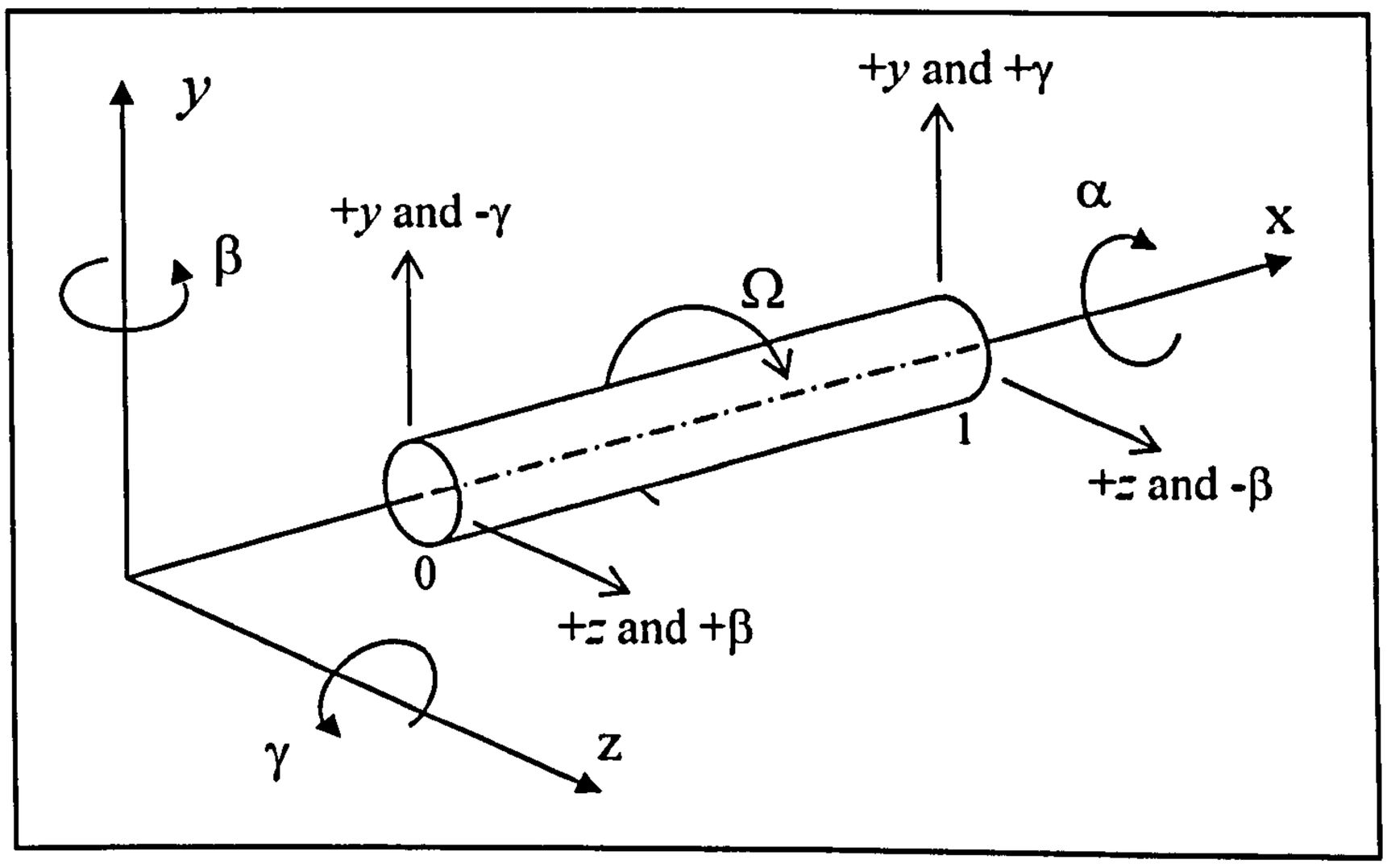

Figure 4.3: Shape Function Matrix Geometry

Thus multiplying out the matrices in Equation 4.15 gives:

$$\mathbf{V'NV'^{T}} = \begin{pmatrix}
0 & 0 & 0 & 0 & 0 & 0 & 0 & 0 & 0 & 0 & 0 & 0 \\
0 & 0 & h_1'h_1' & 0 & h_1'h_2' & 0 & 0 & 0 & h_1'h_3' & 0 & h_1'h_4' & 0 \\
0 & -h_1'h_1' & 0 & 0 & 0 & h_1'h_2' & 0 & -h_1'h_3' & 0 & 0 & 0 & h_1'h_4' \\
0 & 0 & 0 & 0 & 0 & 0 & 0 & 0 & 0 & 0 & 0 & 0 \\
0 & -h_2'h_1' & 0 & 0 & 0 & h_2'h_2' & 0 & -h_2'h_3' & 0 & 0 & 0 & h_2'h_4' \\
0 & 0 & -h_1'h_2' & 0 & -h_2'h_2' & 0 & 0 & 0 & -h_2'h_3' & 0 & -h_2'h_4' & 0 \\
0 & 0 & 0 & 0 & 0 & 0 & 0 & 0 & 0 & 0 & 0 & 0 \\
0 & 0 & h_3'h_1' & 0 & h_3'h_2' & 0 & 0 & 0 & h_3'h_3' & 0 & h_3'h_4' & 0 \\
0 & -h_3'h_1' & 0 & 0 & 0 & h_3'h_2' & 0 & -h_3'h_3' & 0 & 0 & 0 & h_3'h_4' \\
0 & 0 & 0 & 0 & 0 & 0 & 0 & 0 & 0 & 0 & 0 & 0 \\
0 & -h_4'h_1' & 0 & 0 & 0 & h_4'h_2' & 0 & -h_4'h_3' & 0 & 0 & 0 & h_4'h_4' \\
0 & 0 & -h_4'h_1' & 0 & -h_4'h_2' & 0 & 0 & 0 & -h_4'h_3' & 0 & -h_4'h_4' & 0
\end{pmatrix} \tag{4.20}$$

For a cylindrical beam element which has its axis of symmetry coinciding with the axis of rotation, the polar mass moment of inertia per unit length is defined as follows:

$$\theta_P = \frac{\mu r^2}{2} \tag{4.21}$$

Therefore:

$$\mathbf{G}_e = \frac{\Omega \mu r^2}{2} \int_0^l \left[\mathbf{V'NV'^{T}} \right] \partial x \tag{4.22}$$

Given that:

$$\frac{\partial h}{\partial x} = \frac{\partial h}{\partial \xi} \cdot \frac{\partial \xi}{\partial x} \qquad \text{and} \qquad \xi = \frac{x}{l} \tag{4.23) \& (4.24}$$

Then it can be seen that:

$$\frac{\partial h}{\partial x} = \frac{\partial h}{\partial \xi} \cdot \frac{1}{l} \tag{4.25}$$

Also:

$$O' = \frac{\partial}{\partial x} \tag{4.26}$$

Thus the integrals from within the matrix are as follows: (4.27) to (4.36)

$$\int_0^l h_1' h_1' \, \partial x = \frac{6}{5l} \qquad \int_0^l h_2' h_3' \, \partial x = \frac{l}{10l}$$

$$\int_0^l h_1' h_2' \, \partial x = -\frac{l}{10l} \qquad \int_0^l h_2' h_4' \, \partial x = -\frac{l^2}{30l}$$

$$\int_0^l h_1' h_3' \, \partial x = -\frac{6}{5l} \qquad \int_0^l h_3' h_3' \, \partial x = \frac{6}{5l}$$

$$\int_0^l h_1' h_4' \, \partial x = -\frac{l}{10l} \qquad \int_0^l h_3' h_4' \, \partial x = \frac{l}{10l}$$

$$\int_0^l h_2' h_2' \, \partial x = \frac{2l^2}{15l} \qquad \int_0^l h_4' h_4' \, \partial x = \frac{2l^2}{15l}$$

4.2.4 Beam Element Matrix

Inserting terms 4.27 to 4.36 into Equation 4.22 gives the gyroscopic damping matrix for a beam element:

$$\mathbf{G}_e = \frac{\Omega \mu r^2}{60l} \begin{pmatrix} 0 & 0 & 0 & 0 & 0 & 0 & 0 & 0 & 0 & 0 & 0 & 0 \\ 0 & 0 & 36 & 0 & -3l & 0 & 0 & 0 & -36 & 0 & -3l & 0 \\ 0 & -36 & 0 & 0 & 0 & -3l & 0 & 36 & 0 & 0 & 0 & -3l \\ 0 & 0 & 0 & 0 & 0 & 0 & 0 & 0 & 0 & 0 & 0 & 0 \\ 0 & 3l & 0 & 0 & 0 & 4l^2 & 0 & -3l & 0 & 0 & 0 & -l^2 \\ 0 & 0 & 3l & 0 & -4l^2 & 0 & 0 & 0 & -3l & 0 & l^2 & 0 \\ 0 & 0 & 0 & 0 & 0 & 0 & 0 & 0 & 0 & 0 & 0 & 0 \\ 0 & 0 & -36 & 0 & 3l & 0 & 0 & 0 & 36 & 0 & 3l & 0 \\ 0 & 36 & 0 & 0 & 0 & 3l & 0 & -36 & 0 & 0 & 0 & 3l \\ 0 & 0 & 0 & 0 & 0 & 0 & 0 & 0 & 0 & 0 & 0 & 0 \\ 0 & 3l & 0 & 0 & 0 & -l^2 & 0 & -3l & 0 & 0 & 0 & 4l^2 \\ 0 & 0 & 3l & 0 & l^2 & 0 & 0 & 0 & -3l & 0 & -4l^2 & 0 \end{pmatrix} \quad (4.37)$$

This is the complete gyroscopic beam element matrix for a cylindrical element which rotates about its axis of symmetry. The element has been defined as lying along the x-axis such that gyroscopic coupling occurs in the y and z axes. It can

be seen that it is z and beta deflections that create moments about y and gamma, and vice-versa.

4.3 ANSYS GYROSCOPIC DAMPING MATRIX (ANSYS Theory)

Below is the ANSYS gyroscopic matrix as defined in the ANSYS Theory Reference Element Library. ANSYS refers to the matrix as a gyroscopic damping matrix. Although the gyroscopic effect is not strictly that of damping, it is dependant on the velocity component in the same way as damping and is thus often referred to as such. The element type is PIPE 16 – elastic straight pipe. Whilst it shares its stiffness and mass matrices with the standard BEAM 4 ANSYS element, the gyroscopic matrix is unique. Unfortunately, a derivation or reference to other material has not been given, so the matrix is included purely for comparison purposes. Note that ANSYS uses the same axis system for beam elements as that used here.

$$G_{k_{ANSYS}} = 2\Omega\rho Al \begin{pmatrix} 0 & 0 & 0 & 0 & 0 & 0 & 0 & 0 & 0 & 0 & 0 & 0 \\ 0 & 0 & g & 0 & h & 0 & 0 & 0 & -g & 0 & h & 0 \\ 0 & -g & 0 & 0 & 0 & h & 0 & g & 0 & 0 & 0 & h \\ 0 & 0 & 0 & 0 & 0 & 0 & 0 & 0 & 0 & 0 & 0 & 0 \\ 0 & -h & 0 & 0 & 0 & i & 0 & h & 0 & 0 & 0 & j \\ 0 & 0 & -h & 0 & -i & 0 & 0 & 0 & h & 0 & -j & 0 \\ 0 & 0 & 0 & 0 & 0 & 0 & 0 & 0 & 0 & 0 & 0 & 0 \\ 0 & 0 & -g & 0 & -h & 0 & 0 & 0 & g & 0 & -h & 0 \\ 0 & g & 0 & 0 & 0 & -h & 0 & -g & 0 & 0 & 0 & -h \\ 0 & 0 & 0 & 0 & 0 & 0 & 0 & 0 & 0 & 0 & 0 & 0 \\ 0 & -h & 0 & 0 & 0 & j & 0 & h & 0 & 0 & 0 & i \\ 0 & 0 & -h & 0 & -j & 0 & 0 & 0 & h & 0 & -i & 0 \end{pmatrix}$$

Where:

$$g = \frac{6/5R^2}{l^2(1+\varsigma)^2} \qquad h = \frac{-(1/10-1/2\varsigma)R^2}{l(1+\varsigma)^2} \qquad i = \frac{(2/15+1/6\varsigma+1/3\varsigma^2)R^2}{(1+\varsigma)^2}$$

$$j = \frac{-(1/30 + 1/6\varsigma - 1/6\varsigma^2)R^2}{(1+\varsigma)^2} \qquad R = \sqrt{I/A} \qquad \varsigma = \frac{12EI}{GA_s l^2}$$

4.4 SUMMARY

The mathematical formulation of an Euler-Bernoulli finite beam element that can be used to model a shaft and includes gyroscopic effects has been realised. The standard stiffness and mass matrix derivations of an Euler-Bernoulli beam element are widely published in literature and have not been given here. However, the full matrices are given in Appendix A for reference and the author refers to Thomson, W.T., [1993] or Gasch, R., [1976] if the reader requires a complete derivation. The gyroscopic matrix has also been previously published in literature. However, an extensive search has not found the source of derivation. Due to the importance of the gyroscopic effect in this work and the fact that in Chapter 4 the principles used in this chapter are developed and extended to create an element capable of modelling the gyroscopic effects of a propeller, the full derivation has been given. The equivalent ANSYS gyroscopic matrix has also been given as ANSYS has been used to verify the shaft modelling code VIBRATIO into which this gyroscopic matrix has been incorporated.

CHAPTER 5

GYROSCOPIC PROPELLER ELEMENT MATRIX DERIVATION

5.1 INTRODUCTION

This chapter presents the formulation of a gyroscopic propeller element using Euler-Bernoulli theory. The element derivation is based on the same principles as that of the standard beam element derivation shown previously in Chapter 4. However, now the axis of rotation no longer lies along the axis of symmetry belonging to the element, but is instead perpendicular to it. This change does not affect the standard Euler mass and stiffness matrices, but for gyroscopic behaviour the effect of changing this rotational axis is much more significant, making the polar moment of inertia per unit length a variable within the integration. The polar moment of inertia now increases quadratically with the radial distance away from the axis of rotation. Thus the radial distance of the element under consideration from the axis of rotation must be considered and accounted for in the matrix derivation.

5.2 THEORY

5.2.1 Equations of Motion

As before in Chapter 4 the virtual work equation presented by Gasch, R., [1976] is used to derive the equations of motion. The principle of virtual work was first formulated by Bernoulli, J.J. and may be stated as follows: *If a system in equilibrium under the action of a set of forces is given a virtual displacement, the virtual work done by the forces will be zero.* This is more easily understood as the work done by the external forces acting on a system and the work done by the

internal forces must vanish for a virtual displacement. The statement assumes an imaginary virtual displacement given instantaneously, thus there are no significant changes in geometry and the system is assumed to behave linearly.

Therefore:

$$\partial \mathbf{W} = 0 \tag{5.1}$$

As before (in Chapter 4) the virtual work $\partial \mathbf{W}$ for an Euler beam is summed up as follows:

$$\begin{aligned}\partial \mathbf{W} = \sum_{1}^{n} \Bigg\{ & \int_{0}^{l} \partial \mathbf{u}''^{T} EI \mathbf{u}'' dx + \int \partial \mathbf{u}''^{T} d_i EI \left(\dot{\mathbf{u}}'' - \Omega \mathbf{N} \mathbf{u}'' \right) dx + \int \partial \mathbf{u}^{T} \mu \ddot{\mathbf{u}} dx \\ & + \int \partial \mathbf{u}^{T} d_e \dot{\mathbf{u}} dx - \int \partial \mathbf{u}^{T} k_s \mathbf{N} \mathbf{u} dx - \int \partial \mathbf{u}^{T} c_{magn} \mathbf{u} dx \\ & + \left[\partial \mathbf{u}^{T} m \ddot{\mathbf{u}} + \partial \mathbf{u}'^{T} \theta_a \ddot{\mathbf{u}}' - \partial \mathbf{u}'^{T} \Omega \theta_P \mathbf{N} \dot{\mathbf{u}}' \right]_l \Bigg\} \\ & + \sum_{1}^{L} \partial \mathbf{u}^{T} \left(\mathbf{C} \Omega \mathbf{u} + \mathbf{B} \Omega \dot{\mathbf{u}} \right) + \sum_{1}^{n} \Big\{ -\Omega^2 \int \partial \mathbf{u}^{T} \mu \varepsilon_c dx \cos \Omega t \\ & - \Omega^2 \int \partial \mathbf{u}^{T} \mu \varepsilon_s dx \sin \Omega t + \left[-\Omega^2 \partial \mathbf{u}^{T} m \varepsilon_c \cos \Omega t - \Omega^2 \partial \mathbf{u}^{T} m \varepsilon_s \sin \Omega t \right]_l \Big\}\end{aligned} \tag{5.2}$$

From which the gyroscopic virtual work is defined as:

$$\partial \mathbf{W}_G = - \int \left[\partial \mathbf{u}'^{T} \Omega \theta_p \mathbf{N} \dot{\mathbf{u}}' \right]_l \tag{5.3}$$

5.2.2 Gyroscopic Propeller Element Derivation

Gyroscopic bending moments are proportional to the angular velocity of an element. The moments are also coupled such that for an element spinning about the x-axis, a positive rotation in orientation about beta would produce a negative moment about gamma. Note that energy is not being removed from the system by this action, but the moments are simply transposed from one axis to another. However, because this action is proportional to angular velocity the gyroscopic matrix is added to the system damping matrix, and for this reason is often

referred to as the gyroscopic damping matrix even though it is not damping in the conventional sense. In Equation 5.3 this velocity dependence appears as the $\dot{\mathbf{u}}$ term, which is defined as follows:

$$i\dot{l}_k^T = \left(\dot{x}_0 \;\; \dot{y}_0 \;\; \dot{z}_0 \;\; \dot{\alpha}_0 \;\; \dot{\beta}_0 \;\; \dot{\gamma}_0 \;\; \dot{x}_1 \;\; \dot{y}_1 \;\; \dot{z}_1 \;\; \dot{\alpha}_1 \;\; \dot{\beta}_1 \;\; \dot{\gamma}_1\right) \tag{5.4}$$

For the purposes of this analysis the cubic element shape functions Equations 4.4-4.8 as shown in Figure 4.1 have been used.

The equations of motion for the gyroscopic effect can now be derived for a single element using the virtual work principle defined earlier:

$$\partial \mathbf{W}_G = -\int [\partial \mathbf{u}'^T \Omega \theta_P \mathbf{N} \dot{\mathbf{u}}'], \tag{5.5}$$

Since:

$$\partial \mathbf{u}'(x,t) = \mathbf{V}'^T(x) \cdot \partial \mathbf{u}_e(t) \tag{5.6}$$

And:

$$\dot{\mathbf{u}}(x,t) = \mathbf{V}^T(x) \cdot \dot{\mathbf{u}}_e(t) \tag{5.7}$$

Thus the gyroscopic virtual work for an element can be expressed as:

$$\partial \mathbf{W}_{G_{e_p}} = -\partial \mathbf{u}_e^T \int_0^l [\mathbf{V}' \Omega \theta_p \mathbf{N} \mathbf{V}'^T] \, \partial x \cdot \dot{\mathbf{u}}_e \tag{5.8}$$

Since the rotational speed of the shaft is a constant within the integration, this can be expressed as:

$$\partial \mathbf{W}_{G_{e_p}} = -\partial \mathbf{u}_e^T \Omega \int_0^l [\mathbf{V}' \theta_P \mathbf{N} \mathbf{V}'^T] \, \partial x \cdot \dot{\mathbf{u}}_e \tag{5.9}$$

Expressing $\mathbf{G}_{e_p}$ as:

$$\mathbf{G}_{e_p} = \Omega \int_0^l [\mathbf{V}' \theta_P \mathbf{N} \mathbf{V}'^T] \, \partial x \tag{5.10}$$

Then:

$$\partial \mathbf{W}_{G_{e_p}} = -\partial \mathbf{u}_e^T \cdot \mathbf{G}_{e_p} \cdot \dot{\mathbf{u}}_e \tag{5.11}$$

Where $\mathbf{G}_{e_p}$ is now defined as the gyroscopic beam element matrix for a propeller.

In order to describe a propeller-shaft system mathematically, it is first necessary to choose an appropriate axis system. For this study it has been chosen that the shaft should lie along the global X-axis, whilst the propeller blades radiate perpendicularly from the shaft. However, within their local axis systems the propeller and shaft elements can be made to fit any axis system the author chooses, so long as the appropriate matrix transformation is performed during global assembly stages. This can even be taken so far as to both propeller and shaft elements sharing the same local axis system, only to be placed perpendicular to one another on assembly. Thus the propeller and shaft elements are described in the same local axis system, where the element's axis of symmetry is about the x-axis. It is possible to create sub-assemblies for each shaft or propeller blade from however many elements are required before combining them into the global system. This can reduce assembly complications during programming, so that the main consideration is the radial orientation of propeller elements about the X-axis in order to allow for multi-blade systems. However, this is not a prerequisite and it is equally possible to assemble elements into the global matrix in any order the reader chooses.

For a twelve degree of freedom system where x is the axis of rotation but the element's axis of symmetry lies vertically parallel to the y-axis, x and gamma are coupled, and z and alpha are coupled. This geometry is shown in Figure 5.1 and consequently the matrix of element shape functions $\mathbf{V}^T$ becomes:

$$\mathbf{V}^T = \begin{pmatrix} 0 & 0 & h_1 & 0 & h_2 & 0 & 0 & 0 & h_3 & 0 & h_4 & 0 \\ 0 & h_1 & 0 & 0 & 0 & -h_2 & 0 & h_3 & 0 & 0 & 0 & -h_4 \end{pmatrix} \tag{5.12}$$

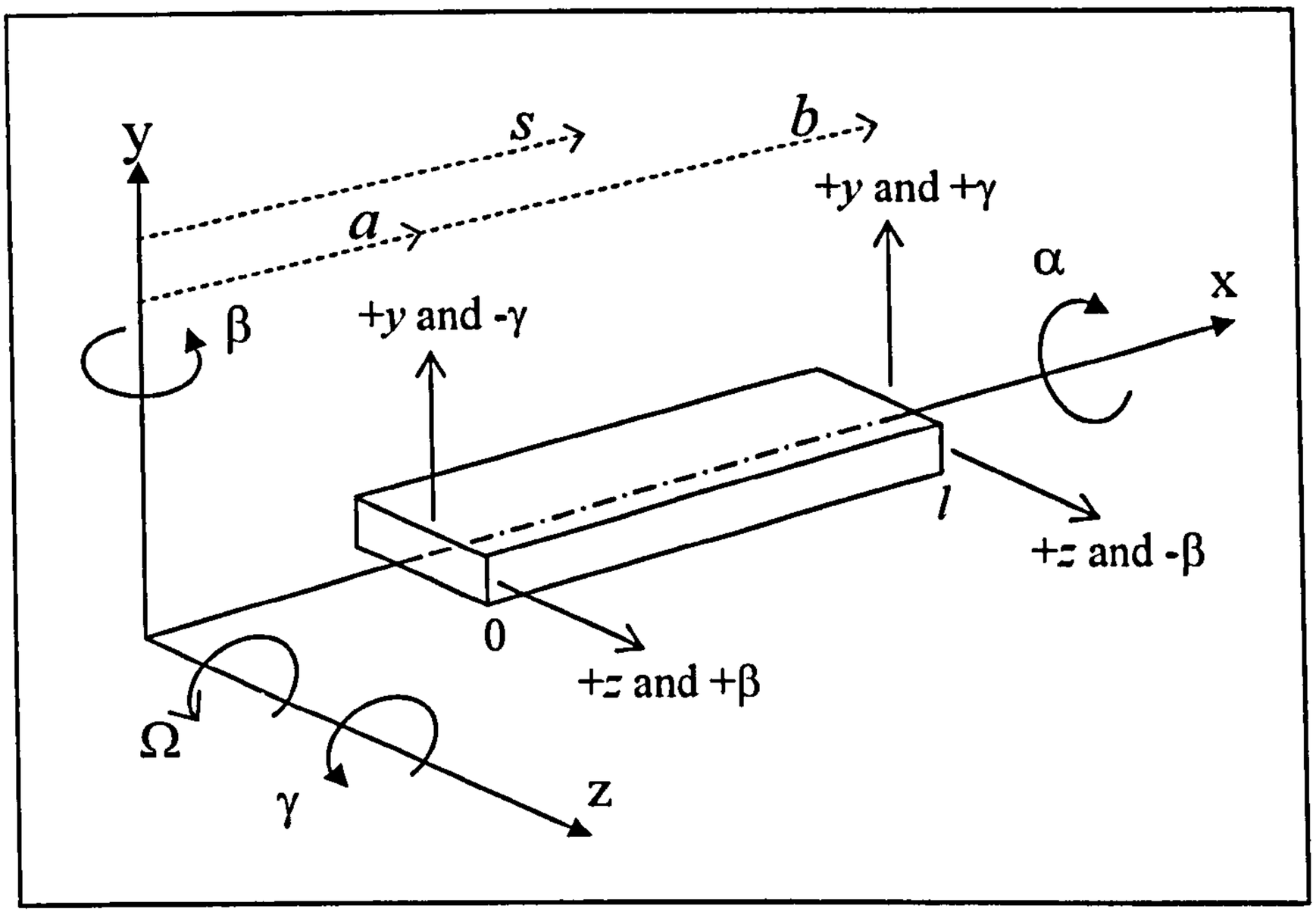

Figure 5.1: Local Axis System

Note: a, b and s are global distances from the axis of rotation

In order to account for the polar moment of inertia per unit length, each propeller blade element is treated as being parallel to the x-axis when attributed to its own local axis system. Therefore, the radial distance to the element under consideration can always be found, whilst coordinates and an angle can be used to determine the orientation of the various propeller blades to the global axis system. The local coordinate system is shown in Figure 5.1 above.

Now since the polar mass moment of inertia per unit length is defined as:

$$\theta_P = \mu s^2 \tag{5.13}$$

Where μ is the mass per unit length. And s is the radial distance to the elemental mass under consideration.

We can express the gyroscopic beam element matrix as:

$$\mathbf{G}_{e_P} = \mu\Omega \int_0^l [\mathbf{V}' s^2 \mathbf{N} \mathbf{V}'^T] \, dx \tag{5.14}$$

Given that $\xi = x/l$ for the element under consideration, then from the Figure 5.1 it can be seen that:

$$s = a + \xi l \tag{5.15}$$

$$s = a + \xi(b - a) \tag{5.16}$$

$$s = a(1 - \xi) + b\xi \tag{5.17}$$

$$s^2 = a^2 + \xi(2ab - 2a^2) + \xi^2(a^2 + b^2 - 2ab) \tag{5.18}$$

Here:

$$O' = \frac{\partial}{\partial x} \tag{5.19}$$

Given that:

$$\frac{\partial h}{\partial x} = \frac{\partial h}{\partial \xi} \cdot \frac{\partial \xi}{\partial x} \tag{5.20}$$

And:

$$\xi = \frac{x}{l} \tag{5.21}$$

Then it can be seen that:

$$\frac{\partial h}{\partial x} = \frac{\partial h}{\partial \xi} \cdot \frac{1}{l} \tag{5.22}$$

Thus the integrals for the various matrix terms are as follows:

$$\int_0^l h_1' s^2 h_1' \, \partial x = \frac{6(2a^2 + 3ab + 2b^2)}{35} \qquad \int_0^l h_1' s^2 h_4' \, \partial x = \frac{l(-5a^2 - 4ab + 2b^2)}{70}$$

$$\int_0^l h_1' s^2 h_2' \, \partial x = \frac{-l(-2a^2 + 4ab + 5b^2)}{70} \qquad \int_0^l h_2' s^2 h_2' \, \partial x = \frac{l^2(9a^2 + 3ab + 2b^2)}{105}$$

$$\int_0^l h_1' s^2 h_3' \, \partial x = \frac{-6(2a^2 + 3ab + 2b^2)}{35} \qquad \int_0^l h_2' s^2 h_3' \, \partial x = \frac{-l(2a^2 - 4ab - 5b^2)}{70}$$

$$\int_0^l h_2' s^2 h_4' \, \partial x = \frac{-l^2(3a^2+ab+3b^2)}{210} \qquad \int_0^l h_3' s^2 h_4' \, \partial x = \frac{l(5a^2+4ab-2b^2)}{70}$$

$$\int_0^l h_3' s^2 h_3' \, \partial x = \frac{6(2a^2+3ab+2b^2)}{35} \qquad \int_0^l h_4' s^2 h_4' \, \partial x = \frac{l^2(2a^2+3ab+9b^2)}{105}$$

(5.23) to (5.32)

Now multiplying out equation 5.11 it can be seen that:

$$\mathbf{V}'s^2\mathbf{N}\mathbf{V}'^T = \begin{pmatrix}
0 & 0 & 0 & 0 & 0 & 0 & 0 & 0 & 0 & 0 & 0 & 0 \\
0 & 0 & -h_1's^2h_1' & 0 & h_1's^2h_2' & 0 & 0 & 0 & h_1's^2h_3' & 0 & h_1's^2h_4' & 0 \\
0 & -h_1's^2h_1' & 0 & 0 & 0 & h_1's^2h_2' & 0 & -h_1's^2h_3' & 0 & 0 & 0 & h_1's^2h_4' \\
0 & 0 & 0 & 0 & 0 & 0 & 0 & 0 & 0 & 0 & 0 & 0 \\
0 & -h_2's^2h_1' & 0 & 0 & 0 & h_2's^2h_2' & 0 & -h_2's^2h_3' & 0 & 0 & 0 & h_2's^2h_4' \\
0 & 0 & -h_2's^2h_1' & 0 & -h_2's^2h_2' & 0 & 0 & 0 & -h_2's^2h_3' & 0 & -h_2's^2h_4' & 0 \\
0 & 0 & 0 & 0 & 0 & 0 & 0 & 0 & 0 & 0 & 0 & 0 \\
0 & 0 & h_3's^2h_1' & 0 & h_3's^2h_2' & 0 & 0 & 0 & h_3's^2h_3' & 0 & h_3's^2h_4' & 0 \\
0 & -h_3's^2h_1' & 0 & 0 & 0 & h_3's^2h_2' & -h_3's^2h_3' & 0 & 0 & 0 & 0 & h_3's^2h_4' \\
0 & 0 & 0 & 0 & 0 & 0 & 0 & 0 & 0 & 0 & 0 & 0 \\
0 & -h_4's^2h_1' & 0 & 0 & 0 & h_4's^2h_2' & -h_4's^2h_3' & 0 & 0 & 0 & 0 & h_4's^2h_4' \\
0 & 0 & -h_4's^2h_1' & 0 & -h_4's^2h_2' & 0 & 0 & 0 & -h_4's^2h_3' & 0 & -h_4's^2h_4' & 0
\end{pmatrix} \tag{5.33}$$

5.2.3 Gyroscopic Propeller Element Matrix

Inserting the terms 5.23 to 5.32 into the relevant positions in matrix 5.33, it can be seen that the gyroscopic beam element matrix for a propeller blade perpendicular to the axis of rotation with distances a and b defined in Figure 5.1 is as follows:

$$\mathbf{G}_{4r} = \frac{\mu\Omega}{210}\begin{pmatrix}
0 & 0 & 0 & 0 & 0 & 0 & 0 & 0 & 0 & 0 & 0 & 0 \\
0 & 0 & 36(2a^2+3ab+2b^2) & 0 & -3l(-2a^2+4ab+5b^2) & 0 & 0 & 0 & -36(2a^2+3ab+2b^2) & 0 & 3l(-5a^2-4ab+2b^2) & 0 \\
0 & -36(2a^2+3ab+2b^2) & 0 & 0 & 0 & -3l(-2a^2+4ab+5b^2) & 0 & 36(2a^2+3ab+2b^2) & 0 & 0 & 0 & 3l(-5a^2-4ab+2b^2) \\
0 & 0 & 0 & 0 & 0 & 0 & 0 & 0 & 0 & 0 & 0 & 0 \\
0 & 3l(-2a^2+4ab+5b^2) & 0 & 0 & 0 & 2l^2(9a^2+3ab+2b^2) & 0 & 3l(2a^2-4ab-5b^2) & 0 & 0 & 0 & -l^2(3a^2+ab+3b^2) \\
0 & 0 & 3l(-2a^2+4ab+5b^2) & 0 & 2l^2(9a^2+3ab+2b^2) & 0 & 0 & 0 & 3l(2a^2-4ab-5b^2) & 0 & l^2(3a^2+ab+3b^2) & 0 \\
0 & 0 & 0 & 0 & 0 & 0 & 0 & 0 & 0 & 0 & 0 & 0 \\
0 & 0 & -36(2a^2+3ab+2b^2) & 0 & -3l(2a^2-4ab-5b^2) & 0 & 0 & 0 & 36(2a^2+3ab+2b^2) & 0 & 3l(5a^2+4ab-2b^2) & 0 \\
0 & 36(2a^2+3ab+2b^2) & 0 & 0 & 0 & -3l(2a^2-4ab-5b^2) & 0 & -36(2a^2+3ab+2b^2) & 0 & 0 & 0 & 3l(5a^2+4ab-2b^2) \\
0 & 0 & 0 & 0 & 0 & 0 & 0 & 0 & 0 & 0 & 0 & 0 \\
0 & -3l(-5a^2-4ab+2b^2) & 0 & 0 & 0 & -l^2(3a^2+ab+3b^2) & 0 & -3l(5a^2+4ab-2b^2) & 0 & 0 & 0 & 2l^2(2a^2+3ab+9b^2) \\
0 & 0 & -3l(-5a^2-4ab+2b^2) & 0 & l^2(3a^2+ab+3b^2) & 0 & 0 & 0 & -3l(5a^2+4ab-2b^2) & 0 & -2l^2(2a^2+3ab+9b^2) & 0
\end{pmatrix} \tag{5.34}$$

5.3 SUMMARY

A novel technique that creates an Euler-Bernoulli finite element that can be used to model a rotating propeller blade including the gyroscopic effects has been realised. The method developed to include gyroscopic effects in propeller models is similar to the derivation of the standard gyroscopic matrix given in Chapter 4. The key difference is the inclusion of the polar moment of inertia per unit length as a variable within the integration. This approach and the resulting gyroscopic matrix have not been previously published.

The main stiffness and mass matrices do not change from that of a standard Euler-Bernoulli shaft element and have been given in Appendix A. With the mass, stiffness and gyroscopic coupling effect accounted for the modelling of a propeller blade is almost complete. However, during operation there is additional centrifugal stiffening imposed on a propeller rotating about an axis perpendicular to its axis of symmetry. These stiffening effects are investigated separately in Chapter 6 since they are in addition to the standard matrices given here and do not replace them. The mathematical formulation used to incorporate the

gyroscopic effect created by propeller deflections could be applied to the derivation of a Timoshenko finite element if required. However, as the gyroscopic effect is itself quite small the difference between a Timoshenko and Euler-Bernoulli model of the effect will be negligible.

CHAPTER 6

CENTRIFUGAL STIFFENING OF PROPELLER ELEMENT MATRIX DERIVATION

6.1 INTRODUCTION

Propeller elements are invariably subjected to axial forces under rotation. These axial forces are created by the angular acceleration the blade undergoes during rotation. So that the axial force in a propeller element will be greatest at the beam's root as this point has to exert enough centrifugal force to support the angular acceleration of the entire blade, the force will fall to zero at the beam's tip. Even for a uniform beam element, the change in force from root to tip will not be linear because the force is proportional to both the mass and radius squared. Hoa, S.V., [1979] produced a paper titled: "Vibration of a Rotating Beam with Tip Mass", which contains a method for deriving the stiffening effect on a uniform propeller element due to centrifugal forces. The paper also includes provision for the additional stiffening effect due to a blade tip mass.

Here the effect of centrifugal stiffening has been considered to warrant investigation for possible inclusion in the formulation of an accurate propeller element. It is assumed that for a heavy element or one rotating quickly the centrifugal stiffening effect has the potential to make significant changes to the ensuing bending mode shapes and frequencies. Furthermore, the full derivation has been included because discrepancies were found with results published by Hoa, S.V., [1979].

6.2 THEORY

6.2.1 Equations of Motion

Under rotation radial beam elements (propeller elements) are stiffened due to the stresses created by centrifugal forces. For a beam which lies parallel to the y-axis and rotates about the x-axis, the centrifugal forces create the stresses σ_x and τ_{xy} in the neutral surface. The following strain energy equation proved by Kapoor, K.K., and Hartz, B.J., [1966] shows that the strain energy stored in the element is higher than the bending strain energy by the amount:

$$\partial W_{cs} = \frac{1}{2}\int_v \left\{\sigma_x (\partial u/\partial x)^2 + 2\tau_{xy}(\partial u/\partial x)(\partial u/\partial y)\right\} dv \qquad (6.1)$$

In the case of slender beams, $\partial u/\partial y = 0$ thus the equation simplifies to:

$$\partial W_{cs} = \frac{1}{2}\int_v \left\{\sigma_x (\partial u/\partial x)^2\right\} dx dy dz \qquad (6.2)$$

6.2.2 Centrifugal Stiffening Propeller Element Derivation

The stress σ_x can be calculated as $\sigma_x = F_x/A$ where F_x is defined as the axial force acting on any section at a distance x from the inner edge of the element, and A is the area of element this force is applied to.

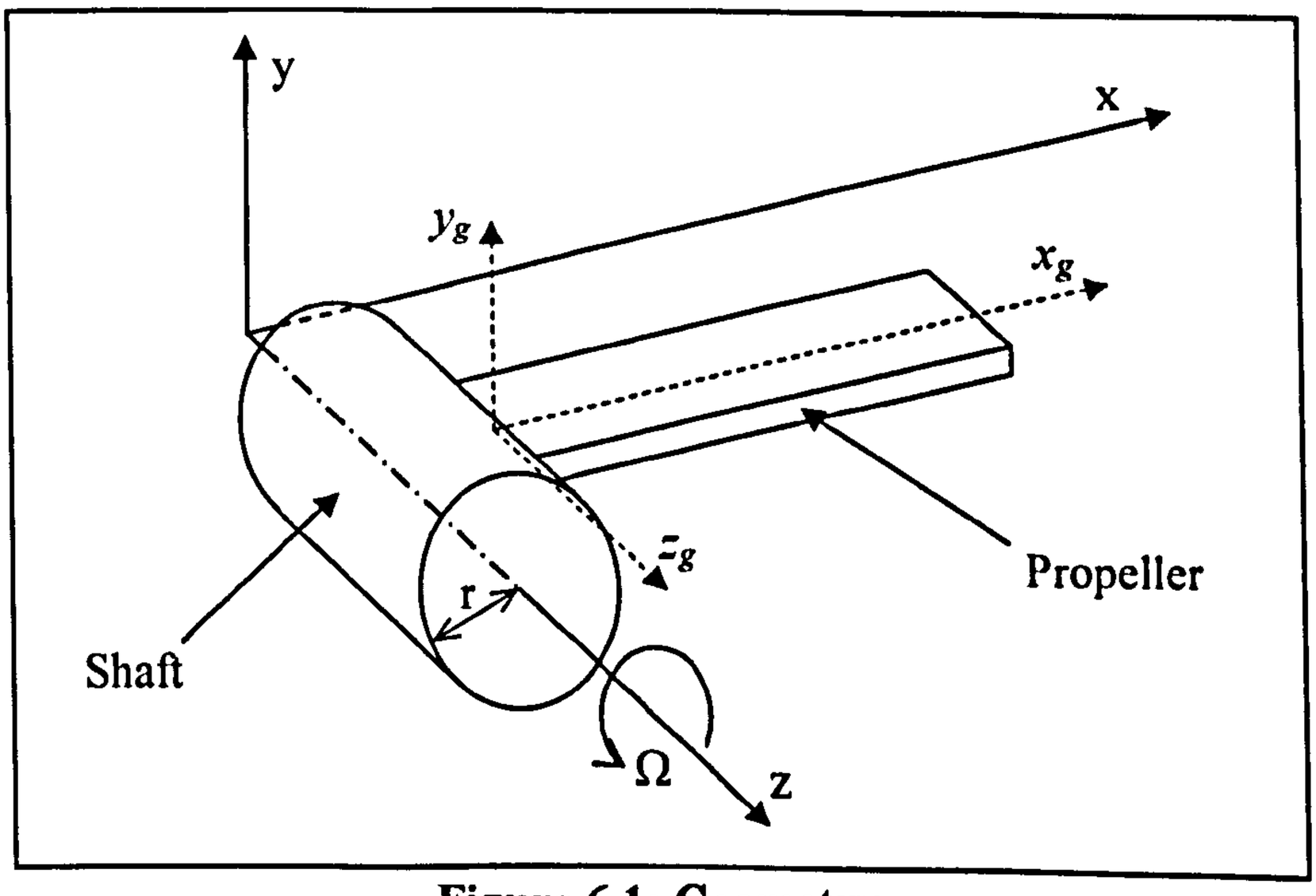

Figure 6.1: Geometry

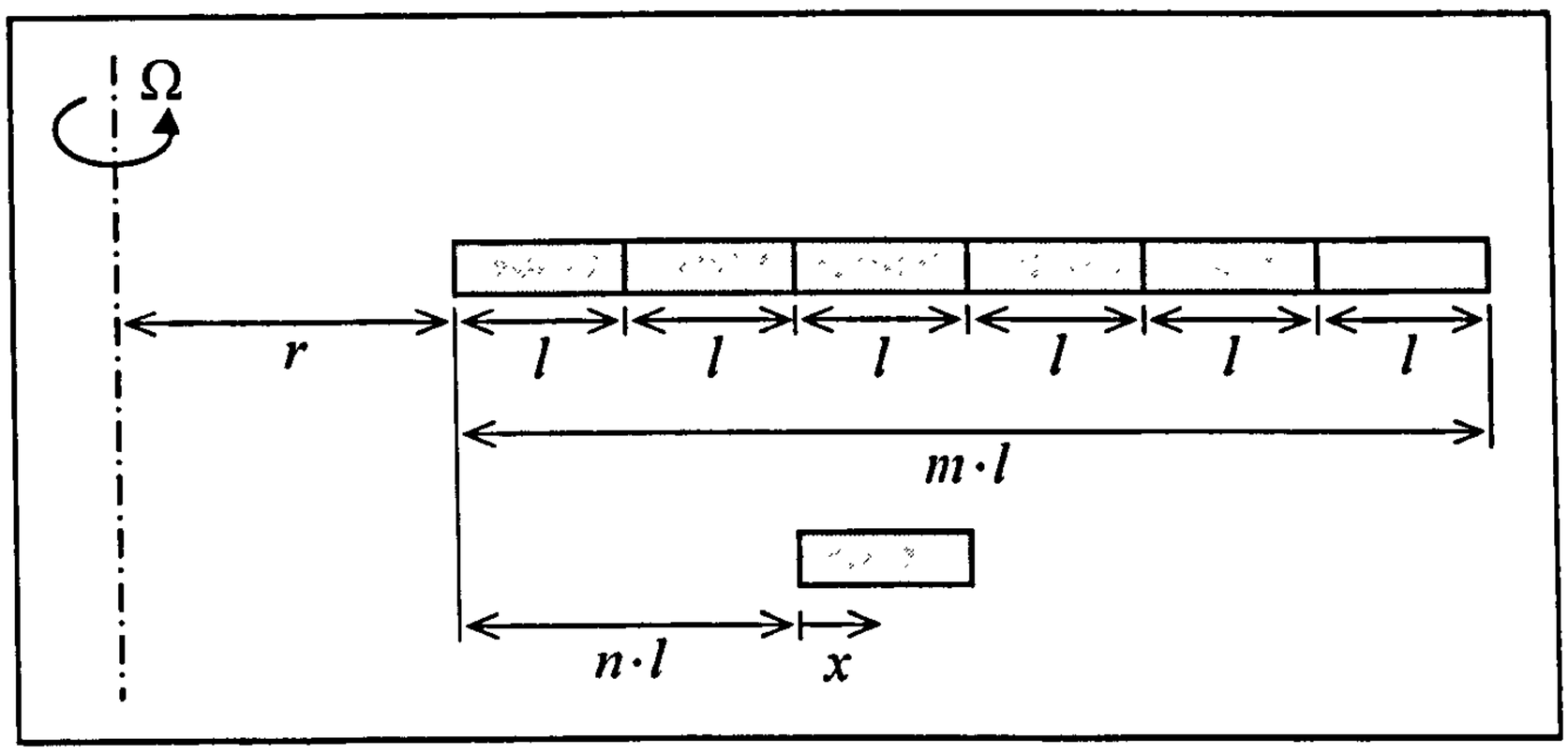

Figure 6.2: Element Location

Given the geometric definitions shown in Figures 6.1 and 6.2, where m is the total number of elements and n is number of elements before the element under consideration, it can be seen that the force acting on any section at the distance y from the element's end is:

$$F_x = A\int_x^l \rho\Omega^2(r+nl+x)dx + A\int_{(n+1)l}^{ml} \rho\Omega^2(r+x_g)dx_g \qquad (6.3)$$

Equation 6.3 can be solved to give the axial stress, σ_x as:

$$\sigma_x = {}^{F_x}\!/_{A} = -\frac{\rho\Omega^2(x^2+2x(l\,\mathrm{n}+r)-l(l(m^2-n^2)+2r(m-n)))}{2} \qquad (6.4)$$

As before in Chapters 4 and 5, the displacement u is approximated by a third order polynomial (As with Equations 4.4-4.8):

$$u = c_1 + c_2x + c_3x^2 + c_4x^3 \qquad (6.5)$$

Expressing this displacement in matrix form, where $\mathbf{V}(x)$ is the matrix of polynomial shape functions and $\mathbf{u}_e$ are the corresponding coordinate displacements expressed in matrix form, gives:

$$\mathbf{u}(x,t) = \mathbf{V}^T(x)\cdot\mathbf{u}_e(t) \qquad (6.6)$$

Using the standard bending shape functions h_1 to h_4 described in Chapter 5 gives:

$$h_1 = 1 - 3\varepsilon^2 + 2\varepsilon^3 \qquad \& \qquad h_2 = -l\left(\varepsilon - 2\varepsilon^2 + \varepsilon^3\right) \qquad (6.7)\ \&\ (6.8)$$

$$h_3 = \left(3\varepsilon^2 - 2\varepsilon^3\right) \qquad \& \qquad h_4 = -l\left(-\varepsilon^2 + \varepsilon^3\right) \qquad (6.9)\ \&\ (6.10)$$

Hence the matrix of shape functions for this geometry becomes:

$$\mathbf{V}^T = \begin{pmatrix} 0 & 0 & h_1 & 0 & h_2 & 0 & 0 & 0 & h_3 & 0 & h_4 & 0 \\ 0 & h_1 & 0 & 0 & 0 & -h_2 & 0 & h_3 & 0 & 0 & 0 & -h_4 \end{pmatrix} \qquad (6.11)$$

Where the displacements are defined as:

$$\mathbf{u}_e^T(t) = \begin{pmatrix} x_0 & y_0 & z_0 & \alpha_0 & \beta_0 & \gamma_0 & x_1 & y_1 & z_1 & \alpha_1 & \beta_1 & \gamma_1 \end{pmatrix} \qquad (6.12)$$

Now given that:

$$\partial W_{cs} = \frac{1}{2}\int_v \left\{\sigma_x \left(\partial u / \partial x\right)^2\right\} dx dy dz \qquad (6.13)$$

And:

$$\mathbf{u}'(x,t) = \mathbf{V}'^T(x) \cdot \mathbf{u}_e(t) \qquad (6.14)$$

Then it can be seen:

$$\partial \mathbf{W}_{e_{cs}} = \frac{1}{2}\mathbf{u}_e^T(t) \cdot \mathbf{K}_{e_{cs}} \cdot \mathbf{u}_e(t) \qquad (6.15)$$

Where:

$$\mathbf{K}_{e_{cs}} = \int_0^l \sigma_x \mathbf{V}'\mathbf{V}'^T dx dy dz \qquad (6.16)$$

Or:

$$\mathbf{K}_{e_{cs}} = A\int_0^l \sigma_x \mathbf{V}'\mathbf{V}'^T dx \qquad (6.17)$$

Thus the elemental centrifugal stiffness matrix $\mathbf{K}_{e_{cs}}$ becomes:

$$\mathbf{K}_{e_{cs}} = A\int_0^1 \begin{pmatrix} 0 & 0 & 0 & 0 & 0 & 0 & 0 & 0 & 0 & 0 & 0 & 0 \\ 0 & \sigma_x h_1' h_1' & 0 & 0 & 0 & -\sigma_x h_1' h_2' & 0 & \sigma_x h_1' h_3' & 0 & 0 & 0 & -\sigma_x h_1' h_4' \\ 0 & 0 & \sigma_x h_1' h_1' & 0 & \sigma_x h_1' h_2' & 0 & 0 & 0 & \sigma_x h_1' h_3' & 0 & \sigma_x h_1' h_4' & 0 \\ 0 & 0 & 0 & 0 & 0 & 0 & 0 & 0 & 0 & 0 & 0 & 0 \\ 0 & 0 & \sigma_x h_1' h_2' & 0 & \sigma_x h_2' h_2' & 0 & 0 & 0 & \sigma_x h_2' h_3' & 0 & \sigma_x h_2' h_4' & 0 \\ 0 & -\sigma_x h_1' h_2' & 0 & 0 & 0 & \sigma_x h_2' h_2' & 0 & -\sigma_x h_2' h_3' & 0 & 0 & 0 & \sigma_x h_2' h_4' \\ 0 & 0 & 0 & 0 & 0 & 0 & 0 & 0 & 0 & 0 & 0 & 0 \\ 0 & \sigma_x h_1' h_3' & 0 & 0 & 0 & -\sigma_x h_2' h_3' & 0 & \sigma_x h_3' h_3' & 0 & 0 & 0 & -\sigma_x h_3' h_4' \\ 0 & 0 & \sigma_x h_1' h_3' & 0 & \sigma_x h_2' h_3' & 0 & 0 & 0 & \sigma_x h_3' h_3' & 0 & \sigma_x h_3' h_4' & 0 \\ 0 & 0 & 0 & 0 & 0 & 0 & 0 & 0 & 0 & 0 & 0 & 0 \\ 0 & 0 & \sigma_x h_1' h_4' & 0 & \sigma_x h_2' h_4' & 0 & 0 & 0 & \sigma_x h_3' h_4' & 0 & \sigma_x h_4' h_4' & 0 \\ 0 & -\sigma_x h_1' h_4' & 0 & 0 & 0 & \sigma_x h_2' h_4' & 0 & -\sigma_x h_3' h_4' & 0 & 0 & 0 & \sigma_x h_4' h_4' \end{pmatrix} dx \tag{6.18}$$

Where σ_x has been previously defined in Equation 6.4.

Now using the previous differential definition shown in Chapter 5 and given as follows:

$$\frac{\partial h}{\partial x} = \frac{\partial h}{\partial \xi} \cdot \frac{1}{l} \tag{6.19}$$

The integrals are defined as:

$$\int_0^1 \sigma_x h_1' h_1' dx = \frac{\rho\Omega^2 3[l(7m^2 - 7n^2 - 7n - 2) + 7r(2m - 2n - 1)]}{35} \tag{6.20}$$

$$\int_0^1 \sigma_x h_1' h_2' dx = -\frac{\rho\Omega^2 l[l(7m^2 - 7n^2 - 14n - 5) + 14r(m - n - 1)]}{140} \tag{6.21}$$

$$\int_0^1 \sigma_x h_1' h_3' dx = -\frac{\rho\Omega^2 3[l(7m^2 - 7n^2 - 7n - 2) + 7r(2m - 2n - 1)]}{35} \tag{6.22}$$

$$\int_0^1 \sigma_x h_1' h_4' dx = -\frac{\rho\Omega^2 l[l(7m^2 - 7n^2 + 2) + 14r(m - n)]}{140} \tag{6.23}$$

$$\int_0^1 \sigma_x h_2' h_2' dx = \frac{\rho\Omega^2 l^2[l(14m^2 - 14n^2 - 7n - 2) + 7r(4m - 4n - 1)]}{210} \tag{6.24}$$

$$\int_0^1 \sigma_x h_2' h_3' dx = \frac{\rho\Omega^2 l[l(7m^2 - 7n^2 - 14n - 5) + 14r(m - n - 1)]}{140} \tag{6.25}$$

$$\int_0^1 \sigma_x h_2' h_4' dx = -\frac{\rho\Omega^2 l^2 [l(7m^2 - 7n^2 - 7n - 3) + 7r(2m - 2n - 1)]}{420} \tag{6.26}$$

$$\int_0^1 \sigma_x h_3' h_3' dx = \frac{\rho\Omega^2 3[l(7\mathrm{m}^2 - 7n^2 - 7n - 2) + 7r(2m - 2n - 1)]}{35} \tag{6.27}$$

$$\int_0^1 \sigma_x h_3' h_4' dx = \frac{\rho\Omega^2 l[l(7m^2 - 7n^2 + 2) + 14r(m - n)]}{140} \tag{6.28}$$

$$\int_0^1 \sigma_x h_4' h_4' dx = \frac{\rho\Omega^2 l^2 [l(14m^2 - 14n^2 - 21n - 9) + 7r(4m - 4n - 3)]}{210} \tag{6.29}$$

6.2.3 Centrifugal Stiffening Propeller Element Matrix

The centrifugal stiffening matrix for a rotating propeller can more simply be described in matrix form as:

$$\mathbf{K}_{e_{cs}} = \mu l\Omega^2 \begin{bmatrix} 0 & 0 & 0 & 0 & 0 & 0 & 0 & 0 & 0 & 0 & 0 & 0 \\ 0 & A & 0 & 0 & 0 & -D & 0 & -A & 0 & 0 & 0 & -E \\ 0 & 0 & A & 0 & D & 0 & 0 & 0 & -A & 0 & E & 0 \\ 0 & 0 & 0 & 0 & 0 & 0 & 0 & 0 & 0 & 0 & 0 & 0 \\ 0 & 0 & D & 0 & B & 0 & 0 & 0 & -D & 0 & F & 0 \\ 0 & -D & 0 & 0 & 0 & B & 0 & D & 0 & 0 & 0 & F \\ 0 & 0 & 0 & 0 & 0 & 0 & 0 & 0 & 0 & 0 & 0 & 0 \\ 0 & -A & 0 & 0 & 0 & D & 0 & A & 0 & 0 & 0 & E \\ 0 & 0 & -A & 0 & -D & 0 & 0 & 0 & A & 0 & -E & 0 \\ 0 & 0 & 0 & 0 & 0 & 0 & 0 & 0 & 0 & 0 & 0 & 0 \\ 0 & 0 & E & 0 & F & 0 & 0 & 0 & -E & 0 & C & 0 \\ 0 & -E & 0 & 0 & 0 & F & 0 & E & 0 & 0 & 0 & C \end{bmatrix} \tag{6.30}$$

Where:

$$A = \frac{3[l(7\mathrm{m}^2 - 7n^2 - 7n - 2) + 7r(2m - 2n - 1)]}{35}$$

$$B = \frac{l^2[l(14m^2 - 14n^2 - 7n - 2) + 7r(4m - 4n - 1)]}{210}$$

$$C = \frac{l^2[l(14m^2 - 14n^2 - 21n - 9) + 7r(4m - 4n - 3)]}{210}$$

$$D = -\frac{l[l(7m^2 - 7n^2 - 14n - 5) + 14r(m - n - 1)]}{140}$$

$$E = -\frac{l[l(7m^2 - 7n^2 + 2) + 14r(m - n)]}{140}$$

$$F = -\frac{l^2[l(7m^2 - 7n^2 - 7n - 3) + 7r(2m - 2n - 1)]}{420}$$

6.3 SUMMARY

The mathematical formulation of an Euler-Bernoulli finite element, that can be used to model the centrifugal stiffening effects of a rotating propeller beam, has been achieved. The resulting matrix does not differ greatly from that published by Hoa, S.V., [1979]. However, most of the terms within the matrix have at least one or two signs that have been published as negative instead of positive and vice versa. These differences are caused by a minor publishing/integration error within the original work whereby *d* in Table 1 should have been expressed as *d* = - (R'+ n). It should also be noted that this stiffness matrix is in addition to the standard Euler-Bernoulli bending, axial and torsional stiffness matrices and does not replace them. This is obviously so since the matrix is dependant on omega squared, and thus without propeller rotation all terms will equal zero.The standard Euler beam stiffness matrices are given in Appendix A, but have not been derived since they are widely published.

Handelman, G., Boyce, W., and Cohen, H., [1958] and also Kumar, R., [1974] have investigated the centrifugal stiffening effect. Concluding that the increase in natural frequencies caused by the increase in stiffness is most significant for the first mode of vibration. An investigation into this claim with published results has been included in Chapter 9.

CHAPTER 7

RESULTS 1: GYROSCOPIC SHAFT ELEMENT

7.1 INTRODUCTION

The Euler beam derivation in Chapter 4 describes the gyroscopic effect of an element bending away from its axis of rotation. Assuming a shaft to lie along the x-axis and be excited in the vertical y-plane (either through y or Gamma) without rotation one would expect to see displacements in this vertical plane only. Even if rotation is included in the model this will still be the case, unless the gyroscopic effects have also been accounted for. Only when the gyroscopic effects are included will the displacements in the vertical plane become coupled with the horizontal plane and induce vibrations in this direction also. This coupling effect also changes the natural frequencies system, thus where the determination of the exact natural frequency is critical it is vital that gyroscopic effects are included.

In order to verify the computer shaft modelling procedure including gyroscopic results, analyses have been performed on a large ship drive shaft simulation. This system was chosen because of a working collaboration with Lloyd's Register of Shipping during which VIBRATIO was verified against results produced by ANSYS 5.1 and Lloyd's experimental data. Since the ANSYS results have been validated a direct comparison between these and VIBRATIO results is possible.

The ship drive shaft is a highly complex model which makes differences in results immediately apparent. For shaft element validation an analysis has been performed omitting the possible disc or propeller attachments. This method is chosen in order to ensure that the relatively small gyroscopic effects of the shaft

elements are not disguised by the large gyroscopic forces associated with such an attachment. This has also been done because of difficulties modelling such a system in ANSYS 5.1. Since ANSYS does not use the hybrid rigid body modelling technique employed here (Chapter 3), a rotational point inertia cannot be simply attached to the free end. Instead a very wide beam element of the same inertia has to be used which in turn creates an ill-conditioned stiffness matrix. For the same reason the axial displacement spring has not been offset from the shaft but is instead treated as being at the node.

7.2 LLOYD'S SHIP DRIVE SHAFT

A model of a ship's drive shaft has been created in both ANSYS and Vibratio; the shaft is 48.01 metres long and manufactured from steel of density 7800 kg/m^3, Young's Modulus 2.07 x 10^{11} N/m^2, and a Poisson's ratio of 0.3. The initial 32.5 metres of shaft connected to the engine is 0.47 metres in diameter, the centre 14.8 metre section is 0.55 metres in diameter with a 0.15 metre diameter hollow centre, and the final 0.71 metres of shaft that would normally be connected to the propeller has a diameter of 1 metre. There are nine support positions along its length, but the propeller end is unsupported and free. The shaft itself rotates at a frequency of 40 Hz. At the opposite end of the shaft to the free end there is a simulated engine. The engine is made from ten rotational inertias, each connected with torsion springs, where the final (tenth) inertia is attached to the shaft. Six of the inertias (numbered four through to nine) are harmonically excited with real forces proportional to omega, where omega is the engine frequency. The harmonic excitation is torsional acting along the axis of the shaft. The propeller attachment point is also harmonically excited at a frequency proportional to omega squared in the vertical plane. Figure 7.1 below shows this in more detail.

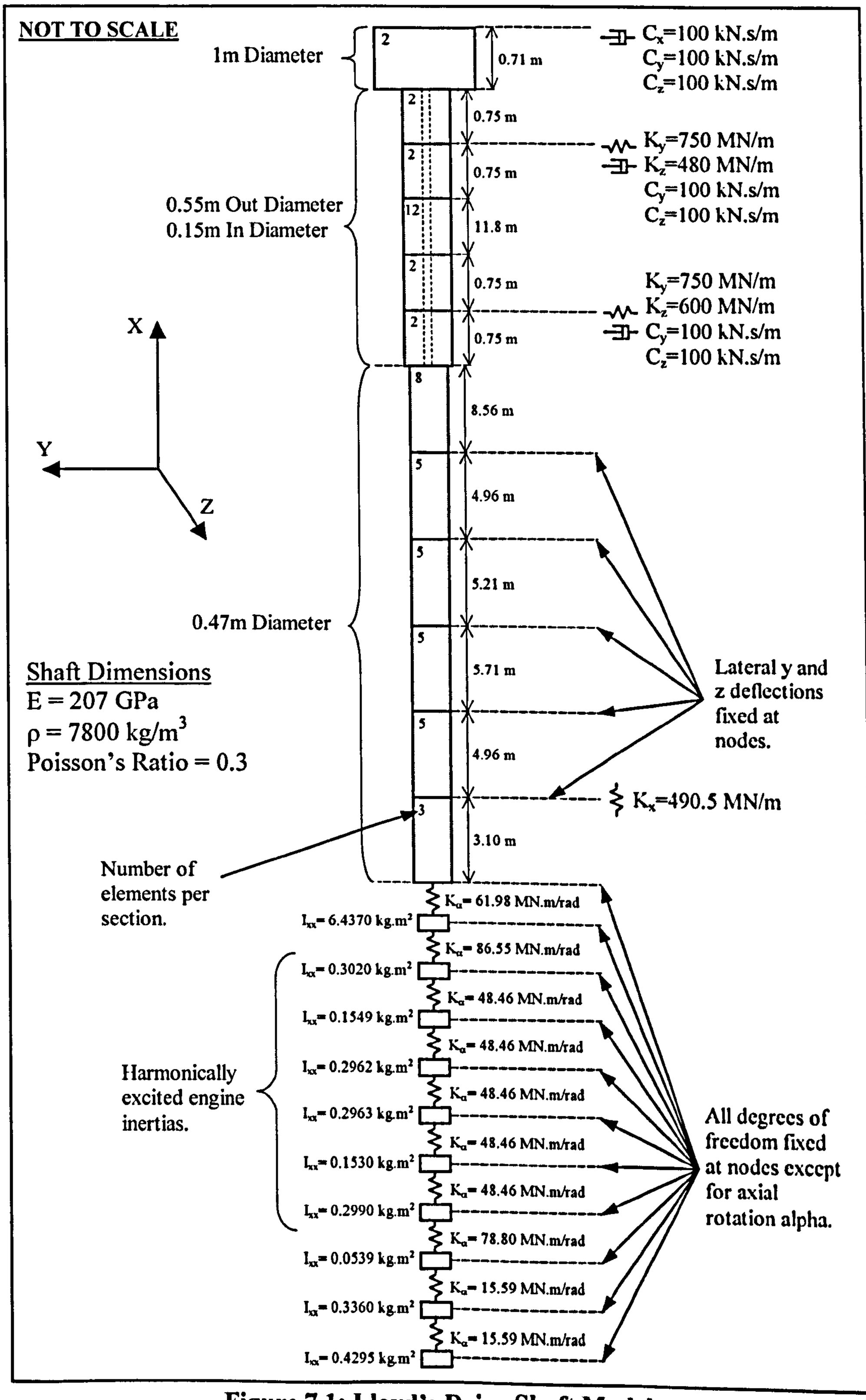

Figure 7.1: Lloyd's Drive Shaft Model

7.3 BEAM ELEMENT RESULTS

The following results compare an ANSYS model against a geometrically identical one developed in VIBRATIO using the gyroscopic beam element formulation derived in Chapter 4. ANSYS has of course been extensively verified by other means, so is a recognised method to verify elements. Unlike the Euler beam elements developed for this study ANSYS uses Timoshenko beam theory and its own gyroscopic matrix that is presented in Chapter 4. Unfortunately, no reference as to how this gyroscopic matrix is derived is given in the ANSYS theory manual and despite an extensive literature review its source has not been found. However, as it has been extensively tested and verified including an experimental model for this particular problem it is assumed that the ANSYS results are correct.

For this type of model VIBRATIO is capable of producing many different results including displacement, velocity, acceleration, stress and eigenvalue. Eigenvalues have not been compared for this model because the forced vibration results are superior, checking both the natural response frequencies and mode shapes simultaneously. The displacement values are published since these are the simplest to interpret. Stress results have not been compared since they rely on further mathematic calculations that may differ from those used by ANSYS.

VIBRATIO produces displacement results for each degree of freedom at each shaft node. The Lloyd's shaft has nineteen nodes giving one hundred and fourteen different sets of results to compare with the ANSYS model. Results correlate with those produced by ANSYS so it is pointless publishing all the available graphs. Thus, only the six degrees of freedom belonging to the free (unsupported) propeller end are shown in Figures 7.1 to 7.6. However it can be taken as read that results at other shaft positions have equally good or better correlation with ANSYS than those of the free end.

It can be seen that correlation between results is almost perfect with those produced by ANSYS. However, for lateral deflections there is a slight frequency shift in response of approximately 0.5Hz towards the upper end of the frequency

analysis. This shift increases with frequency and is a known phenomenon that exists between Euler and Timoshenko modelling techniques. Davis, R., et al., [1972] previously noted the tendency for Euler theory to overestimate vibration frequency increases with the ratio of beam depth to the wavelength of vibration.

Displacements for both models can be seen to be of the same magnitude. Furthermore the reader should note the small blips in the graphs around 36 Hz (vertical) and 44 Hz (horizontal). This small detail is of interest because entirely different modelling techniques reproduce the same minor disturbances on a complex system.

Figures 7.2 and 7.6 are very similar as are those of 7.3 and 7.5. This is due to the direct relationship between the vertical deflection and corresponding Gamma rotation, and the same relationship that exists for the horizontal deflection with Beta. However despite only the gyroscopic effect coupling the vertical and horizontal responses, the two graphs are not of the same shape as may be expected.

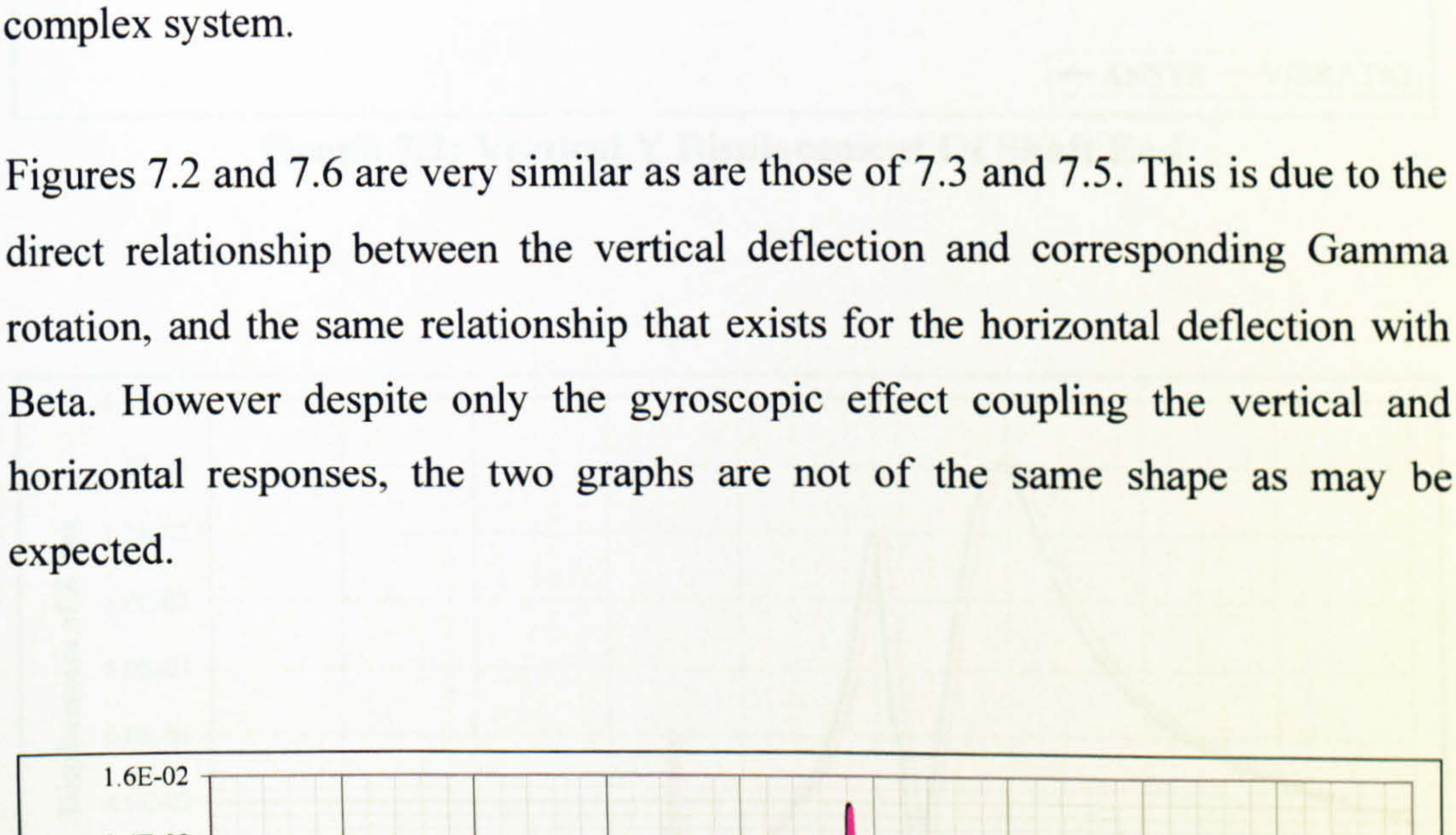

Graph 7.1: Axial X Displacement Of Shaft End

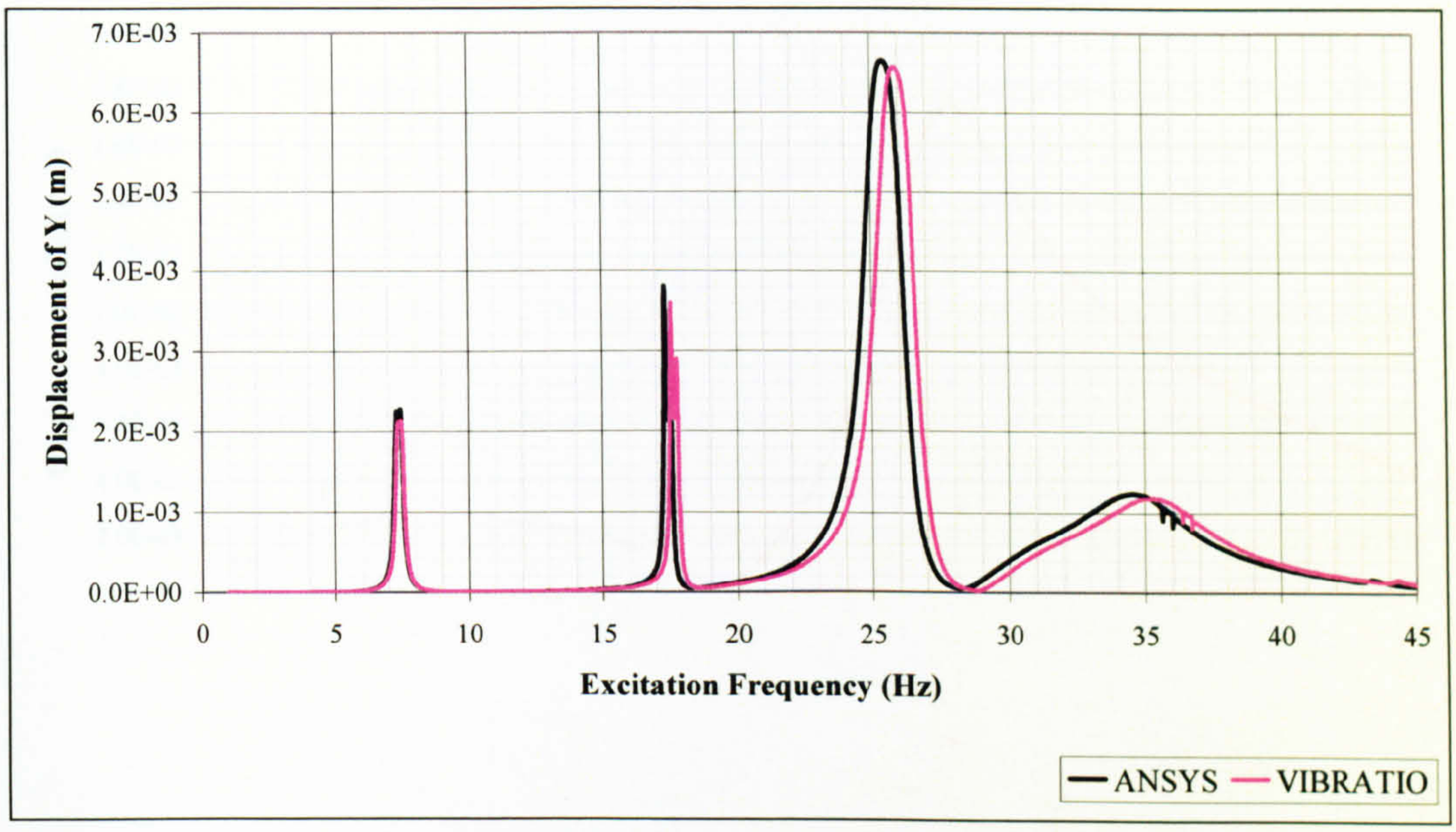

Graph 7.2: Vertical Y Displacement Of Shaft End

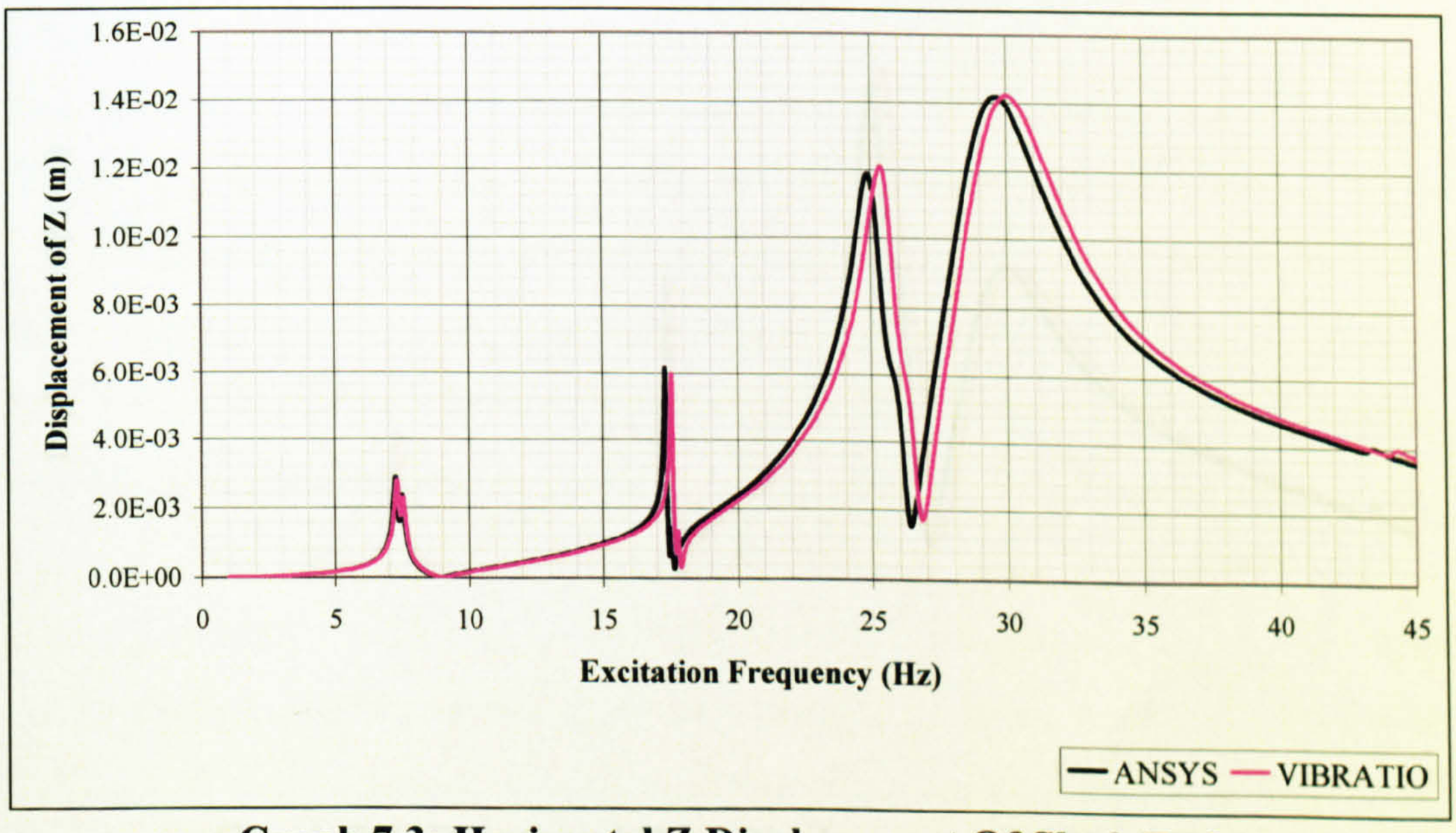

Graph 7.3: Horizontal Z Displacement Of Shaft End

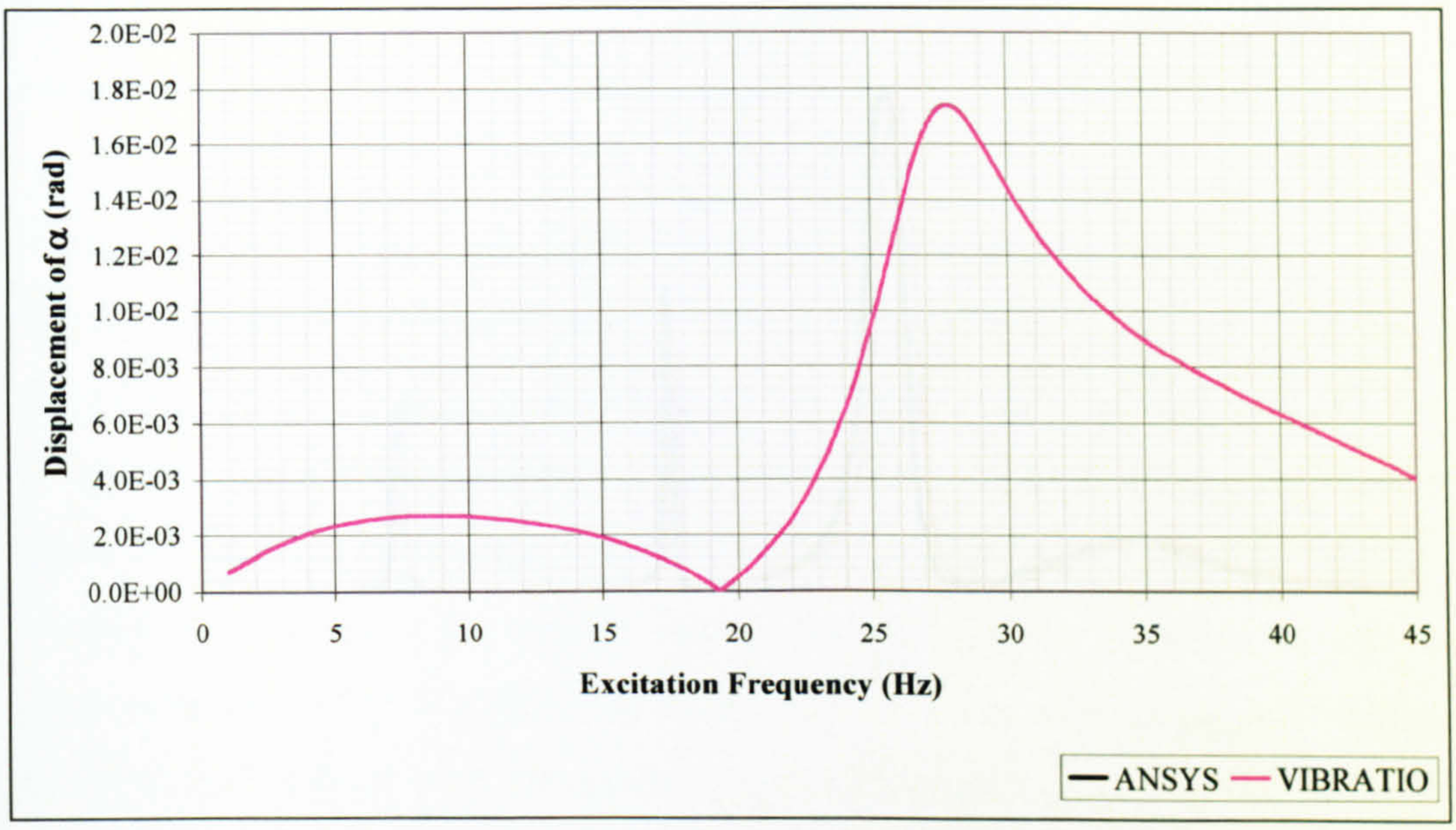

Graph 7.4: Rotational Alpha Displacement Of Shaft End

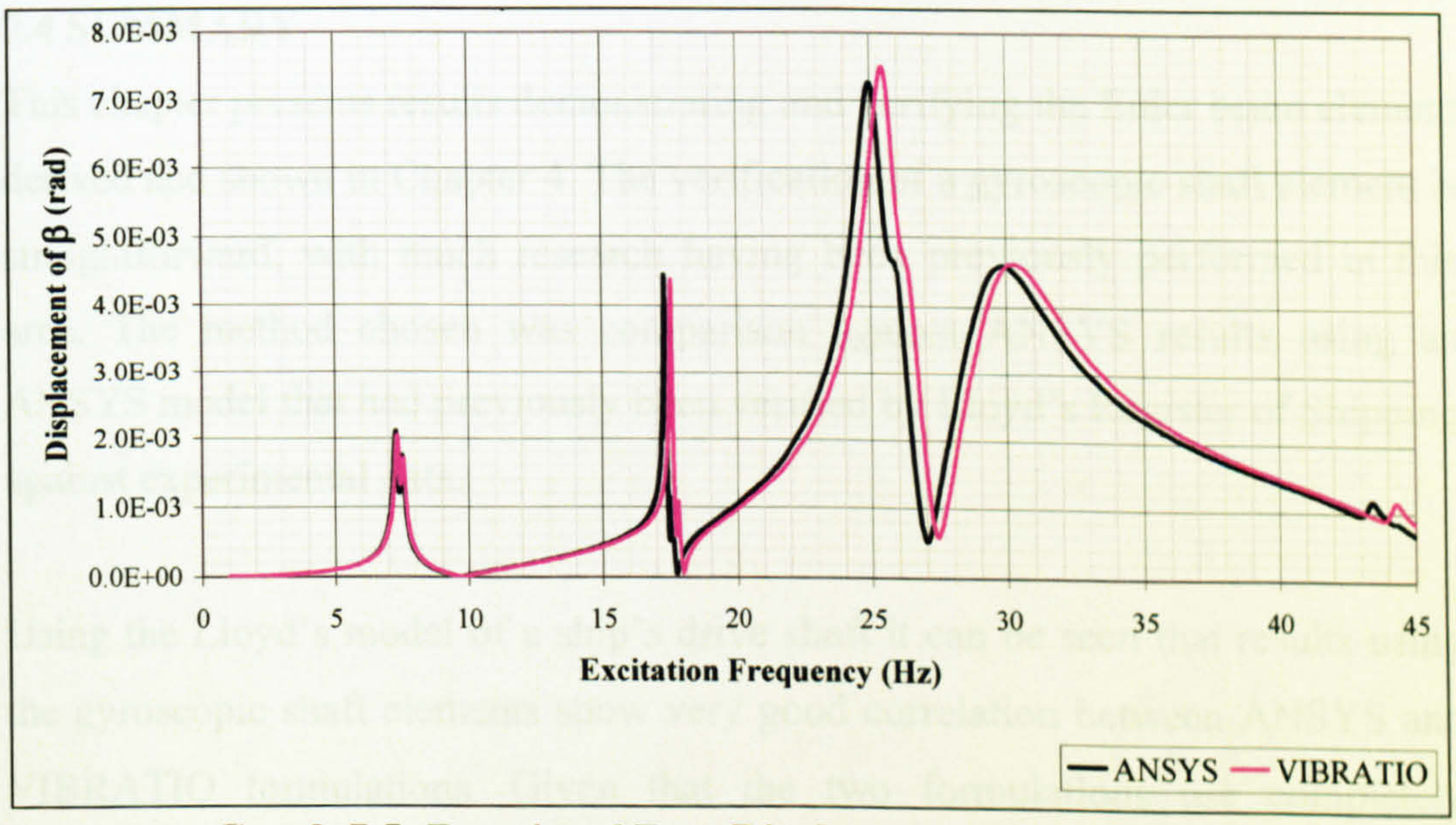

Graph 7.5: Rotational Beta Displacement Of Shaft End

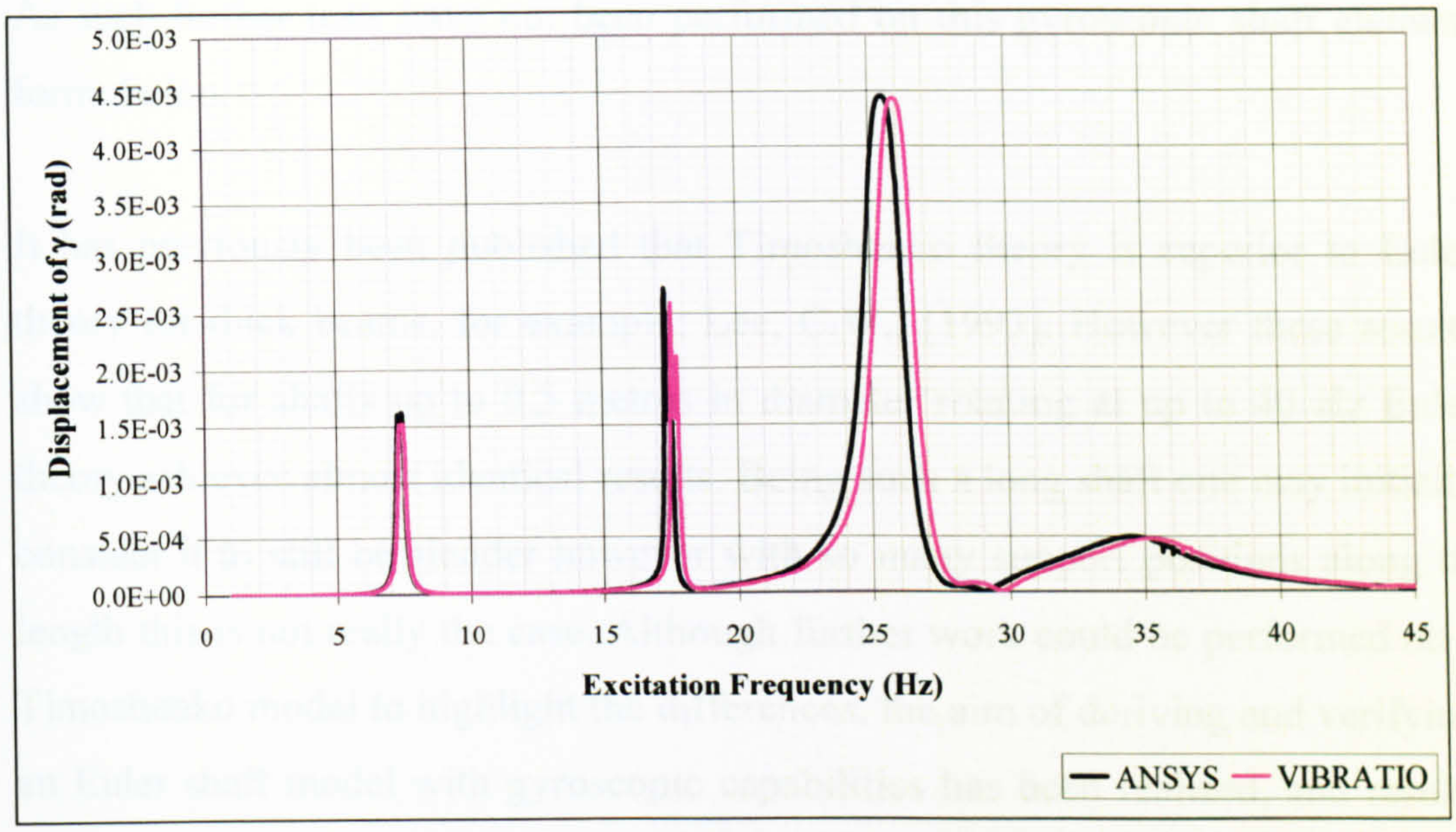

Graph 7.6: Rotational Gamma Displacement Of Shaft End

7.4 SUMMARY

This chapter presents results demonstrating and verifying the Euler beam element derived and shown in Chapter 4. The verification of a gyroscopic shaft element is straightforward, with much research having been previously performed in this area. The method chosen was comparison against ANSYS results using an ANSYS model that had previously been verified by Lloyd's Register of Shipping against experimental data.

Using the Lloyd's model of a ship's drive shaft it can be seen that results using the gyroscopic shaft elements show very good correlation between ANSYS and VIBRATIO formulations. Given that the two formulations use completely different theory (ANSYS uses Timoshenko and VIBRATIO uses Euler) and solvers, these results are exceptional. This particular drive shaft has been chosen as a reliable benchmark, because the problem's complexity immediately highlights differences, and also previous corroboration with Lloyd's Register of Shipping has verified results. Since the ANSYS simulation has been verified by Lloyd's Register of Shipping against a full model it is reliable to conclude that the VIBRATIO gyroscopic shaft formulations and computer coding are correct.

As such further tests have not been performed on this gyroscopic shaft element formulation.

It has previously been published that Timoshenko theory is superior to Euler theory for thick beams, for example; Lee, C.W., [1993]. However these results show that for shafts up to 0.5 metres in diameter rotating at up to 40 Hz Euler theory achieves almost identical results. Being such a long shaft one may initially consider it to still be slender however with so many support positions along its length this is not really the case. Although further work could be performed on a Timoshenko model to highlight the differences, the aim of deriving and verifying an Euler shaft model with gyroscopic capabilities has been realised, and results are considered accurate.

CHAPTER 8

RESULTS 2: GYROSCOPIC PROPELLER ELEMENT

8.1 INTRODUCTION

This chapter presents results of the verification of the gyroscopic element formulations. Perhaps the most obvious method of verification for a propeller element is comparison to experimental results. Unfortunately this can also be the most problematic technique. The main difficulty of using an experiment for verification is experimental error which can never be fully eliminated. Even assuming this error could be reduced to less than five percent, its effect may still be greater than the gyroscopic effects. Thus, at best experimental methods could be used to verify trends. Thus experimental results have not been used and a computational technique is employed. Eigenvalue and forced frequency results have been compared against theoretical values for simple cantilevers and then a parametric study has been performed.

8.2 EIGENVALUE RESULTS

Results have been obtained for simple cantilever beams since the natural frequencies are widely available. The beams have then been treated as rotating about an axis perpendicular to their axis of symmetry as in propellers for comparison. Using Euler beam theory Thomson, W.T., [1993] shows the first three modes of vibration can be calculated as follows:

$$\omega_n = \pm(\beta_n l)^2 \sqrt{\frac{EI}{\mu l^4}} \tag{8.1}$$

Where for a cantilever beam the following coefficients are given:

Fundamental	$(\beta_1 l)^2 = 3.52$
Second Mode	$(\beta_2 l)^2 = 22.0$
Third Mode	$(\beta_3 l)^2 = 61.7$

Figure 8.1 below depicts a typical rectangular cross-section of a beam element so that I_y and I_z can be calculated. For a beam of differing width and thickness the natural frequencies will not be the same in each direction as I_y and I_z will be distinct.

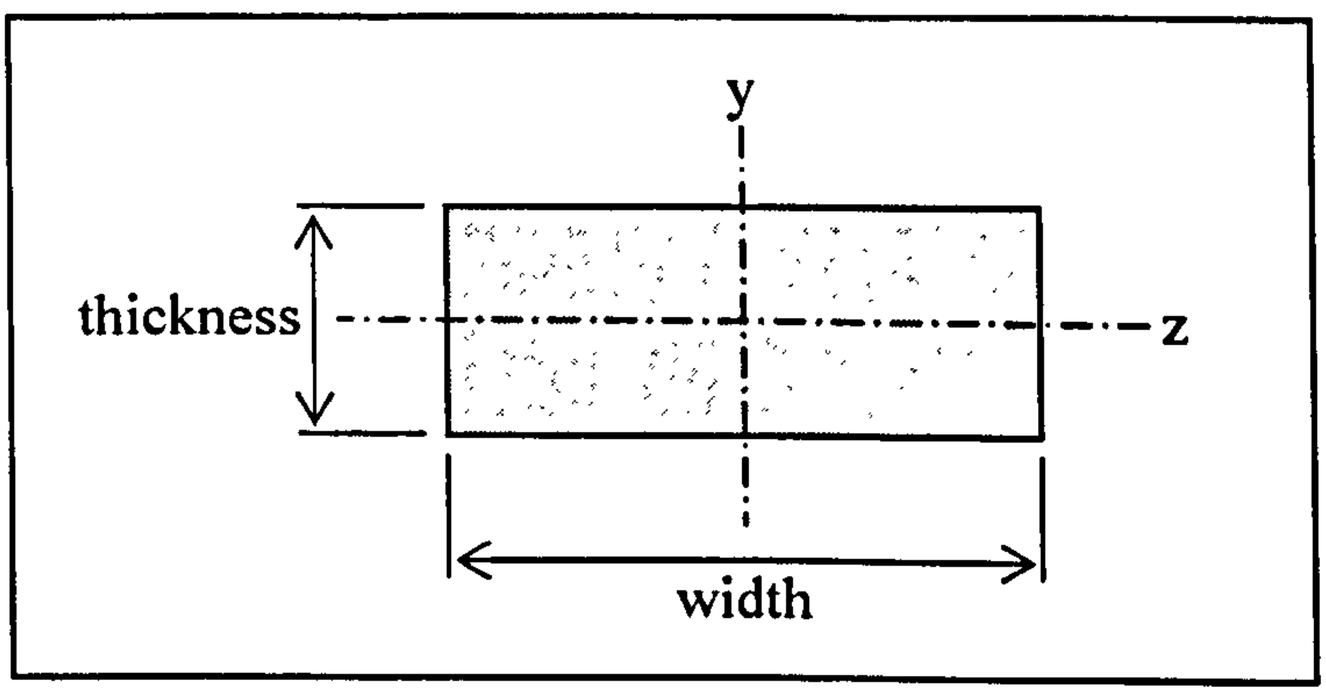

Figure 8.1: Rectangular Cross-Section of a Beam Element

$$I_y = \frac{width^3 \times thickness}{12} \tag{8.2}$$

$$I_z = \frac{width \times thickness^3}{12} \tag{8.3}$$

Since the mass per unit length increases linearly with the width and thickness in Equation 8.1 the natural frequency about I_y is independent of the beam thickness, and the natural frequency about I_z is independent of the beam width. This is only true for a beam of rectangular cross-section. Thus the following values given in Table 8.1 are for various beam thicknesses only. This of course is not true when gyroscopic coupling is considered since the natural frequencies about I_y and I_z become coupled. For simplicity each beam is divided into three elements of

equal length. The total length is maintained at one metre in all cases, and the slenderness ratio is given since this is the ultimate determinate of the natural frequency. The propeller is fixed at the root as in the case of a cantilever. The material is steel where Young's Modulus = 207 GPa, Poisson's Ratio = 0.3, and Density = 7800 kg/m^3. Natural frequencies are given in radians per second. One can see that with error values of just 1.24 % for the third natural frequency of vibration there is little point in increasing the number of finite elements further for this type of test.

Thick -ness (m)	Slender -ness Ratio	Exact ω_1	Exact ω_2	Exact ω_3	PC ω_1	PC ω_2	PC ω_3	Err. % ω_1	Err. % ω_2	Err. % ω_3
0.01	100	52.3	327	918	52.3	329	929	0.10	0.49	1.24
0.02	50	105	654	1835	105	658	1858	0.10	0.49	1.24
0.04	25	209	1309	3670	209	1315	3716	0.10	0.49	1.24
0.10	10	523	3271	9175	523	3287	9289	0.10	0.49	1.24

Table 8.1: Eigenfrequencies for Standard Euler Beams

Not surprisingly the inclusion of gyroscopic effects (assuming there is a propeller rotation speed) complicates the eigenfrequencies somewhat. Due to coupling in the damping matrix the width and thickness are now not independent of each other for eigenfrequencies in each axis of symmetry. Thus the width and thickness must be considered together. In order not to complicate the problem unnecessarily initial results are for systems where the thickness and width of the beams are the same.

Table 8.2 (below) shows the effect of adding a propeller rotation speed to the eigenfrequencies of two simple propeller beams. Where propeller rotation speed is included the first six natural frequencies have been provided. The reason for this is the tendency for the gyroscopic effect to 'split' the natural frequencies. This is a normal gyroscopic phenomenon that results clearly show in Table 8.2. For example the first natural frequency of the 0.01 x 0.01m propeller is 52.3 rad/s. Once the propeller speed is set to 250 rpm this eigenfrequency splits into

two eigenfrequencies either side of the original, 45.4 rad/s and 59.0 rad/s. This trend continues throughout results and can be seen to be true for the second and third eigenfrequencies also. Another point the reader should note is that as the beam becomes thicker (and therefore stiffer) the splitting of eigenfrequencies becomes less pronounced despite the associated increase in inertia. This can be stated since although the numerical difference is similar the eigenfrequencies are higher so the percentage change is smaller.

Thickness (m)	Width (m)	Speed (rpm)	PC ω_1	PC ω_2	PC ω_3	PC ω_4	PC ω_5	PC ω_6
0.01	0.01	0	52.3	329	929			
0.01	0.01	250	45.4	59.0	253	400	655	1116
0.01	0.01	500	39.0	65.2	194	462	484	1134
0.02	0.02	0	105	658	1858			
0.02	0.02	250	97.7	111	581	731	1584	2070
0.02	0.02	500	90.9	118	507	800	1311	2231
0.04	0.04	0	209	1315	3716			
0.04	0.04	250	202	216	1239	1390	3454	3944
0.04	0.04	500	195	223	1162	1462	3168	4139
0.10	0.10	0	523	3287	9289			
0.10	0.10	250	516	530	3212	3363	9037	9528
0.10	0.10	500	509	537	3135	3438	8772	9752

Table 8.2: Eigenfrequencies for Square Gyroscopic Euler Propeller

The interaction and 'splitting' of natural eigenfrequencies due to gyroscopic coupling is however much harder predict intuitively for systems where the width and thickness of the propeller element are not the same. This is due to interaction with two sets of eigenfrequencies which differ in I_y and I_z. Table 8.3 shows results for such a system.

The first three eigenfrequencies in I_y (for a 0.1m thick beam) will in fact be 523, 3287 and 9289 rad/s respectively as shown in Table 8.1, however these do not necessarily appear as the higher order eigenfrequencies in Table 8.3 since the

fourth natural mode in I_z is often achieved first. The 'splitting' of eigenfrequencies is no longer seen as was the case in the square propeller blades; instead the eigenfrequencies tend to shift to a higher or lower value. Results show this shift to be intuitively unpredictable, so it is vital as analysis such as this is performed. As before as the beam thickness and stiffness increase the change in eigenfrequencies tends to become less pronounced.

Thickness (m)	Width (m)	Speed (rpm)	PC ω_1	PC ω_2	PC ω_3	PC ω_4	PC ω_5	PC ω_6
0.01	0.10	0	52.3	329	523	929	2092	3288
0.01	0.10	500	52.2	321	528	919	1976	3134
0.01	0.10	1000	51.9	300	541	889	1735	2934
0.01	0.10	1500	51.5	274	554	849	1535	2803
0.02	0.10	0	105	523	658	1858	3288	4184
0.02	0.10	500	104	512	667	1821	3241	4089
0.02	0.10	1000	104	487	688	1717	3098	3933
0.02	0.10	1500	103	456	73	1577	2916	3856
0.04	0.10	0	209	523	1315	3288	3716	8368
0.04	0.10	500	209	522	1309	3210	3767	7767
0.04	0.10	1000	207	520	1293	3038	3867	6882
0.04	0.10	1500	205	517	1266	2837	3967	6154

Table 8.3: Gyroscopic Eigenfrequencies for Rectangular Euler Propeller

Furthermore since the width and thickness of the beam are no longer independent of one another it is not easy to tabulate results according to the slenderness ratio as is the case for centrifugal stiffening (Chapter 9, Table 9.2). This is clearly demonstrated below in Table 8.4 where a steel cantilever blade of the same thickness but differing width shows different eigenvalues for the first three modes of vibration about I_z. For a stationary propeller these three modes of vibration are associated only with the thickness of the blade. It can be seen that

the thinner the width the greater the effect becomes as the blade becomes more flexible and natural frequencies in both axis become closer together.

Thickness (m)	Width (m)	Speed (rpm)	PC ω_1	PC ω_2	PC ω_3
0.01	0.075	0	52.3	329	929
0.01	0.075	500	52.1	308	903
0.01	0.075	1000	51.6	273	833
0.01	0.075	1500	50.8	239	748
0.01	0.100	0	52.3	329	929
0.01	0.100	500	52.2	321	919
0.01	0.100	1000	51.9	300	889
0.01	0.100	1500	51.5	274	849
0.01	0.125	0	52.3	329	929
0.01	0.125	500	52.2	324	927
0.01	0.125	1000	52.0	311	923
0.01	0.125	1500	51.8	293	918

Table 8.4: Gyroscopic Eigenfrequencies for Rectangular Euler Propeller of Varying Width

8.3 FORCED FREQUENCY RESULTS

The eigenvalue results given in Section 8.2 are adequate for the understanding of gyroscopic coupling, however it is considered beneficial to demonstrate effects graphically as well. For this purpose forced frequency results for various models have been produced. Initial results (Graphs 8.1-8.4) have been formed to simultaneously display the gyroscopic coupling and 'splitting' phenomenon. As such a square section propeller blade has been used with a slenderness ratio (S.R.) of 50. Specifically it is one metre long and two centimetres thick (for both width and thickness). A nominal force and moment has been applied to Y and γ at the tip node. No damping has been included and as such amplitude (especially peak amplitudes at resonant frequencies) should be ignored. This propeller model

has been run at various speeds including the analysis of a stationary propeller. Results for the first mode of vibration which is shown to split into two natural frequencies as the propeller rotates are displayed below (Graphs 8.1-8.4). X and α results are not shown since they are zero. In addition to the splitting which can be clearly seen, gyroscopic coupling is displayed. This shows as the lack of response in the Z and β axis when the propeller is not rotating.

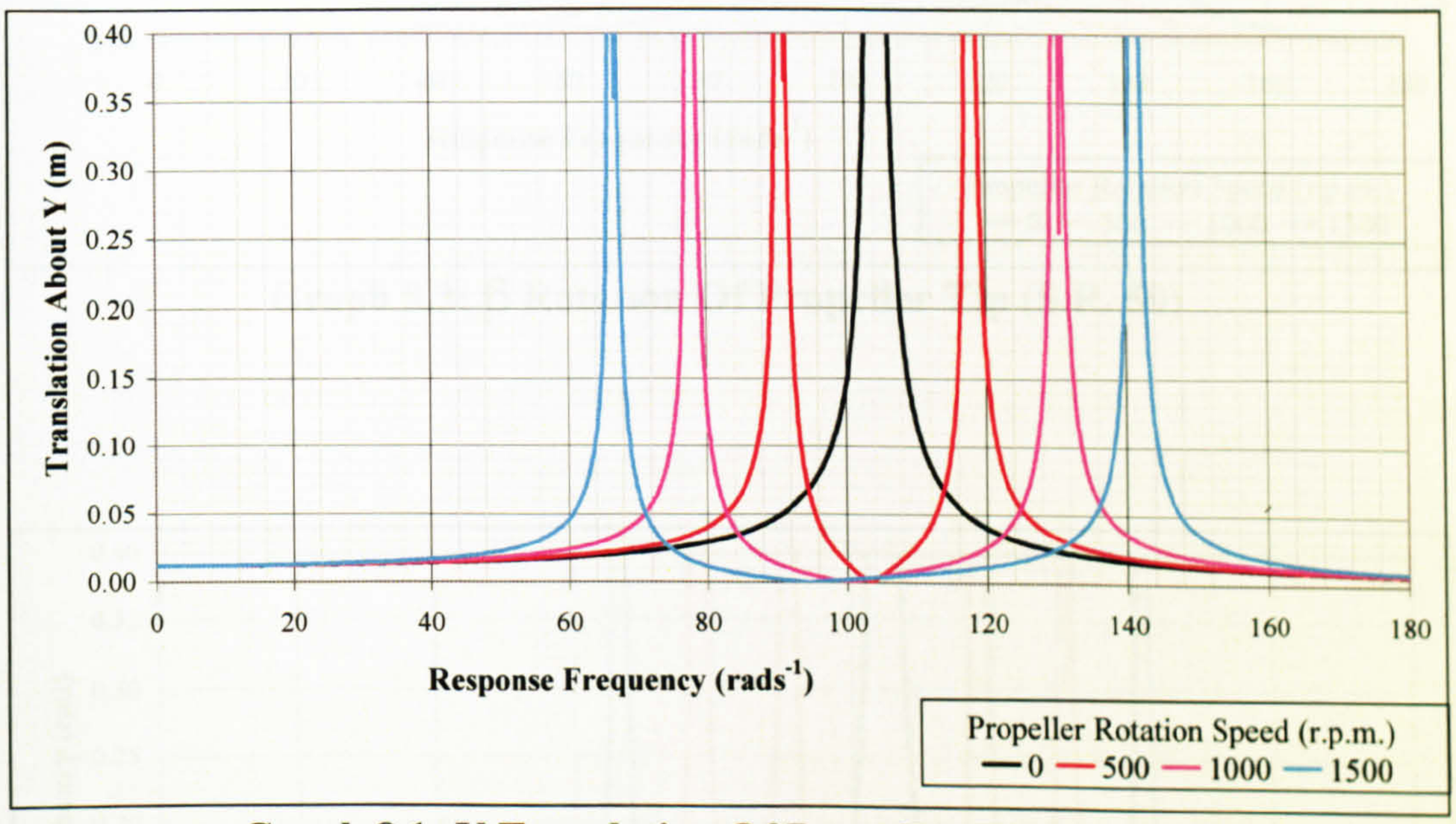

Graph 8.1: Y Translation Of Propeller Tip (S.R. 50)

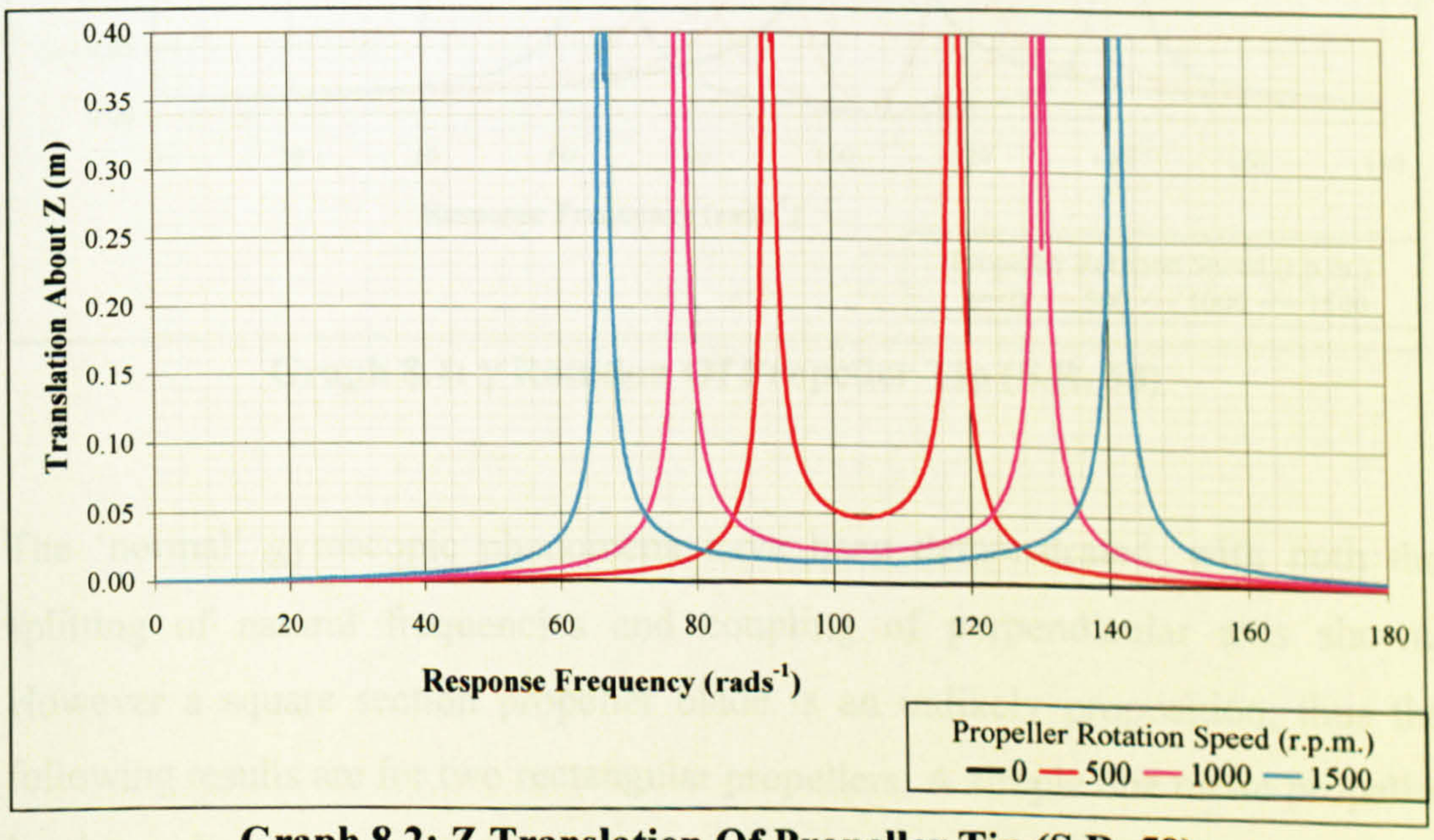

Graph 8.2: Z Translation Of Propeller Tip (S.R. 50)

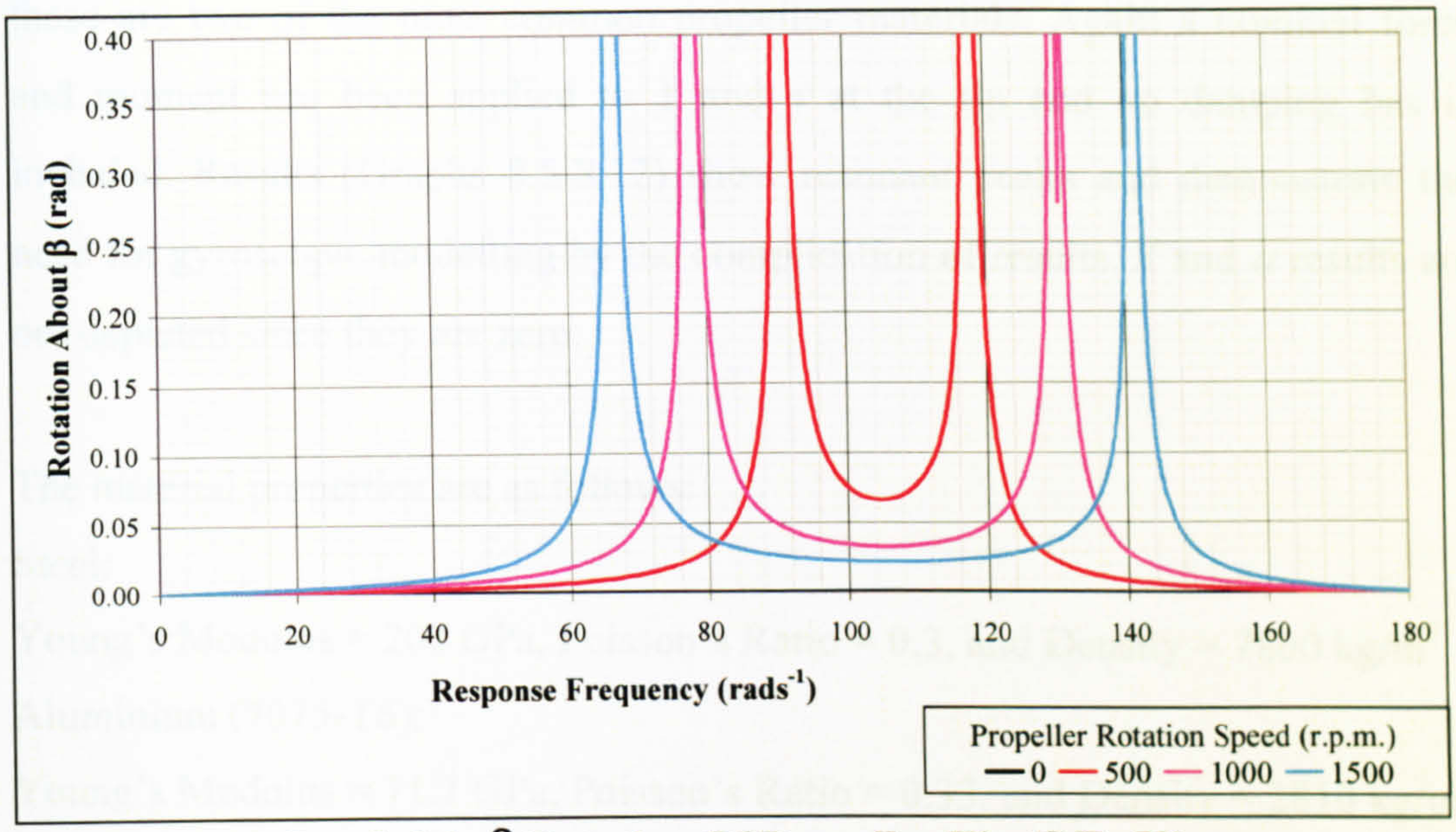

Graph 8.3: β Rotation Of Propeller Tip (S.R. 50)

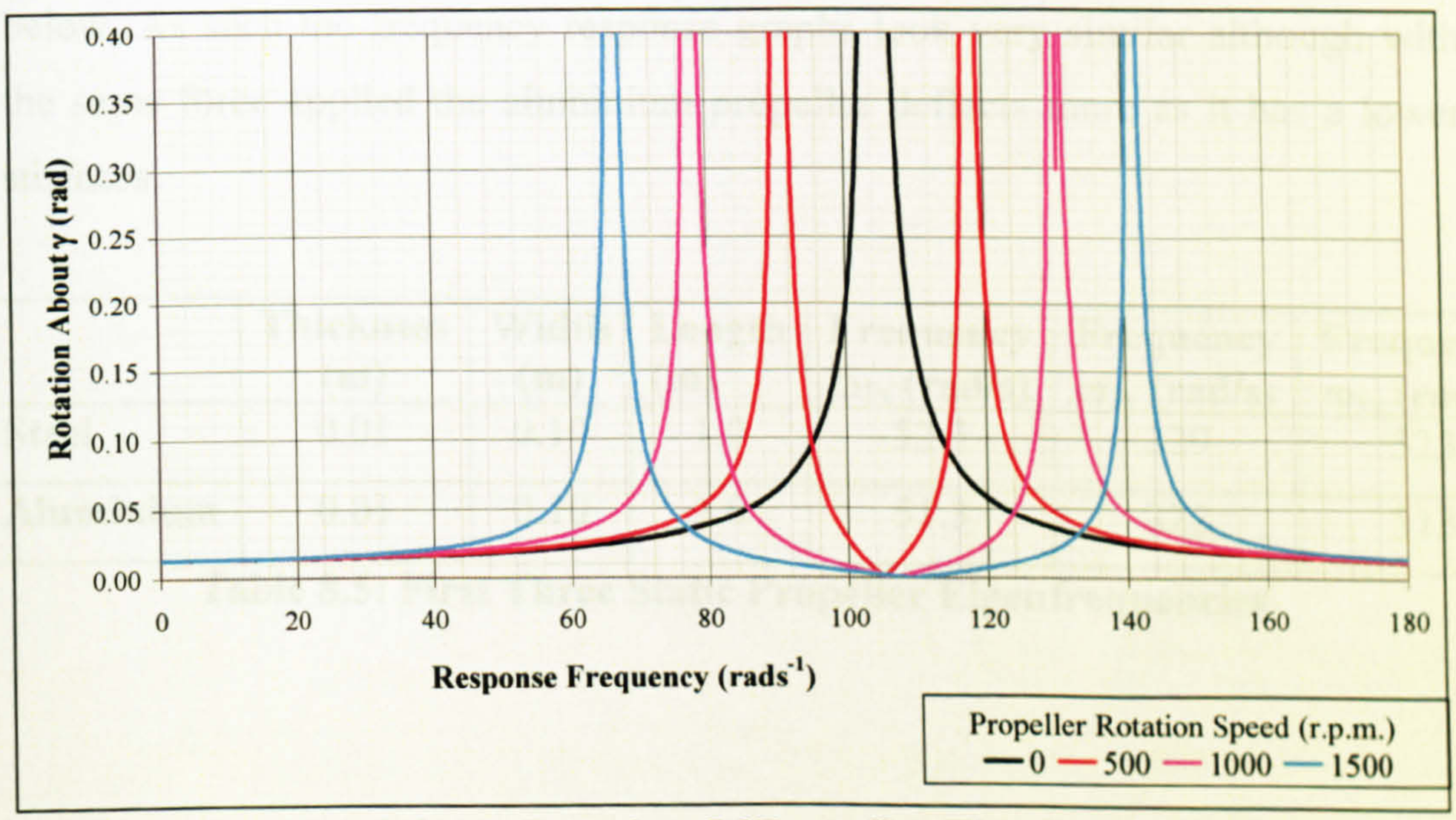

Graph 8.4: γ Rotation Of Propeller Tip (S.R. 50)

The 'normal' gyroscopic phenomena have been demonstrated, with both the splitting of natural frequencies and coupling of perpendicular axis shown. However a square section propeller blade is an unlikely proposition, thus the following results are for two rectangular propellers. A simple one metre propeller has been chosen, ten centimetres wide and one centimetre thick. Although these

dimensions are fictional a steel and aluminium comparison has be drawn since these are two of the most common propeller materials. Again a nominal force and moment has been applied to Y and γ at the tip and no damping has is included. Results (Graphs 8.5-8.12) show resonant peaks and demonstrate the need for gyroscopic modelling by the complication of results. X and α results are not depicted since they are zero.

The material properties are as follows:

Steel:

Young's Modulus = 207 GPa, Poisson's Ratio = 0.3, and Density = 7800 kg/m^3

Aluminium (7075-T6):

Young's Modulus = 71.7 GPa, Poisson's Ratio = 0.33, and Density = 2810 kg/m^3

Ironically since both Young's Modulus and Density are reduced for Aluminium the eigenvalues for both materials are very similar. This is shown in Table 8.5 below. As such the frequency response graphs look very similar although with the same force applied the aluminium propeller deflects more as it has a lower stiffness.

	Thickness (m)	Width (m)	Length (m)	Frequency ω_{1y} (rad/s)	Frequency ω_{2y} (rad/s)	Frequency ω_{1z} (rad/s)
Steel	0.01	0.10	1.0	52.3	329	523
Aluminium	0.01	0.10	1.0	51.3	322	513

Table 8.5: First Three Static Propeller Eigenfrequencies

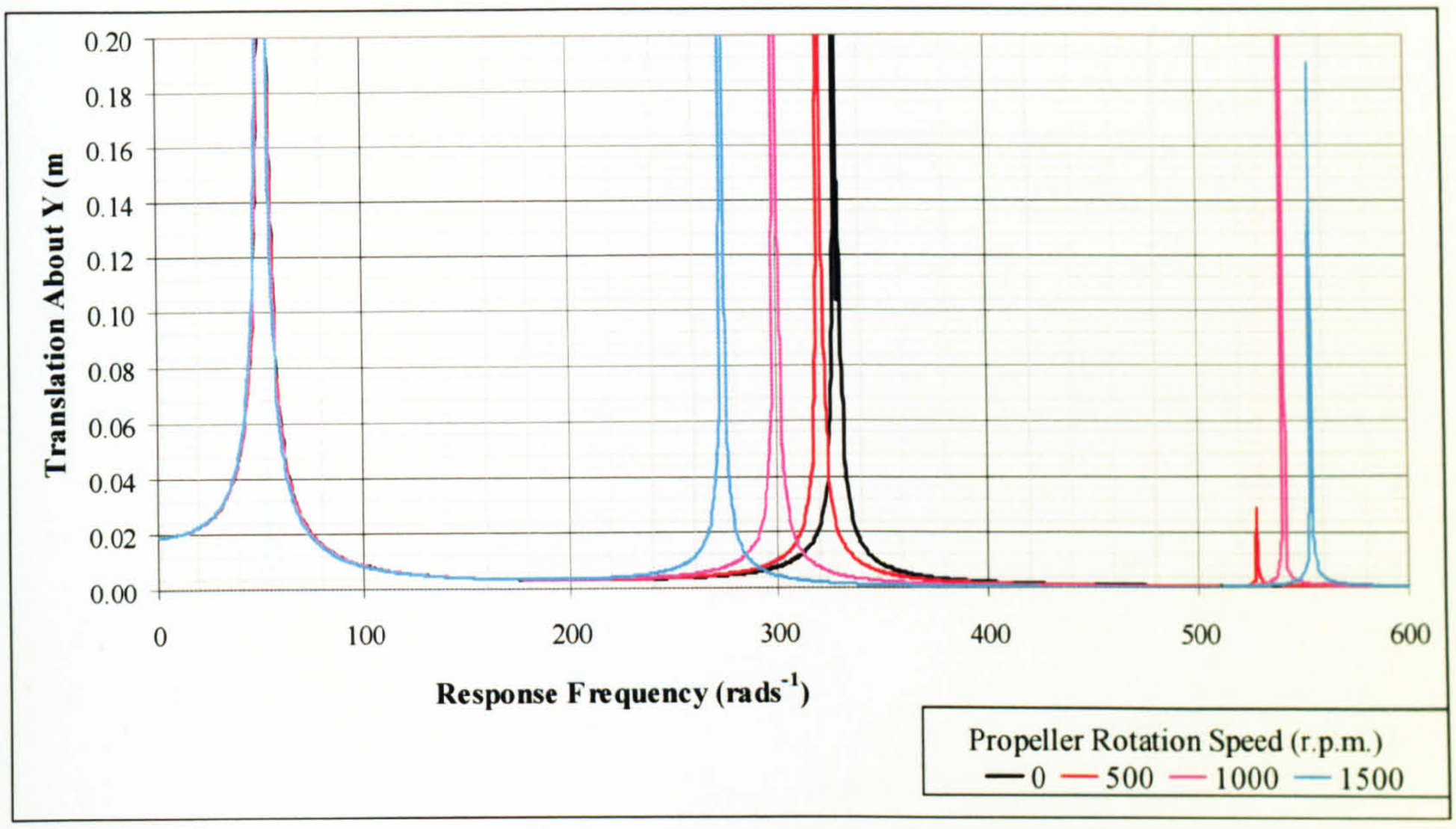

Graph 8.5: Y Translation Of Steel Propeller Tip

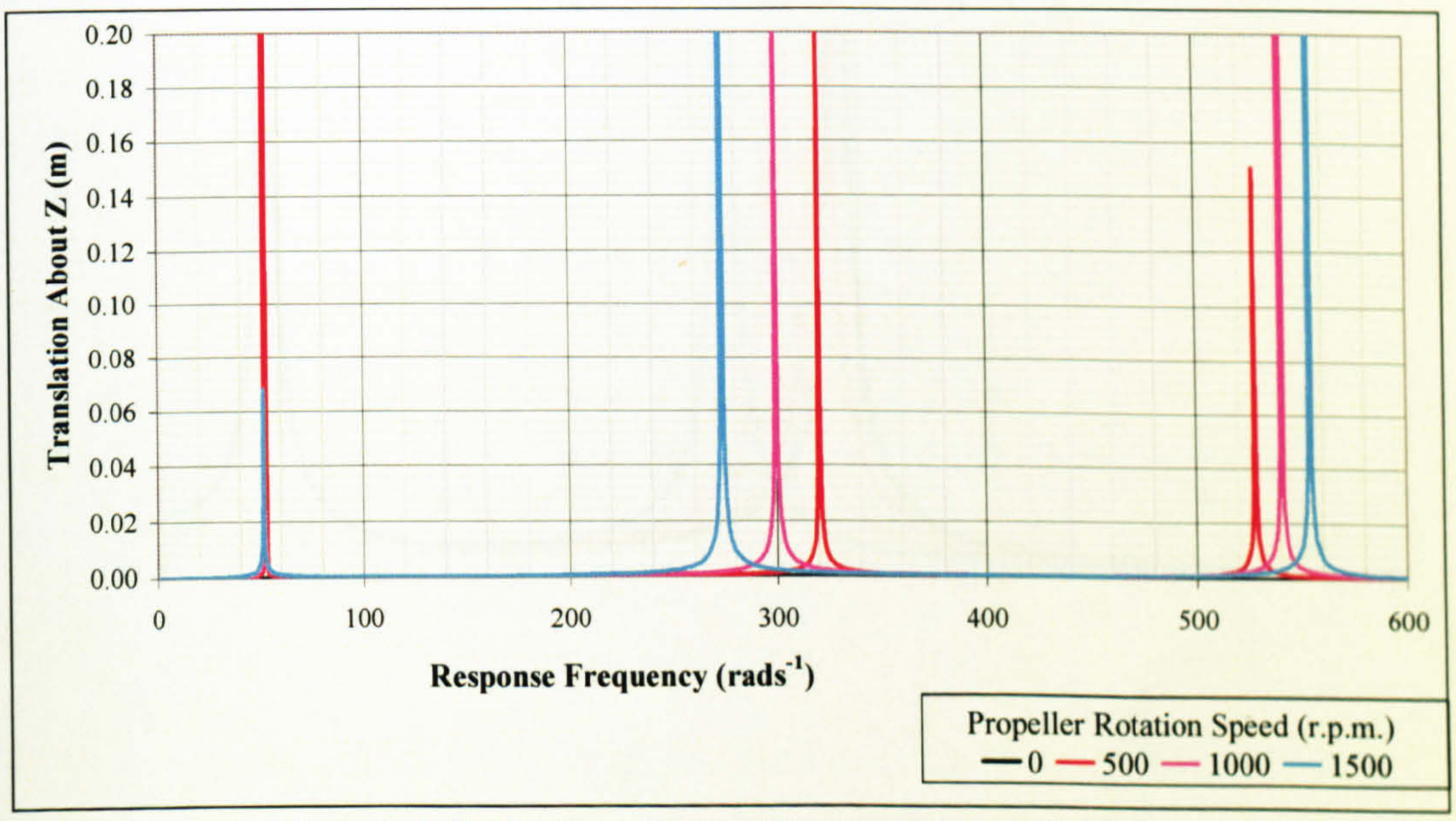

Graph 8.6: Z Translation Of Steel Propeller Tip

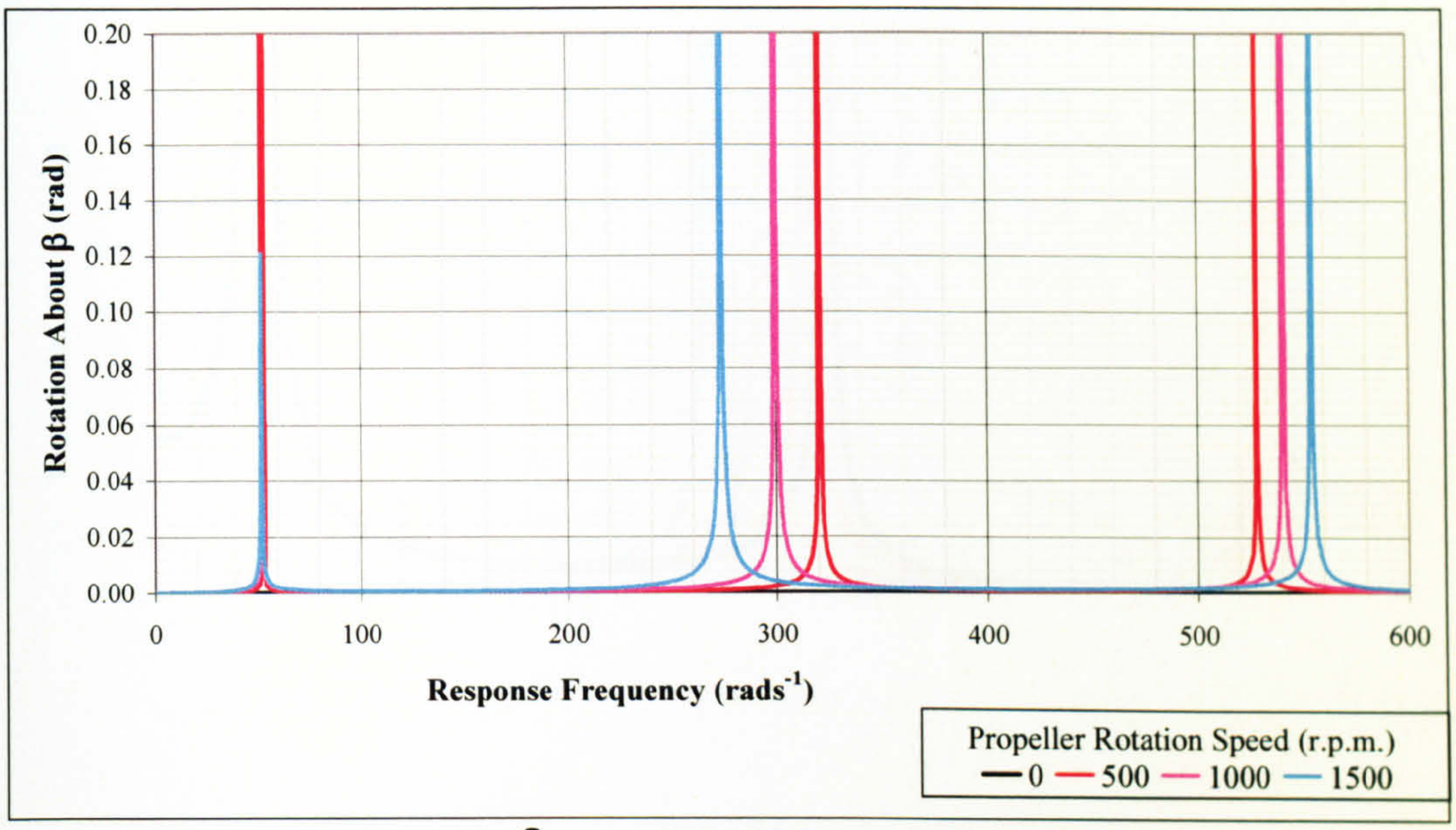

Graph 8.7: β Rotation Of Steel Propeller Tip

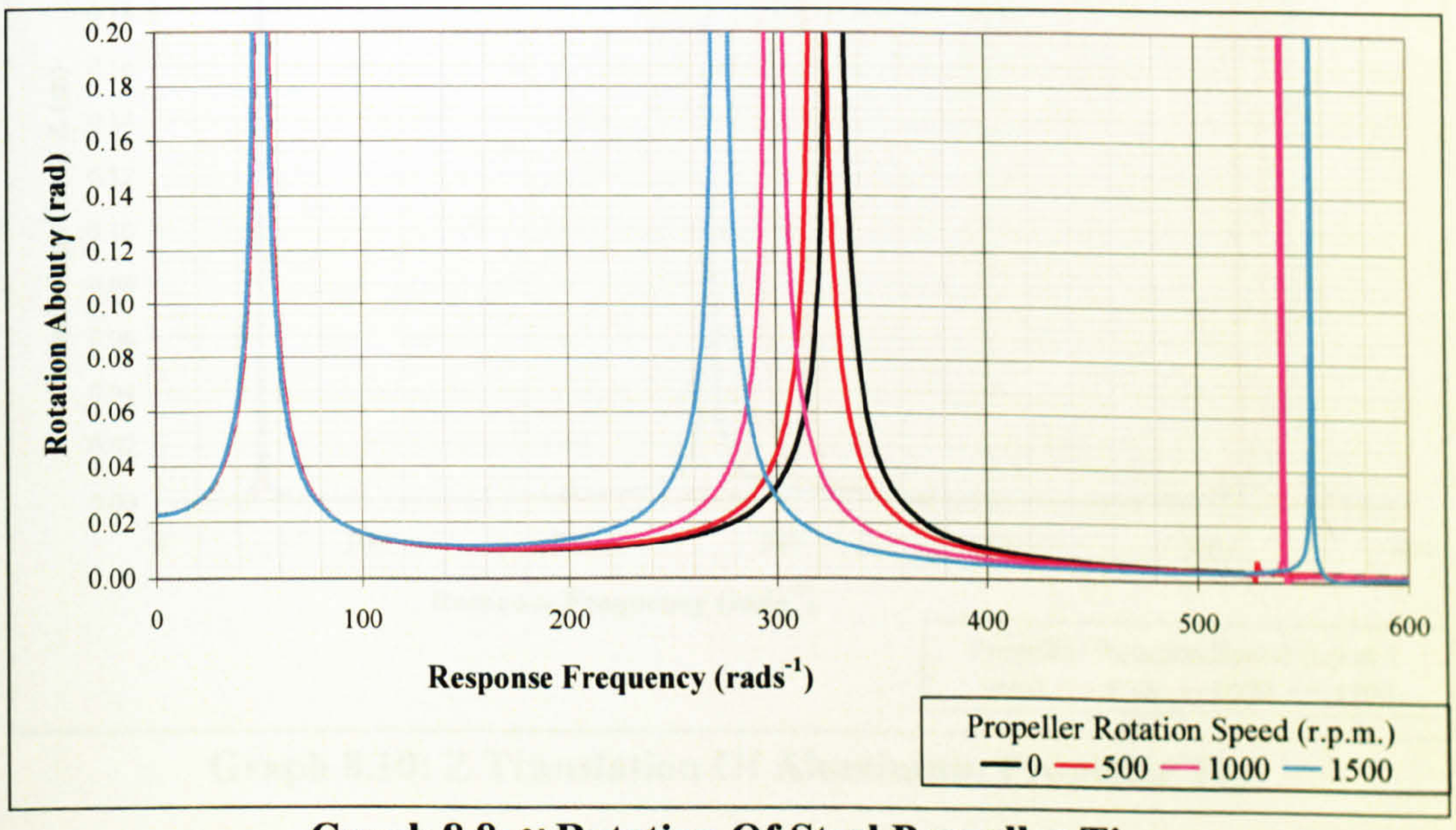

Graph 8.8: γ Rotation Of Steel Propeller Tip

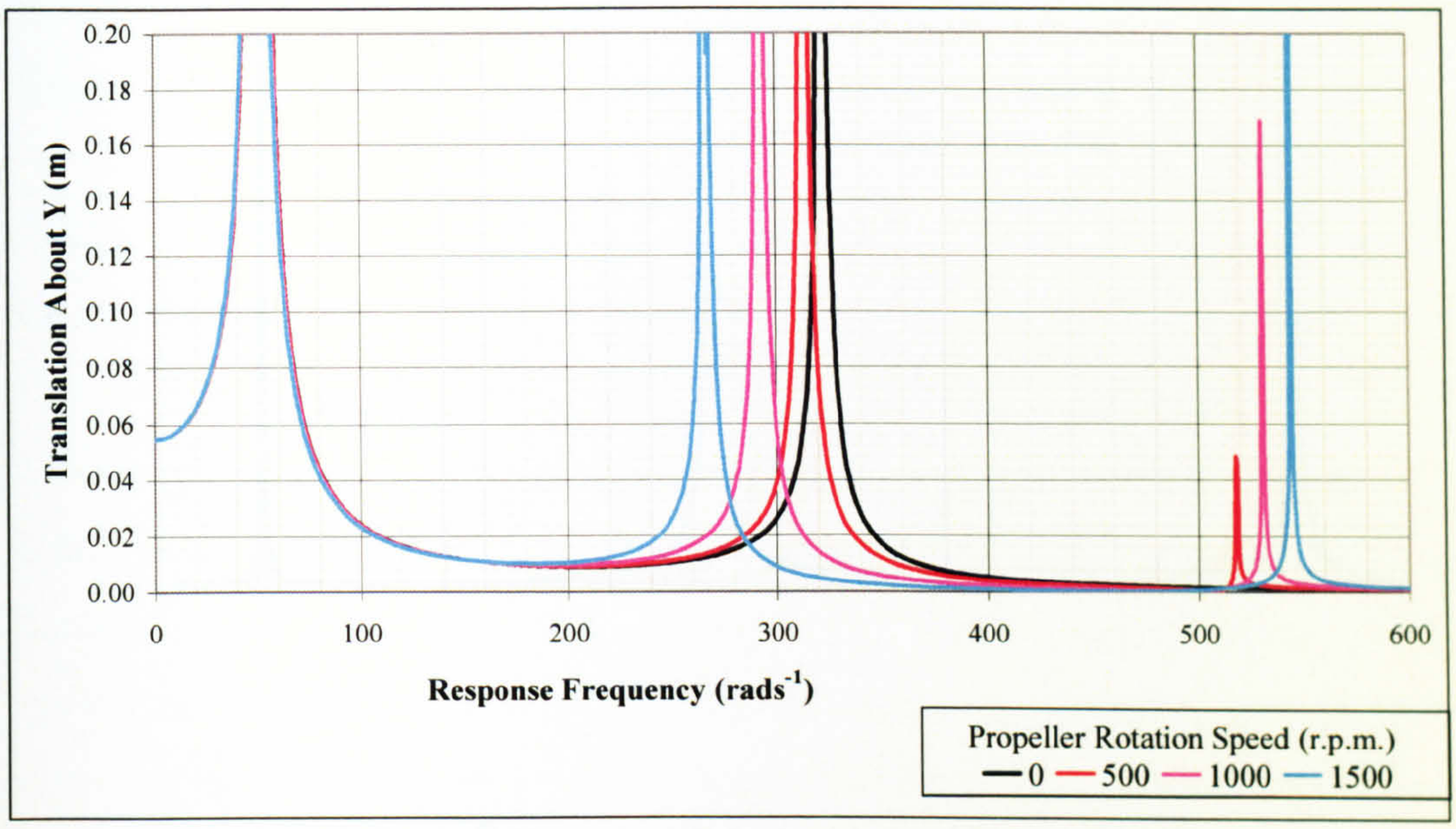

Graph 8.9: Y Translation Of Aluminium Propeller Tip

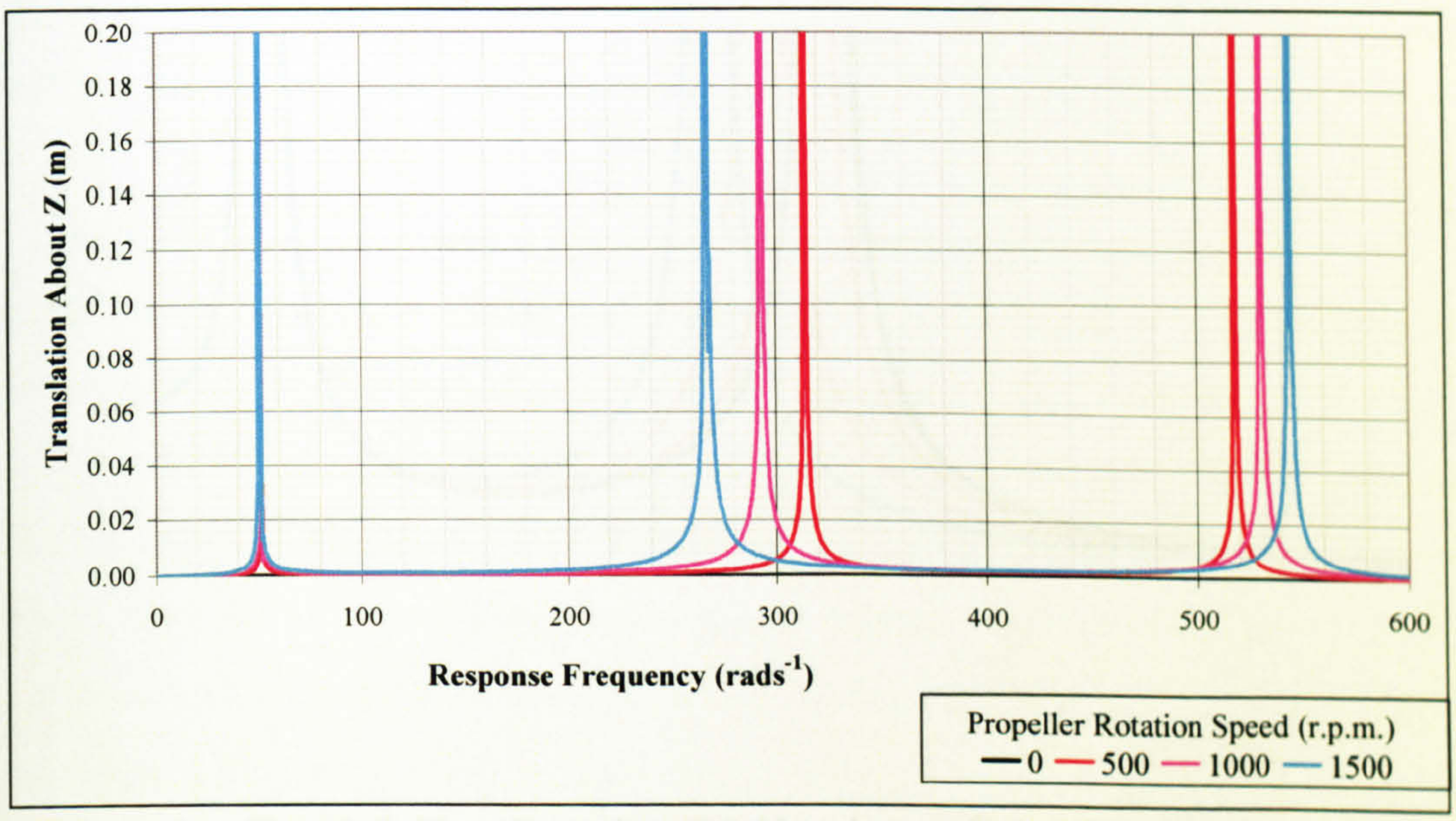

Graph 8.10: Z Translation Of Aluminium Propeller Tip

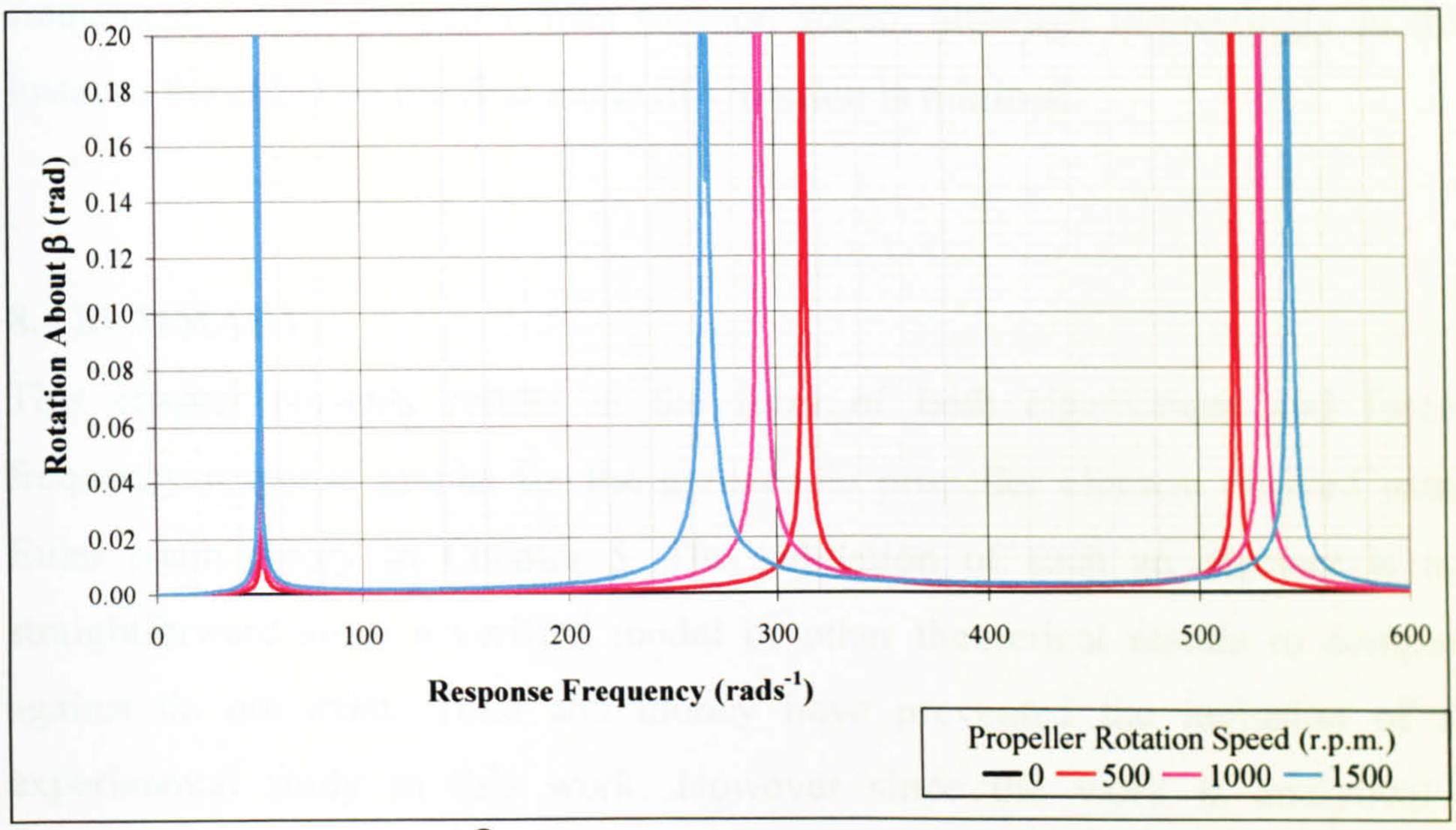

Graph 8.11: β Rotation Of Aluminium Propeller Tip

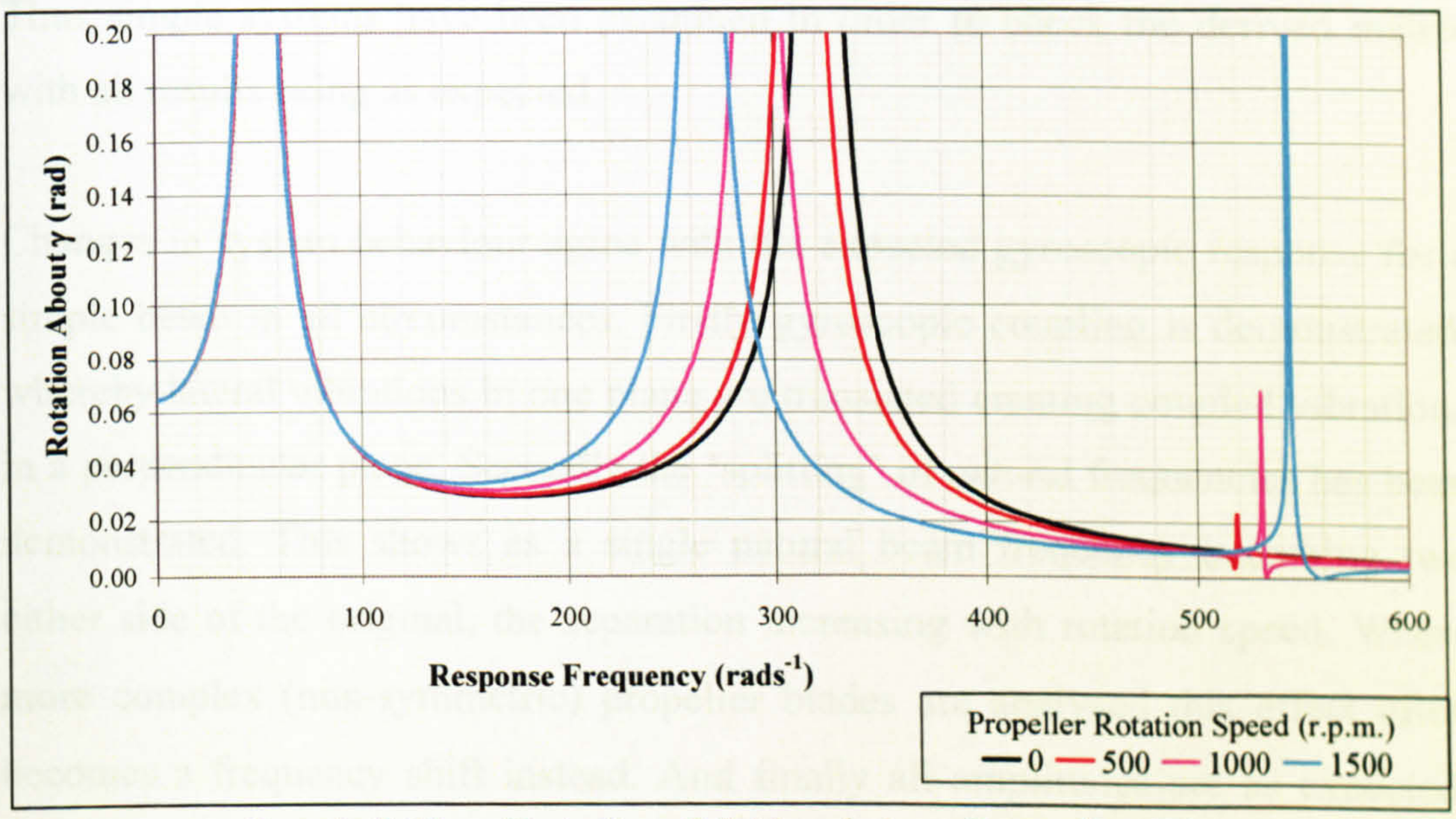

Graph 8.12: γ Rotation Of Aluminium Propeller Tip

Gyroscopic coupling is immediately evident as a response around 525-550 rad/s, this is only seen in results where rotation is present since this eigenvalue belongs to the I_z axis not the I_y axis in which the system is excited. The response becomes more significant in amplitude with rotation frequency as the gyroscopic forces increase. Coupling is also evident in the Z and β results which are only present when there is rotation. Furthermore the gyroscopic effect changes the natural

frequencies of the propeller with rotation speed, although interestingly in this instance the effect on the first mode of vibration is minimal.

8.4 SUMMARY

This chapter presents results in the form of both eigenvalues and forced frequency response graphs for the gyroscopic propeller element derived using Euler beam theory in Chapter 5. The validation of such an element is not straightforward since a verified model or other theoretical results to compare against do not exist. Time and money have prevented the inclusion of an experimental study in this work. However since the work is analytical a verification examining the gyroscopic coupling effect is itself is considered sufficient given that the gyroscopic effects are not too difficult to understand. Thus simple systems have been examined in order to check the derived matrix with all results being as expected.

Changes in system behaviour agree with the expected gyroscopic response for a simple beam in all circumstances. Firstly gyroscopic coupling is demonstrated, whereby lateral vibrations in one plane are translated creating coupled vibrations in a perpendicular plane. Secondly the 'splitting' of natural frequencies has been demonstrated. This shows as a single natural beam frequency becoming two either side of the original, the separation increasing with rotation speed. Where more complex (non-symmetric) propeller blades are analysed this effect often becomes a frequency shift instead. And finally all amplitudes are as expected, with vibration amplitudes in perpendicular axes being approximately equal. This is important since as various whirl conditions are achieved at different speeds the lateral displacements will tend to be equal. Thus if these displacements vastly differed the gyroscopic coupling effect would likely prove to be incorrect.

Finally results show that for propellers lateral changes in system response due to gyroscopic forces must not be ignored due to the possibility of significant changes in system behaviour. The effect is greater the closer the width and thickness of the blade are dimensionally since the coupled natural frequencies in

both axes are then closer together. The change is also more significant for more flexible blades.

CHAPTER 9

RESULTS 3: CENTRIFUGAL STIFFENING ELEMENT

9.1 INTRODUCTION

This chapter presents results showing the effects of centrifugal stiffening of propeller systems using the formulation developed from Hoa, S.V., [1979] in Chapter 6. For the purpose of this investigation all gyroscopic effects have been eliminated such that the centrifugal effect is studied in isolation. This is in order to simplify the problem and save confusion between the gyroscopic and centrifugal stiffening effects.

It can be seen that if tests are initiated with a stationary propeller and then the rotation frequency is increased, one would expect to the resonant vibration frequencies of the propeller increase due to the additional stiffening effect. Handelman, G., Boyce, W., and Cohen, H., [1958] and Kumar, R., [1974] showed that the increase in natural frequencies caused by the increase in stiffness, is most significant for the first mode of vibration. However this may only be true for certain types of system and as such is an expected system response to be investigated.

This type of stress stiffening is most significant for very slender beams that have a very low initial lateral stiffness, thus the effect will also be investigated for beams of differing slenderness ratios in order to determine at what point it may become insignificant.

9.2 EIGENVALUE RESULTS

All results have been produced for systems where the propeller is 1 metre long and split into three finite elements of equal length (since three elements are shown to provide good accuracy in Chapter 8). The thickness of the blade has then been changed in order to provide results for systems of different slenderness ratios. Since gyroscopic effects have been removed there is no coupling between the two bending planes (Figure 8.1), thus for a rectangular section the natural frequencies for the thickness and width are independent of each other. As such the width and associated natural frequencies are not given in the results. Once again steel is used where Young's Modulus = 207 GPa, Poisson's Ratio = 0.3, and Density = 7800 kg/m^3.

Thickness (m)	Slenderness Ratio	Speed (rpm)	ω_1 (Rad/s)	Wright et al.	ω_2 (Rad/s)	Wright et al.	ω_3 (Rad/s)	Wright et al.
0.01	100	0	52.3	52.3	329	328	929	918
0.01	100	500	77.3	77.4	355	354	954	944
0.01	100	1000	124	124	423	422	1031	1018
0.01	100	1500	175	175	518	517	1145	1131

Table 9.1: Eigenfrequency Comparison with Results from Wright et al., [1982]

Table 9.1 shows eigenfrequencies for a slender beam with results compared to those of Wright et al., [1982]. Results from Wright et al have been interpolated from Table 3 in the published paper. Results show excellent agreement despite the use of just three finite elements for this model. As such further comparison against other results has been deemed unnecessary as this study is focused on propeller behaviour. A complete comparison of different methods of analysing the effects of centrifugal stiffening is given by Wright et al., [1982].

Thickness (m)	Slenderness Ratio	Speed (rpm)	ω_1 (Rad/s)	ω_2 (Rad/s)	ω_3 (Rad/s)
0.01	100	0	52.3	329	929
0.01	100	500	77.3	355	954
0.01	100	1000	124	423	1031
0.01	100	1500	175	518	1145
0.02	50	0	105	658	1858
0.02	50	500	119	671	1871
0.02	50	1000	155	709	1911
0.02	50	1500	199	770	1975
0.04	25	0	209	1315	3716
0.04	25	500	217	1322	3723
0.04	25	1000	238	1342	3743
0.04	25	1500	270	1374	3776
0.10	10	0	523	3287	9289
0.10	10	500	526	3290	9292
0.10	10	1000	535	3298	9300
0.10	10	1500	550	3312	9314

Table 9.2: Euler Propeller Eigenfrequencies Including Centrifugal Stiffening

The first thing to notice about centrifugal stiffening is that it can be very significant even for relatively slow rotation speeds. Also since the stiffening is dependant on the rotation speed squared, as the rotation speed increases the effect becomes considerably more important although not exponentially so.

Centrifugal stiffening also proves to be far more significant for slender propellers. This is due to the low bending stiffness associated with a slender propeller, thus the additional effect of centrifugal stiffening is more significant. This is most obvious comparing eigenfrequencies for the thick and thinnest (10 and 100 slenderness ratio) propellers in Table 9.2. Due to the modelling technique used it can be seen that eigenfrequencies for the thick propeller are

exactly ten times that of the thin propeller when there is no rotation. However this trend does not continue once rotation is invoked and therefore centrifugal stiffening effects are included. In fact for the thick shaft eigenfrequencies hardly change, while mode one for the slender shaft shows the eigenfrequency more than triple by 1500 rpm.

For further clarification the percentage change in eigenfrequencies is displayed graphically below (Graphs 9.1-9.4) for all four slenderness ratios up to a propeller rotation speed of 10000 rpm. This clearly shows how the effect can be is much greater for a slender beam where a 1967 % increase in eigenfrequency is seen for the first mode of vibration for the one centimetre thick propeller at 10000 rpm, while for the ten centimetre thick propeller under the same conditions a 137 % increase is seen.

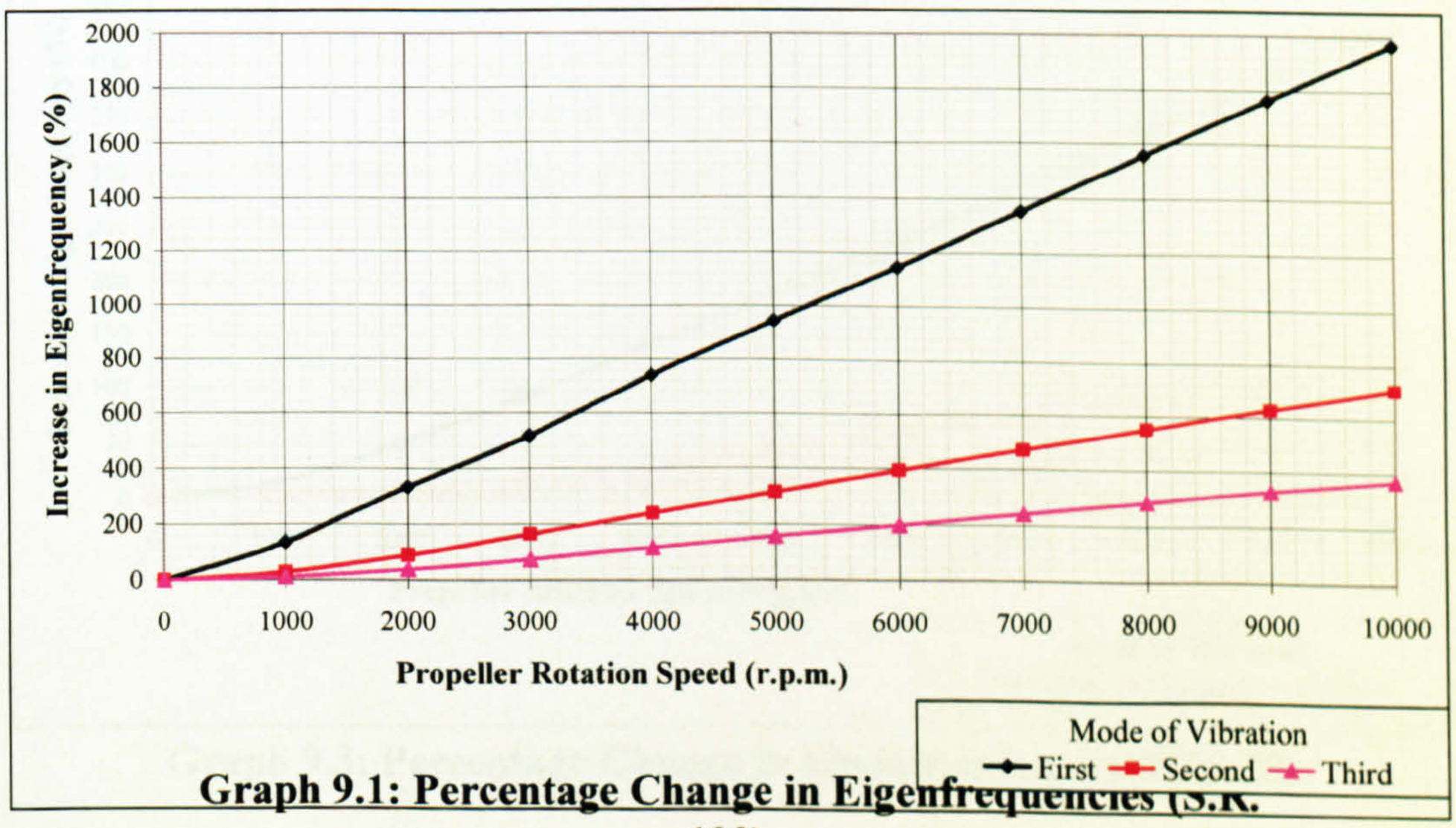

Graph 9.1: Percentage Change in Eigenfrequencies (S.R. 100)

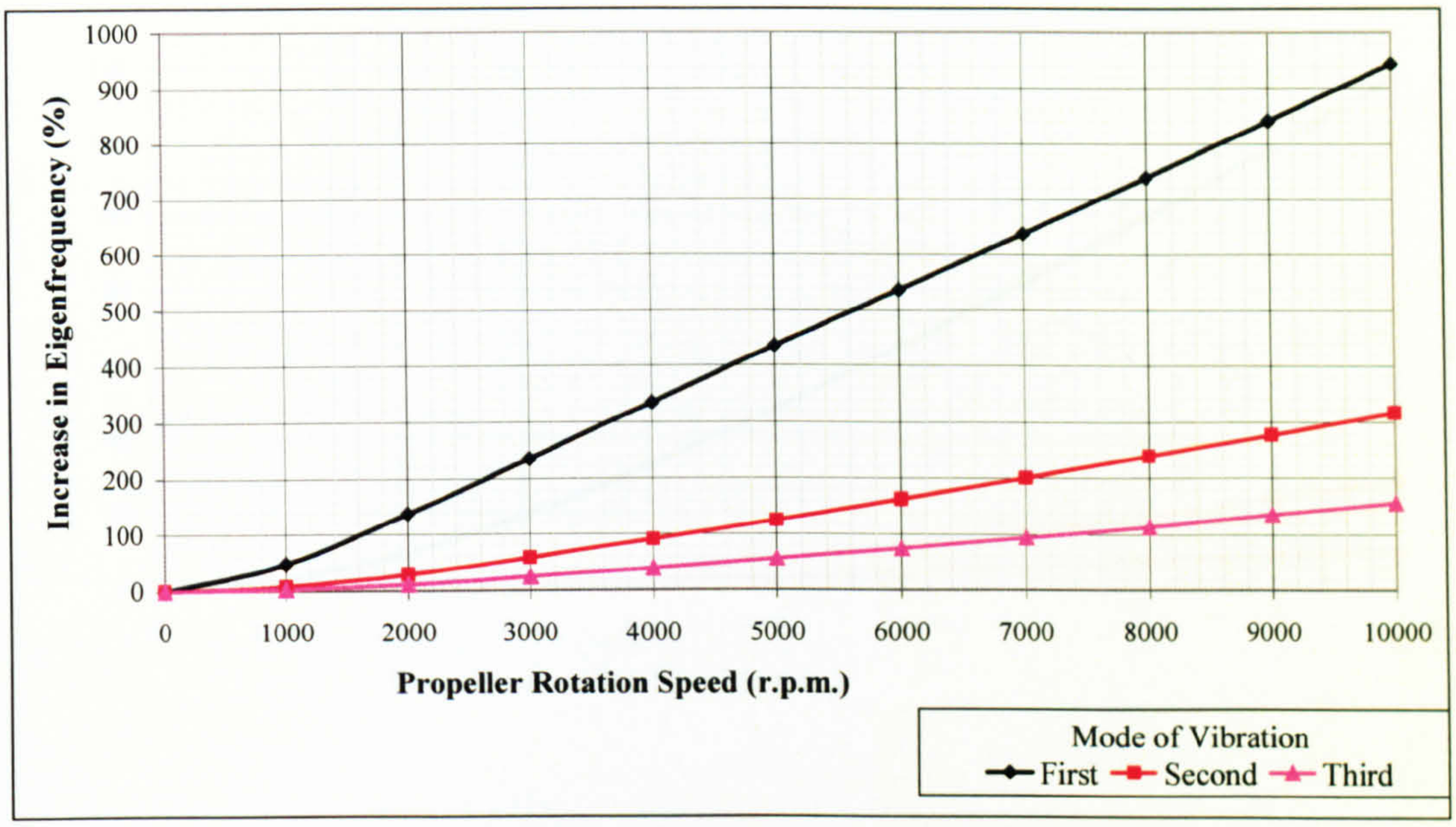

Graph 9.2: Percentage Change in Eigenfrequencies (S.R. 50)

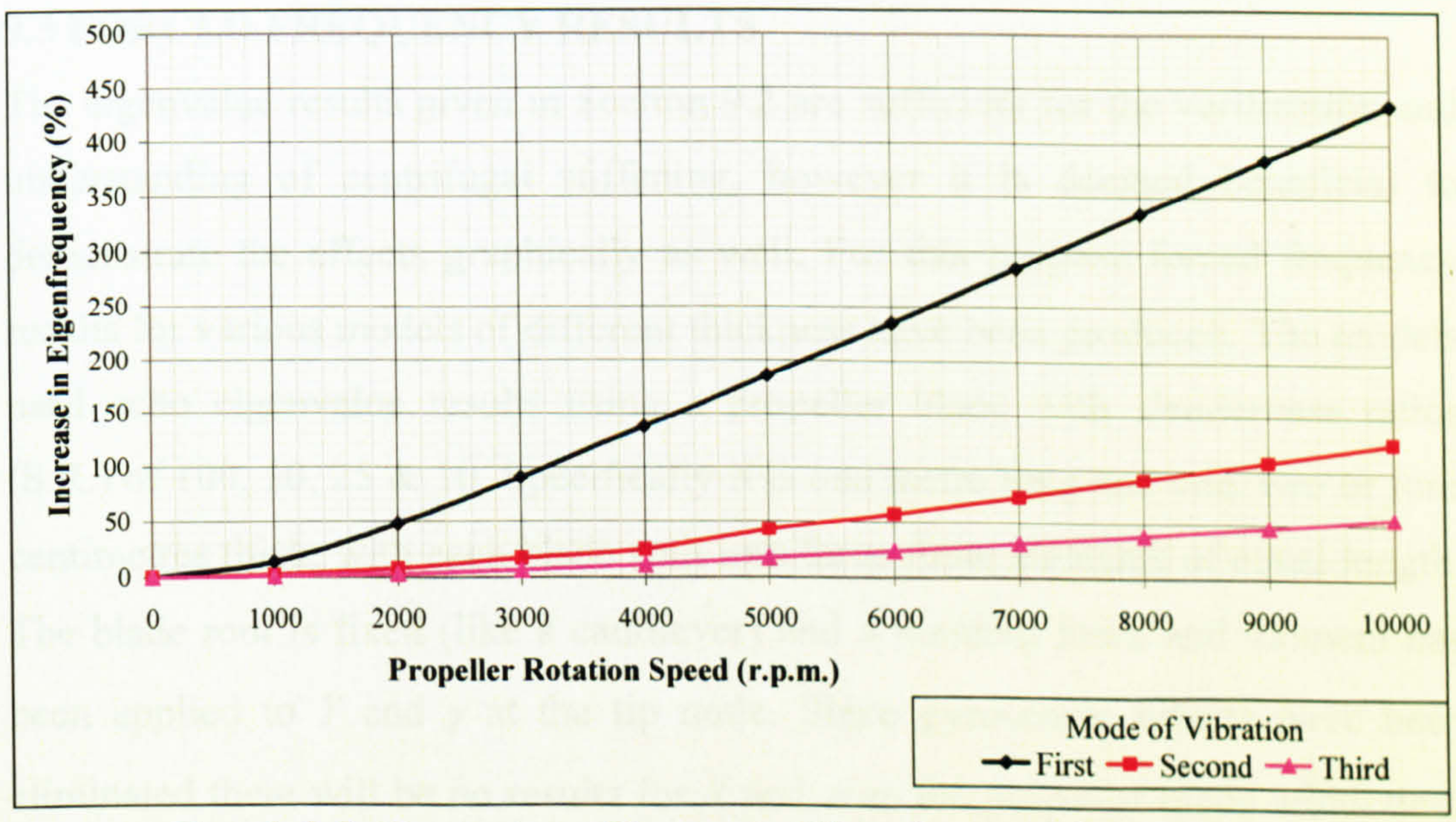

Graph 9.3: Percentage Change in Eigenfrequencies (S.R. 25)

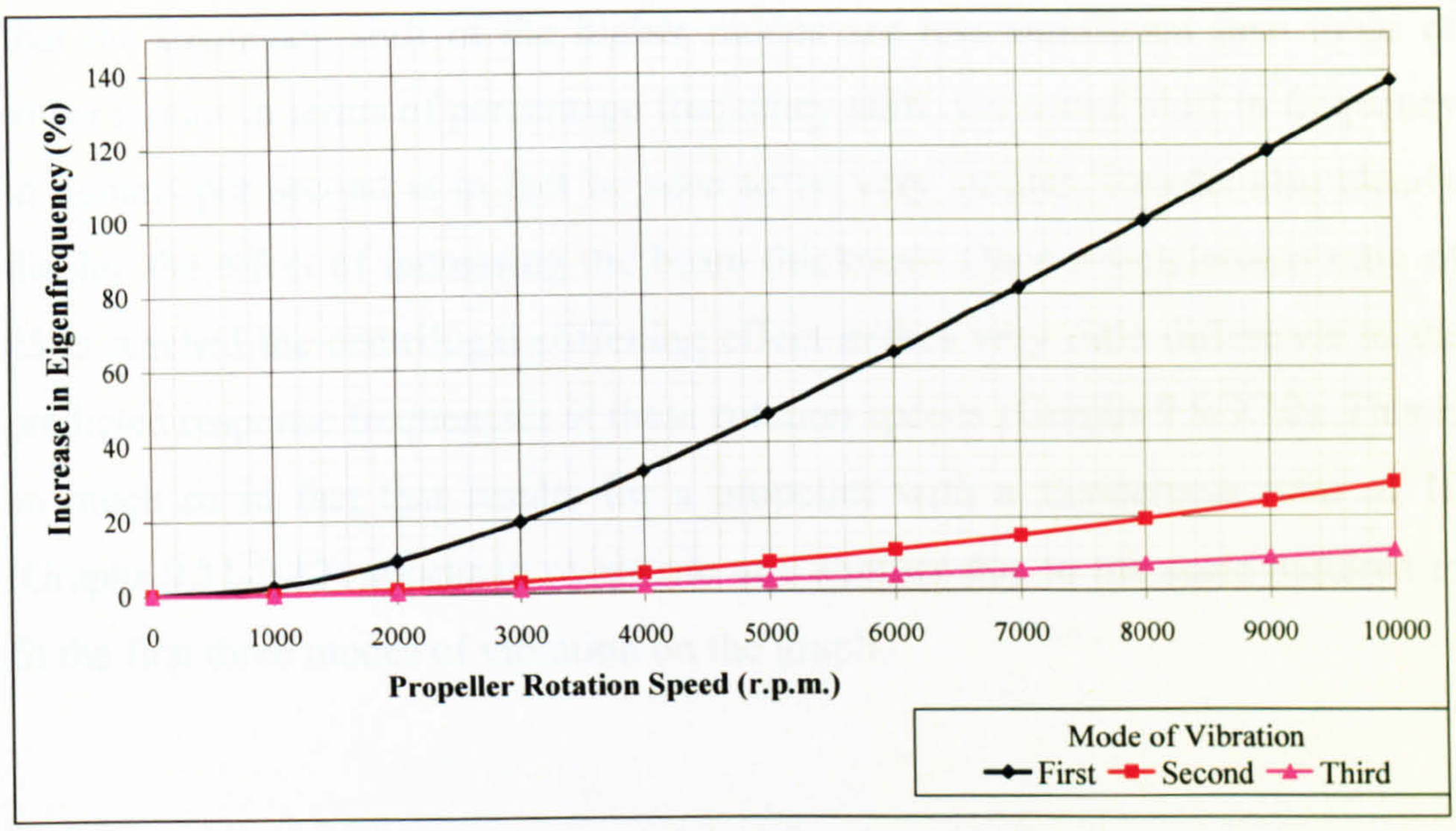

Graph 9.4: Percentage Change in Eigenfrequencies (S.R. 10)

9.3 FORCED FREQUENCY RESULTS

The eigenvalue results given in Section 9.2 are sufficient for the verification and understanding of centrifugal stiffening, however it is deemed beneficial to demonstrate the effects graphically as well. For this purpose forced frequency results for various models of different thickness have been produced. The models used echo eigenvalue results using a propeller blade with slenderness ratios (S.R.) of 100, 50, 25 & 10. Specifically it is one metre long and one, two or four centimetres thick, with each blade split into three finite elements of equal length. The blade root is fixed (like a cantilever) and a nominal force and moment has been applied to Y and γ at the tip node. Since gyroscopic effects have been eliminated there will be no results for X and α so the propeller blade width does not effect results. X and α results are also zero so only Y and γ results are given (Graphs 9.5-9.12). No damping has been included and as such amplitude (that is peak amplitudes at resonant frequencies) should be ignored. The models have been run at various speeds including the analysis of a stationary propeller.

Results show as the rotation speed increases so does the resonant frequency in all cases. As expected these match the eigenfrequencies. Although it is true to say

that the frequency shift of the higher modes are less significant than those of lower modes in terms of percentage frequency shift, the actual shift in frequency in radians per second is in fact be seen to be very similar. Results also clearly display the effect of increasing the beam thickness. Once a slenderness ratio of 25 is reached the centrifugal stiffening effect makes very little difference to the predicted response frequencies at these rotation speeds (Graphs 9.9-9.10). This is so much so in fact that results for a propeller with a slenderness ratio of 10 (Graphs 9.11-9.12) appear to overwrite one another due to the scale required to fit the first three modes of vibration on the graph.

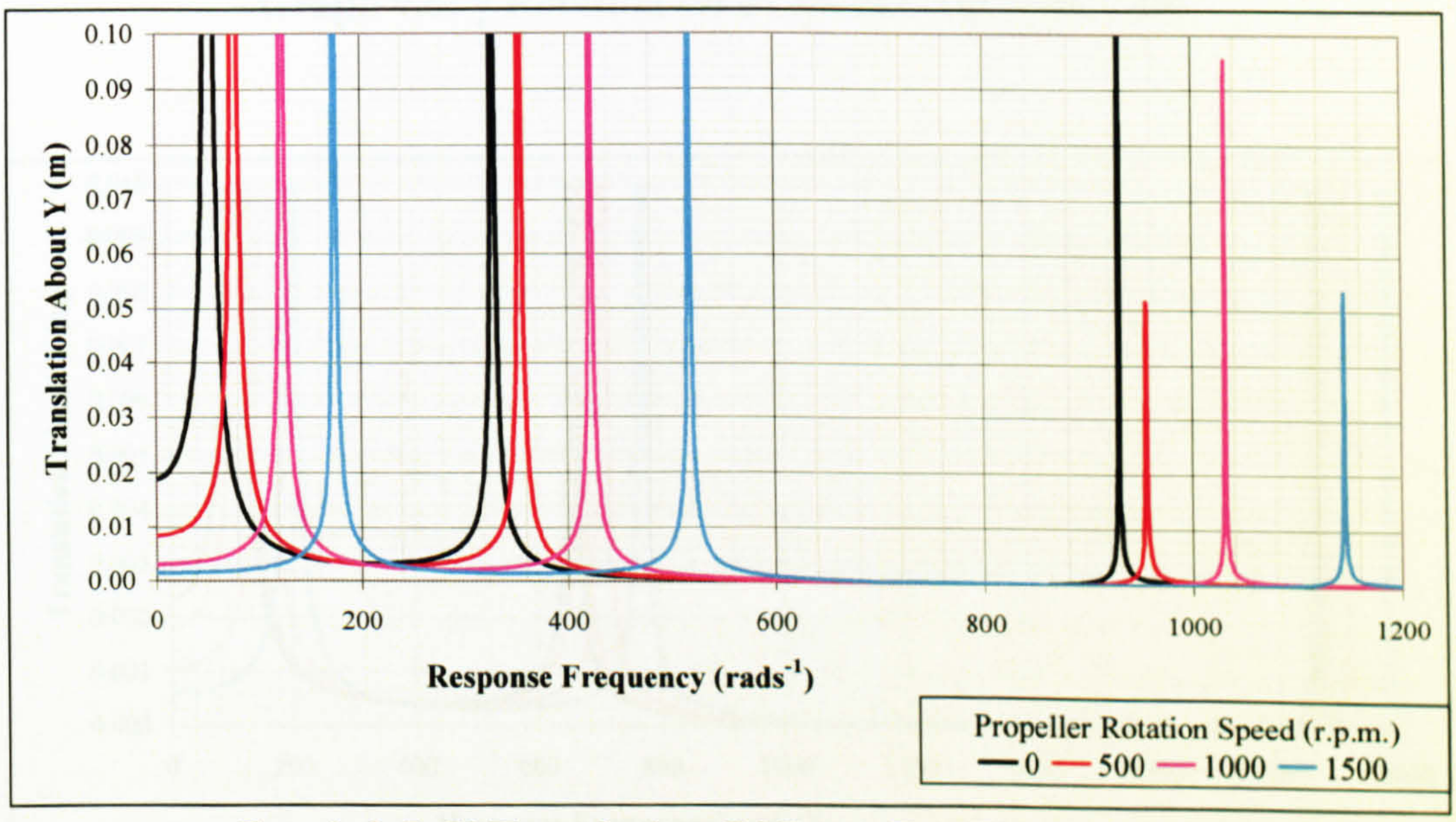

Graph 9.5: Y Translation Of Propeller Tip (S.R. 100)

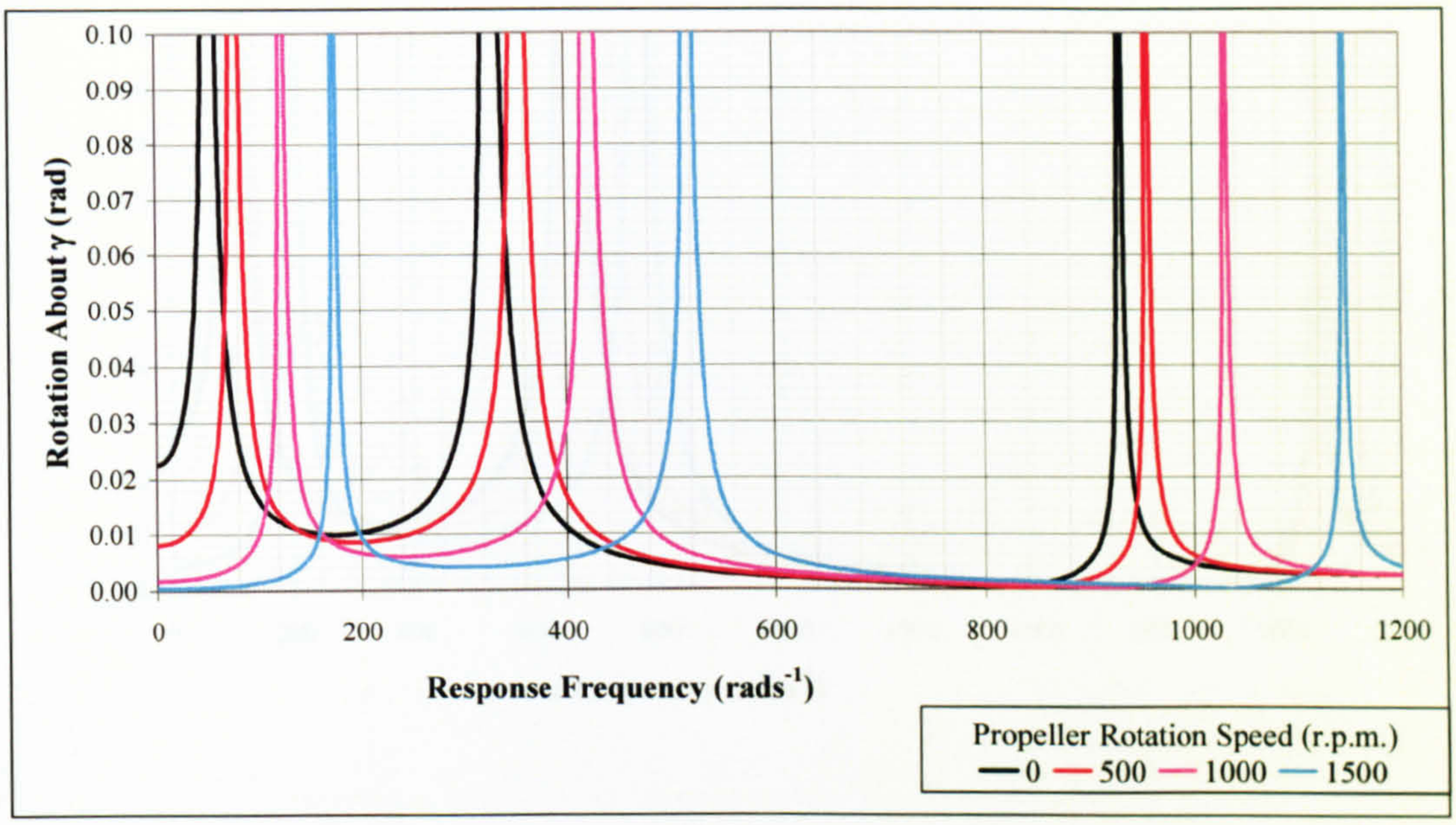

Graph 9.6: γ Rotation Of Propeller Tip (S.R. 100)

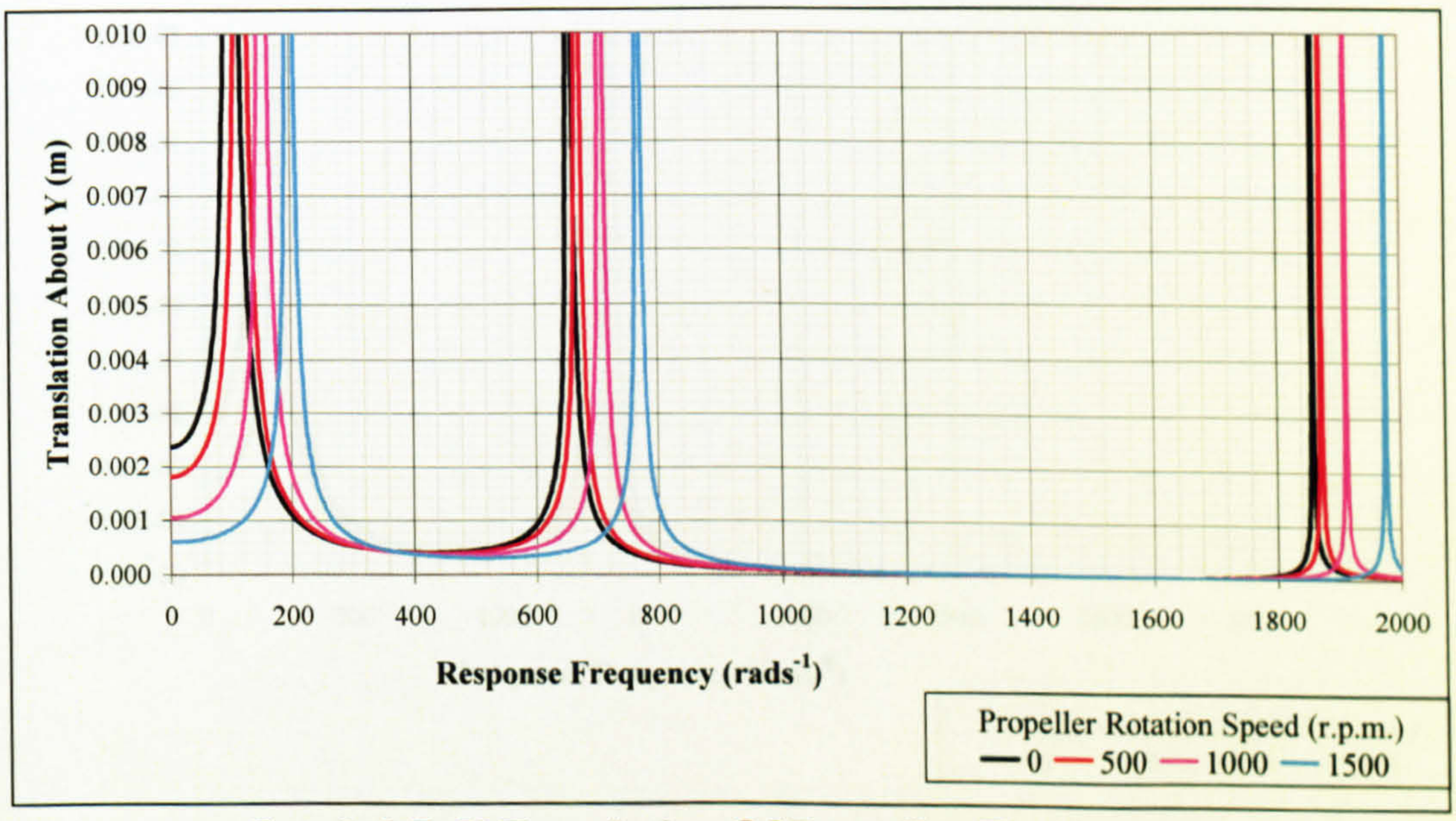

Graph 9.7: Y Translation Of Propeller Tip (S.R. 50)

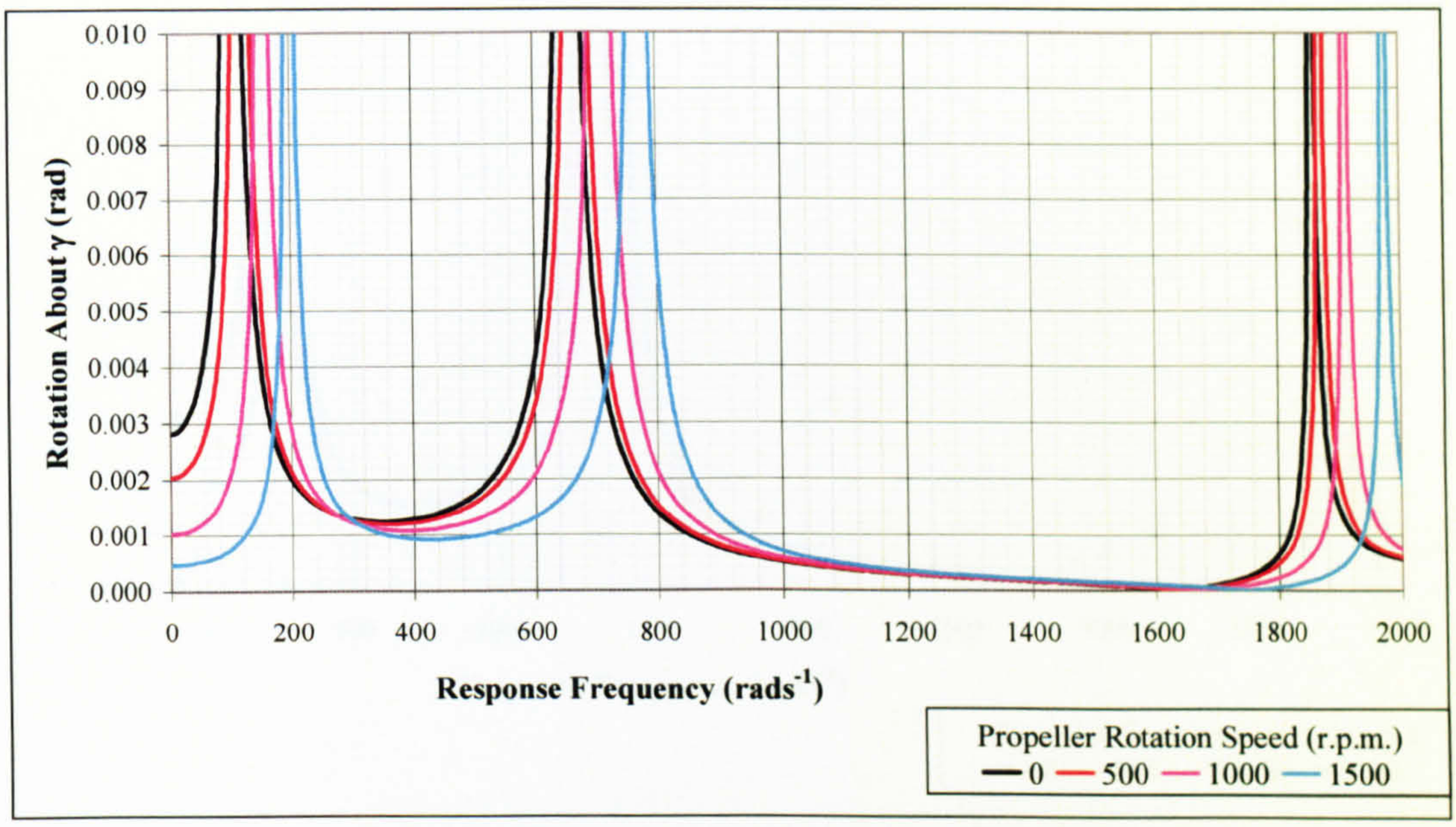

Graph 9.8: γ Rotation Of Propeller Tip (S.R. 50)

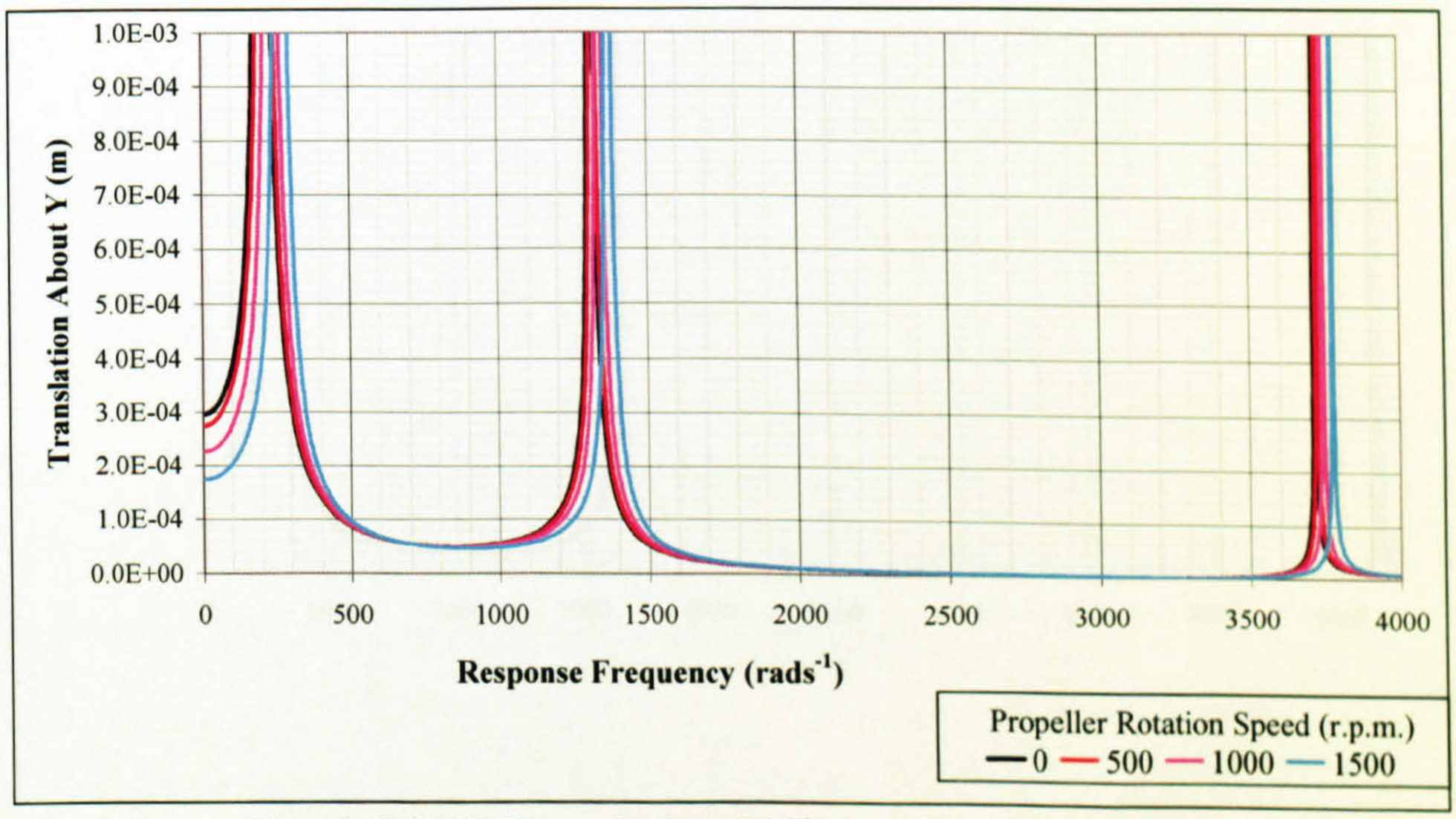

Graph 9.9: Y Translation Of Propeller Tip (S.R. 25)

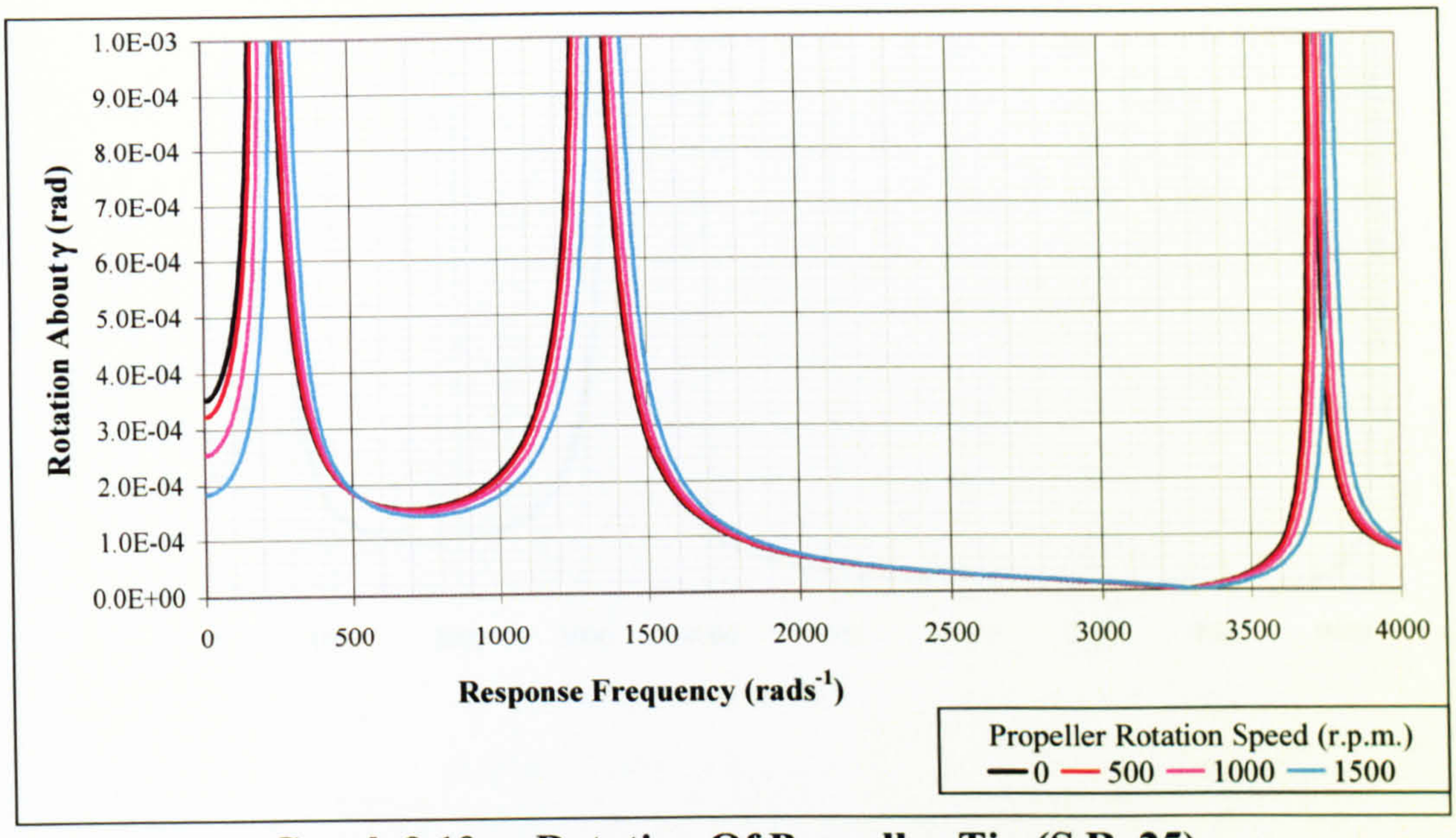

Graph 9.10: γ Rotation Of Propeller Tip (S.R. 25)

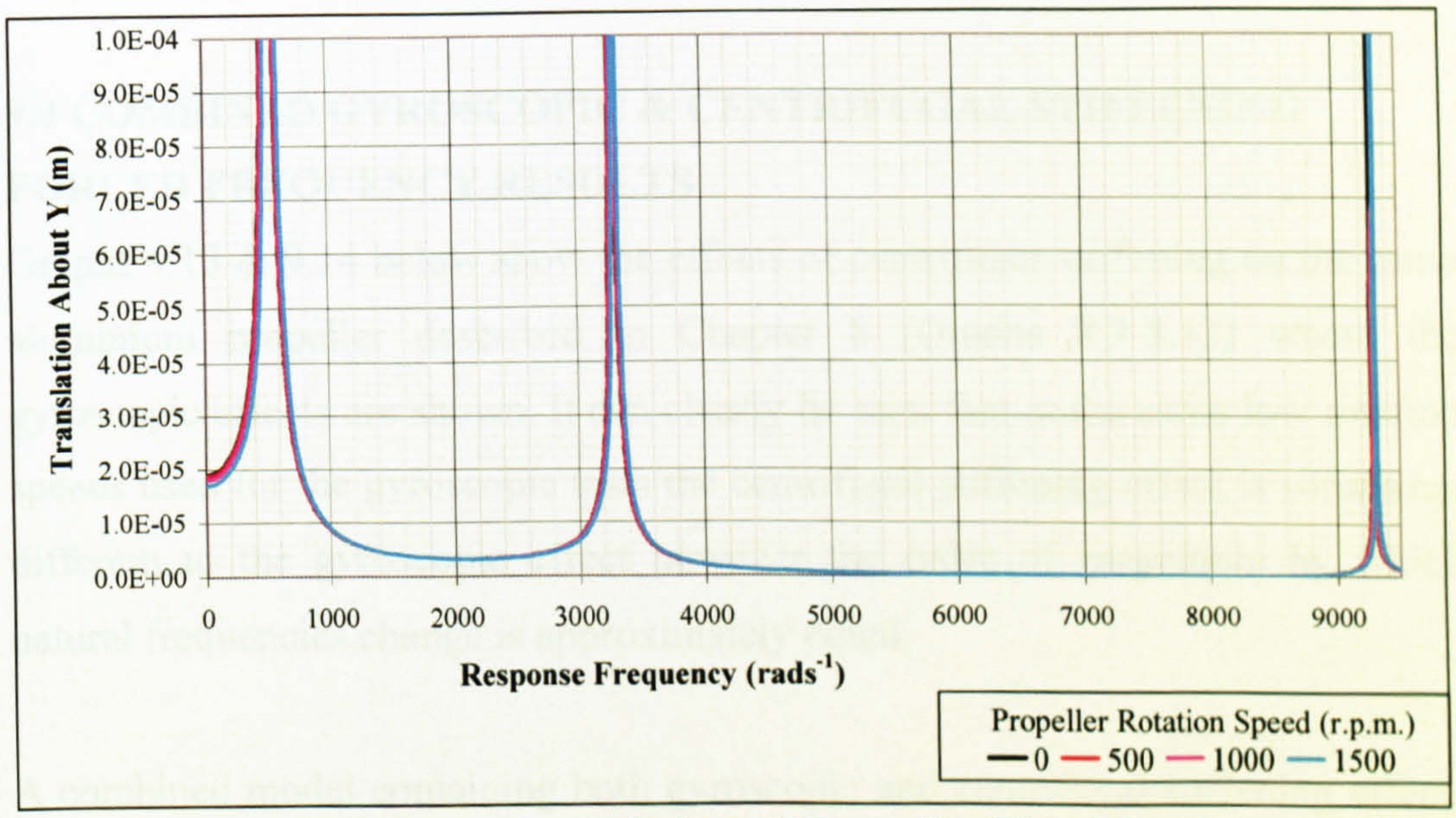

Graph 9.11: Y Translation Of Propeller Tip (S.R. 10)

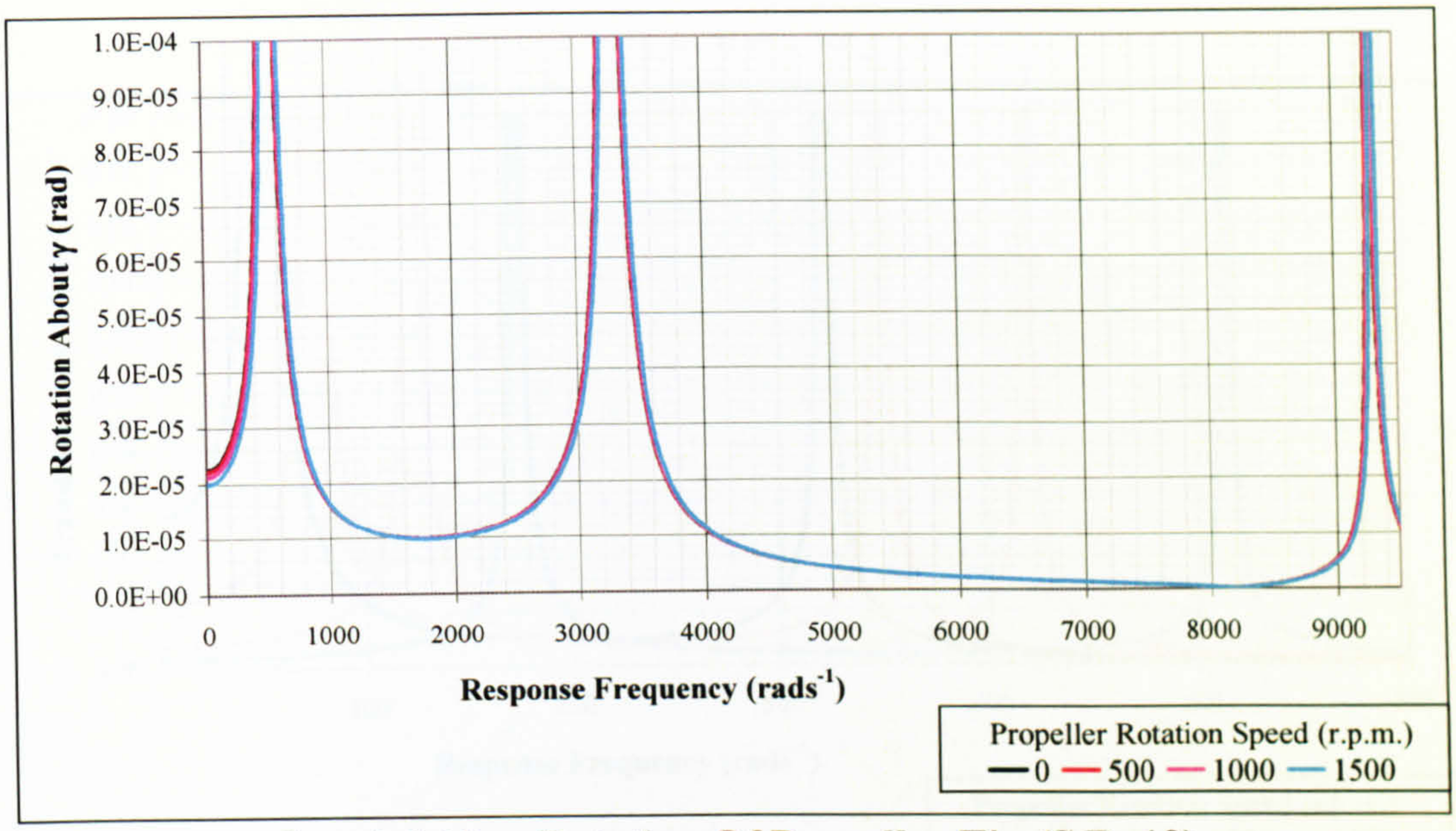

Graph 9.12: γ Rotation Of Propeller Tip (S.R. 10)

9.4 COMBINED GYROSCOPIC & CENTRIFUGAL STIFFENING FORCED FREQUENCY RESULTS

Graphs 9.13 & 9.14 below show the effects of centrifugal stiffening on the same aluminium propeller described in Chapter 8 (Graphs 8.9-8.12) where the gyroscopic effects are shown. It can clearly be seen that at the same low rotation speeds used for the gyroscopic tests the centrifugal stiffening effect is somewhat different to the gyroscopic effect however the order of magnitude by which natural frequencies change is approximately equal.

A combined model containing both gyroscopic and centrifugal stiffening effects is then shown in Graphs 9.15-9.18 below. The graphs are very similar in shape to Graphs 8.9-8.12 which show only gyroscopic effects, however centrifugal stiffening is apparent in the increased natural frequencies. For clarity a direct comparison can be made with Graphs 8.9, 9.13, & 9.15, which show gyroscopic, centrifugal stiffening and combined effects for the same system respectively. It is most obvious for the first mode of vibration since this hardly changes under gyroscopic influence alone. Also since in some cases both effects can conspire to increase a natural frequency there are significant increases seen.

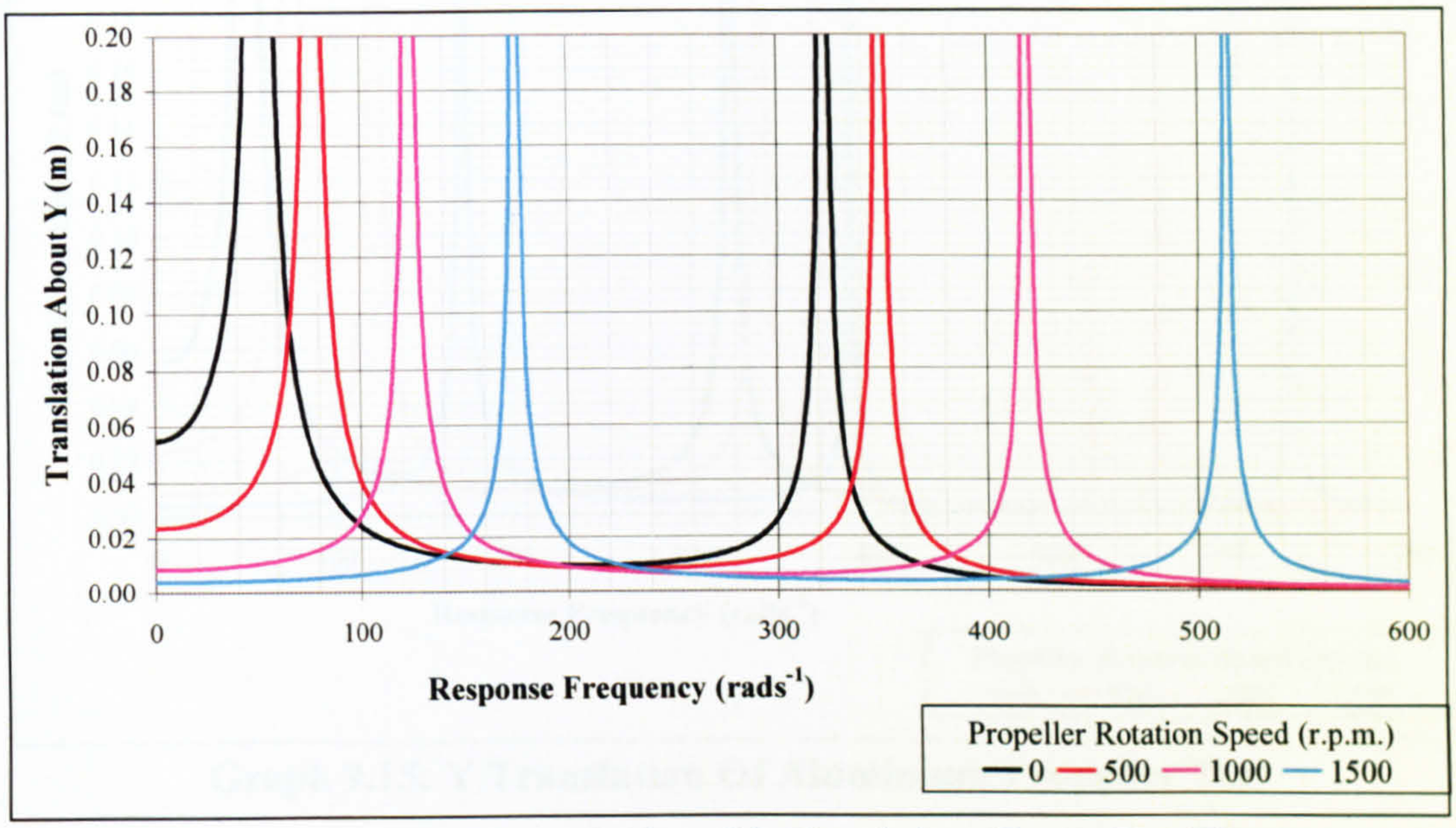

Graph 9.13: Y Translation Of Aluminium Propeller Tip

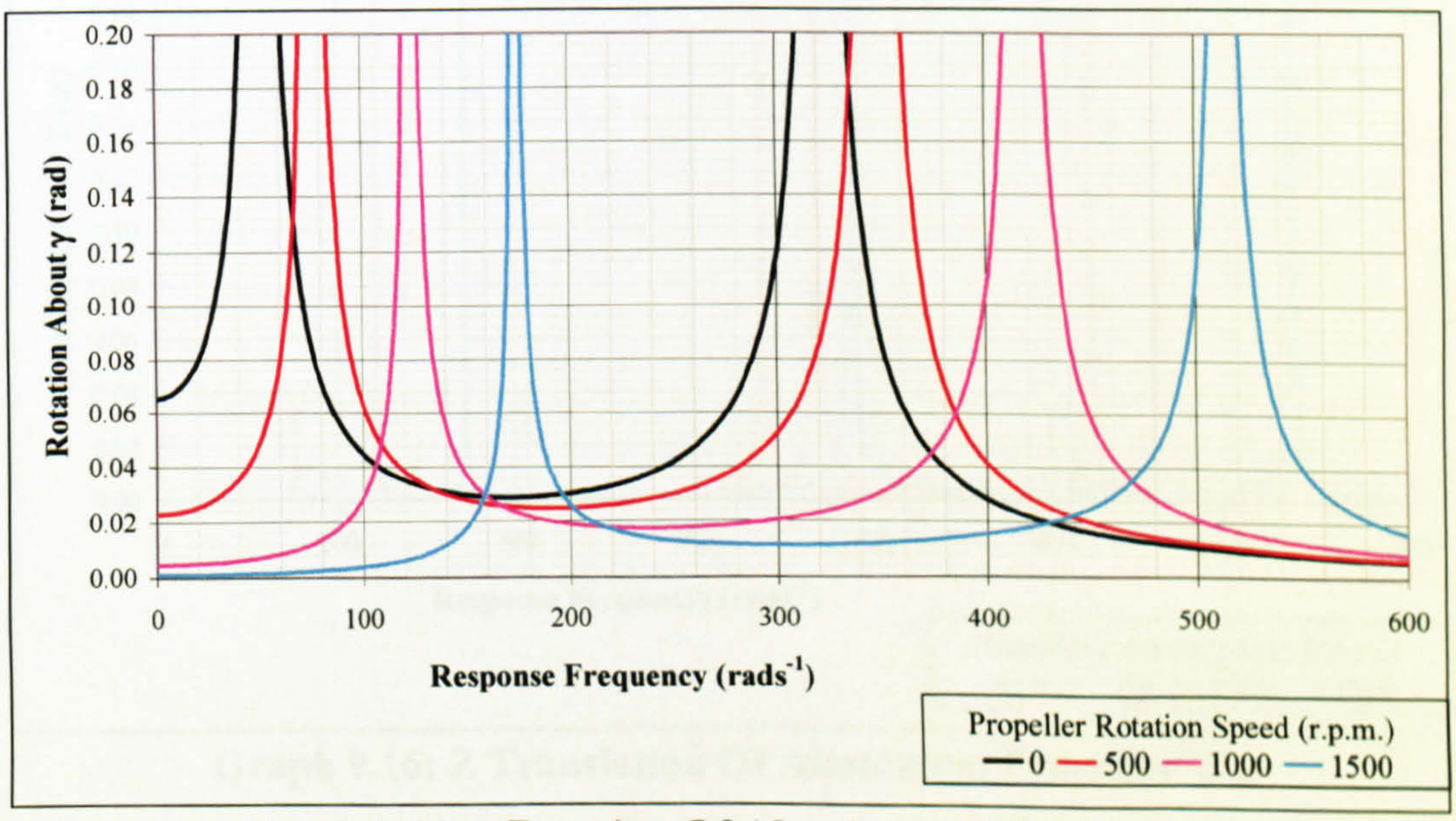

Graph 9.14: γ Rotation Of Aluminium Propeller Tip

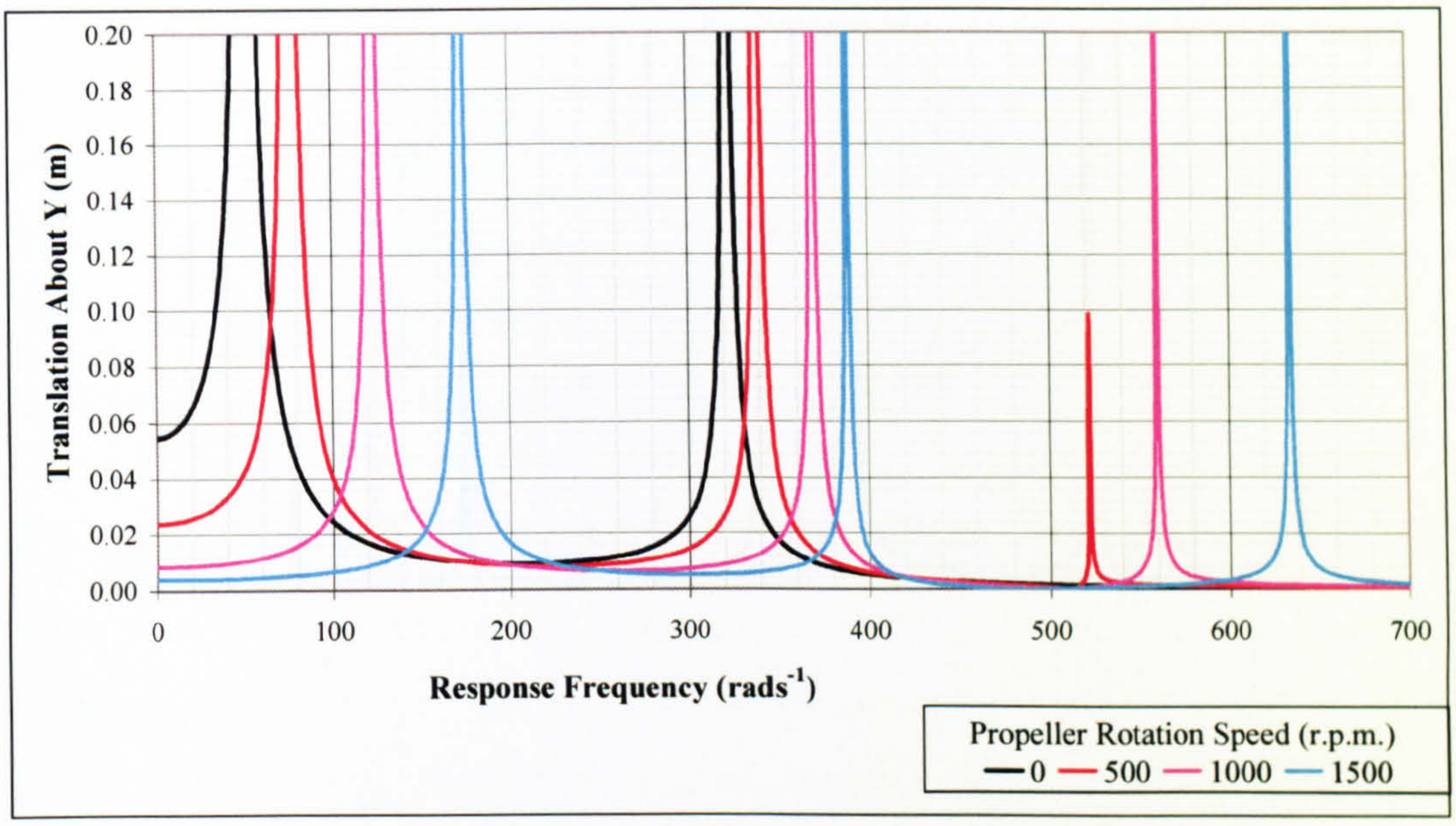

Graph 9.15: Y Translation Of Aluminium Propeller Tip

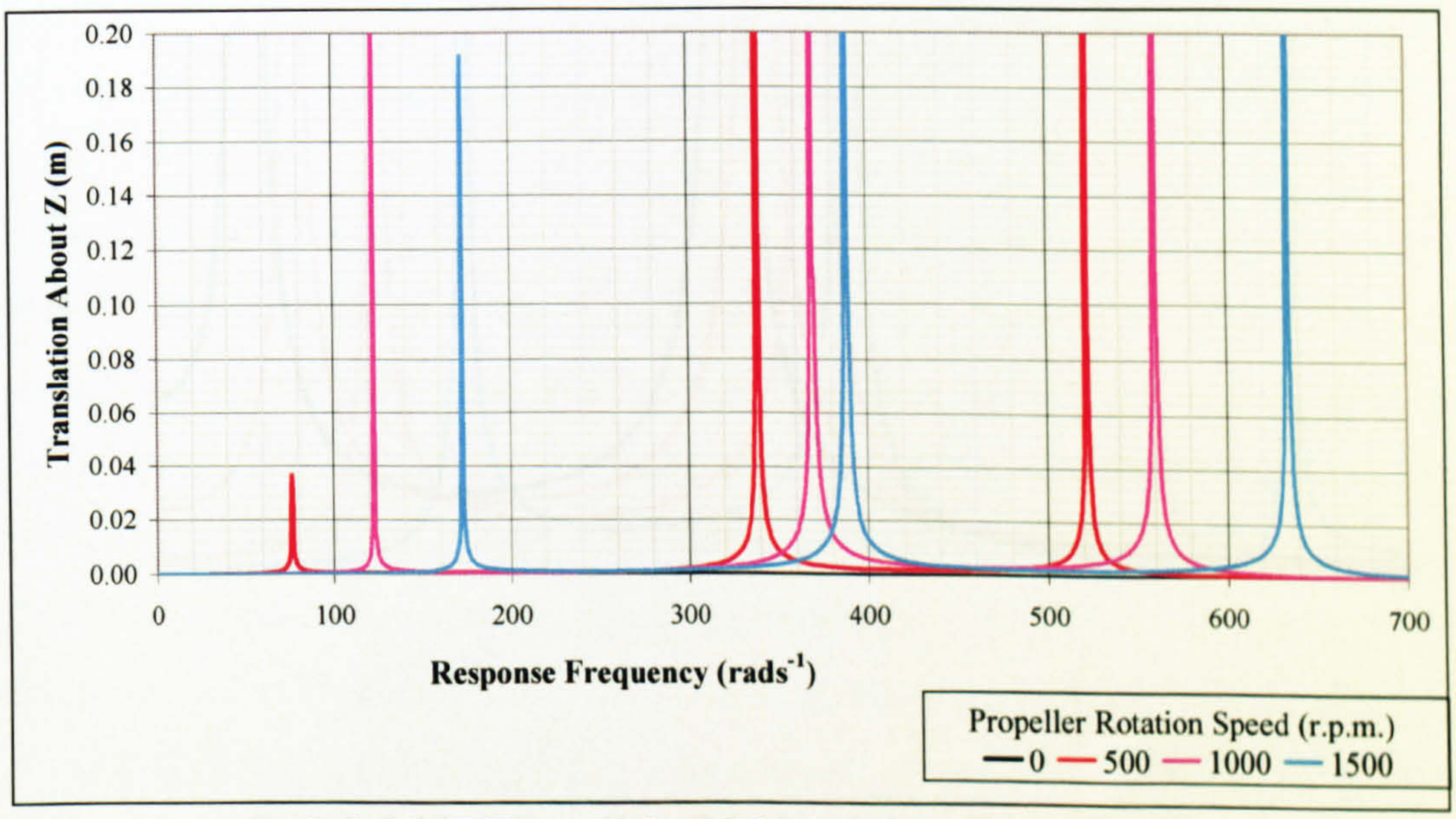

Graph 9.16: Z Translation Of Aluminium Propeller Tip

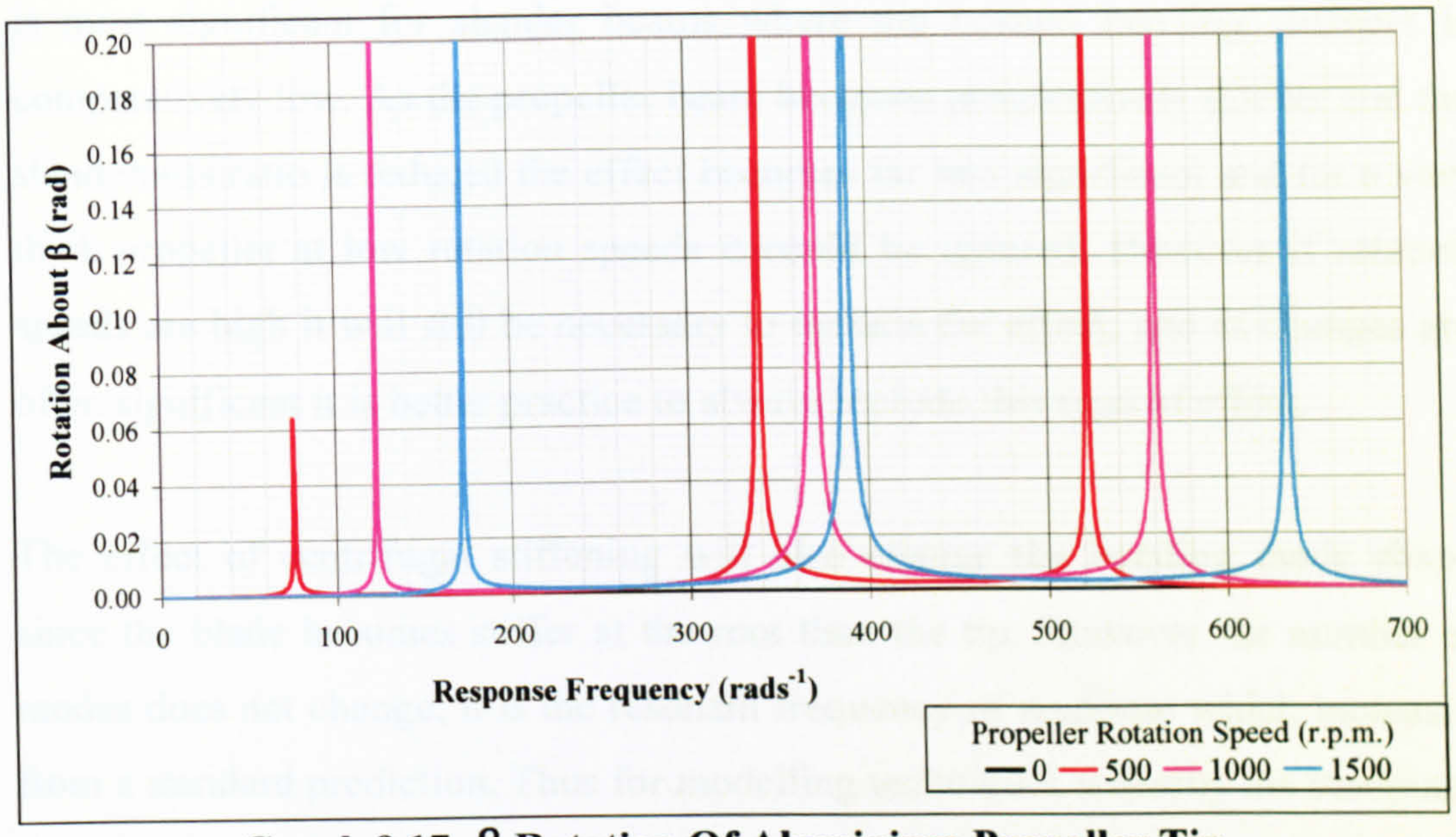

Graph 9.17: β Rotation Of Aluminium Propeller Tip

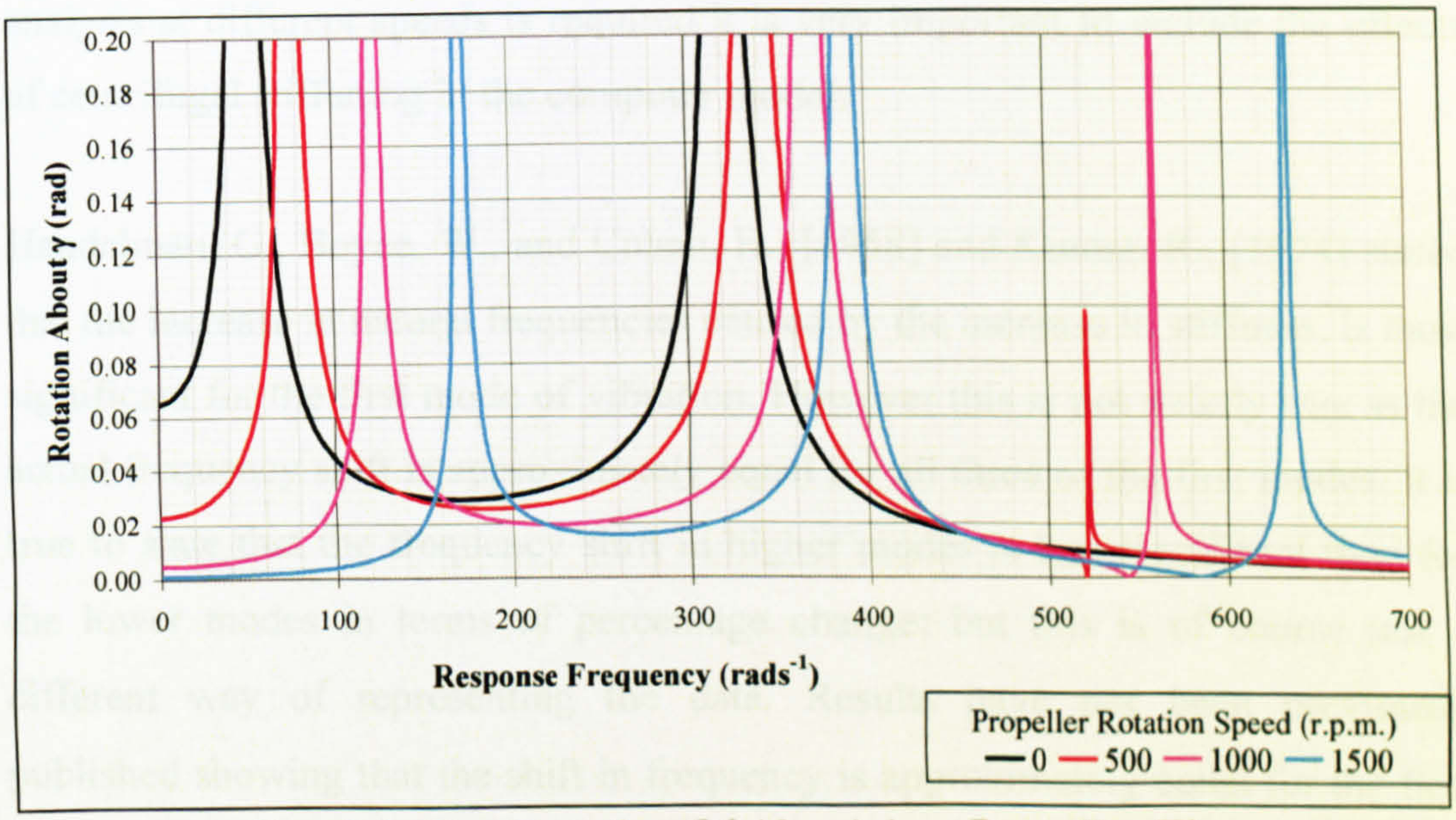

Graph 9.18: γ Rotation Of Aluminium Propeller Tip

9.5 SUMMARY

This chapter presents results for propellers including the effects of centrifugal stiffening derived in Chapter 6. Eigenvalues have been verified against results published by Wright et al., [1982]. As expected the increase in bending mode stiffness due to the axial stress caused by centrifugal stiffening increases the natural response frequencies, this continues to increase with rotation speed. This

is most significant for slender beams where the normal bending stiffness is comparatively low. As the propeller beam becomes progressively thicker and the slenderness ratio is reduced the effect becomes far less significant and for a very thick propeller at low rotation speeds it could be ignored. However if rotation speeds are high it will still be necessary to include the effect, and as changes are often significant it is better practice to always include this type of effect.

The effect of centrifugal stiffening will also change the bending mode shape since the blade becomes stiffer at the root than the tip. However the number of modes does not change; it is the resonant frequency of response which increases from a standard prediction. Thus for modelling techniques whereby the computer model is 'corrected' to match experimental results it may be deemed possible to ignore the effects and compensate in later model 'correction'. However if analysis at different speeds is required it is very important to include the effects of centrifugal stiffening in the computer model.

Handelman, G., Boyce, W., and Cohen, H., [1958] and Kumar, R., [1974] stated that the increase in natural frequencies caused by the increase in stiffness, is most significant for the first mode of vibration. However this is not strictly true as the actual frequency shift is approximately equal for all three of the first modes. It is true to state that the frequency shift in higher modes is less significant than for the lower modes in terms of percentage change; but this is of course just a different way of representing the data. Results have not been previously published showing that the shift in frequency is approximately equal for the first three modes in this manner.

Finally it is shown that at the same rotation speed the gyroscopic effect is approximately equal to that of centrifugal stiffening for propellers in terms of numerical frequency shift for symmetric propellers. Due to this it is important to include both effects in a model; especially as for some modes of vibration both effects will increase a particular natural frequency making the potential total shift very large indeed. It should be noted that because gyroscopic coupling sometimes lowers a natural frequency this will not always be the case. As the

increase in computation time for such additions is now minimal due to improvements in modern computer speeds it is considered wise to include both effects during modelling.

CHAPTER 10

DISCUSSIONS & CONCLUSIONS

10.1 DISCUSSIONS

Over the past forty or so years since computers have become available for scientific use much effort has been devoted to the study of flexible beam elements for rotor-dynamic analysis. The analysis is of great importance mainly due to the need of improving efficiencies of power plants since vast sums of money are involved. However there are many other problems that this type of analysis is applicable to, some of which include manufacturing equipment, drive shafts, rotor-arms for helicopters, propellers, and turbine blades.

To reduce design costs and improve understanding of such systems complete dynamic modelling of such systems has to be achieved. In recent years since computers has become exponentially more powerful the Finite Element Method has been regarded as the best choice for the approximation of such continuums. The method is very flexible permitting the analysis of structures with complex geometry using a limited number of simple elements. Finite Element modelling is now long established and there are many possible methods of achieving the end goal, the method chosen for this study is the rigid body and flexible element hybrid modelling technique described in Chapter 3. This type of modelling proves much more flexible than a system such as ANSYS uses since it allows the inclusion of rotational point inertias or spring attachments at a distance from the shaft node. Achieving this in ANSYS creates an ill-conditioned stiffness matrix because in each case a finite element of very high stiffness will have to be used.

In the past the programming of a mathematical finite element model demanded a balance between the requirements of high accuracy and computational efficiency. In order to achieve good accuracy a detailed model incorporating all possible effects is required. However this type of detail would create computational problems limiting the practical value of the model. As such much previous research has focused on reducing computational time whilst retaining accuracy. However now since computers are now easily powerful enough to deal with complex modelling techniques the principal issue often boils down to the inclusion of all possible system idiosyncrasies in order to ensure an accurate model. The main objective of this research was to improve the understanding of propeller behaviour since over the course of time there has been considerably less research in the area of rotor-dynamic propeller elements than of shaft elements. To this end the main two considerations are the gyroscopic and centrifugal stiffening effects, because the gyroscopic effect is very different to that of a rotating shaft and the centrifugal stiffening effect does not exist at all in shaft elements.

The theory presented in this thesis permits propeller blades to be modelled using Euler-Bernoulli beam elements. This is a much faster technique than models which employ a fine mesh of small elements. To this end a novel mathematical approach has been used to describe the gyroscopic bending moments and forces of such an element. The literature survey in Chapter 2 shows that an attempt to describe the gyroscopic effects in this manner has not been previously attempted. The method is fully described in Chapter 5. The technique is based on the derivation of a standard Euler gyroscopic matrix for an element rotating about its own axis of symmetry as described in Chapter 4. However the crucial difference when a propeller type element is being considered is that the axis of rotation is now perpendicular to the elements axis of symmetry. Thus the polar moment of inertia per unit length now becomes a variable within the integration. This moment of inertia increases quadratically with the distance away from the axis of rotation. Thus the radial distance of the elemental mass under consideration from the axis of rotation must be considered in the matrix derivation. The final result

shows the effect to be directly dependant on the rotation speed and the radial distance squared as can be expected.

Gyroscopic behaviour is often considered a difficult subject to understand because forces and moments do not necessarily occur in the direction one might initially expect. Additionally where rotation speeds are small or the polar moment of inertia is small it is often possible to produce an accurate model without the inclusion of gyroscopic effects and thus they can get ignored. Gyroscopic motion occurs whenever the axis about which a body is spinning is itself rotating about another axis. A common example of this is a disc rotating on a shaft as shown in Figure 10.1 below. Where the moment is applied about the *z*-axis the reaction is not about the same axis as it would be if the rotor were stationary, but is instead about the *y*-axis, perpendicular to both the applied moment and axis of rotation.

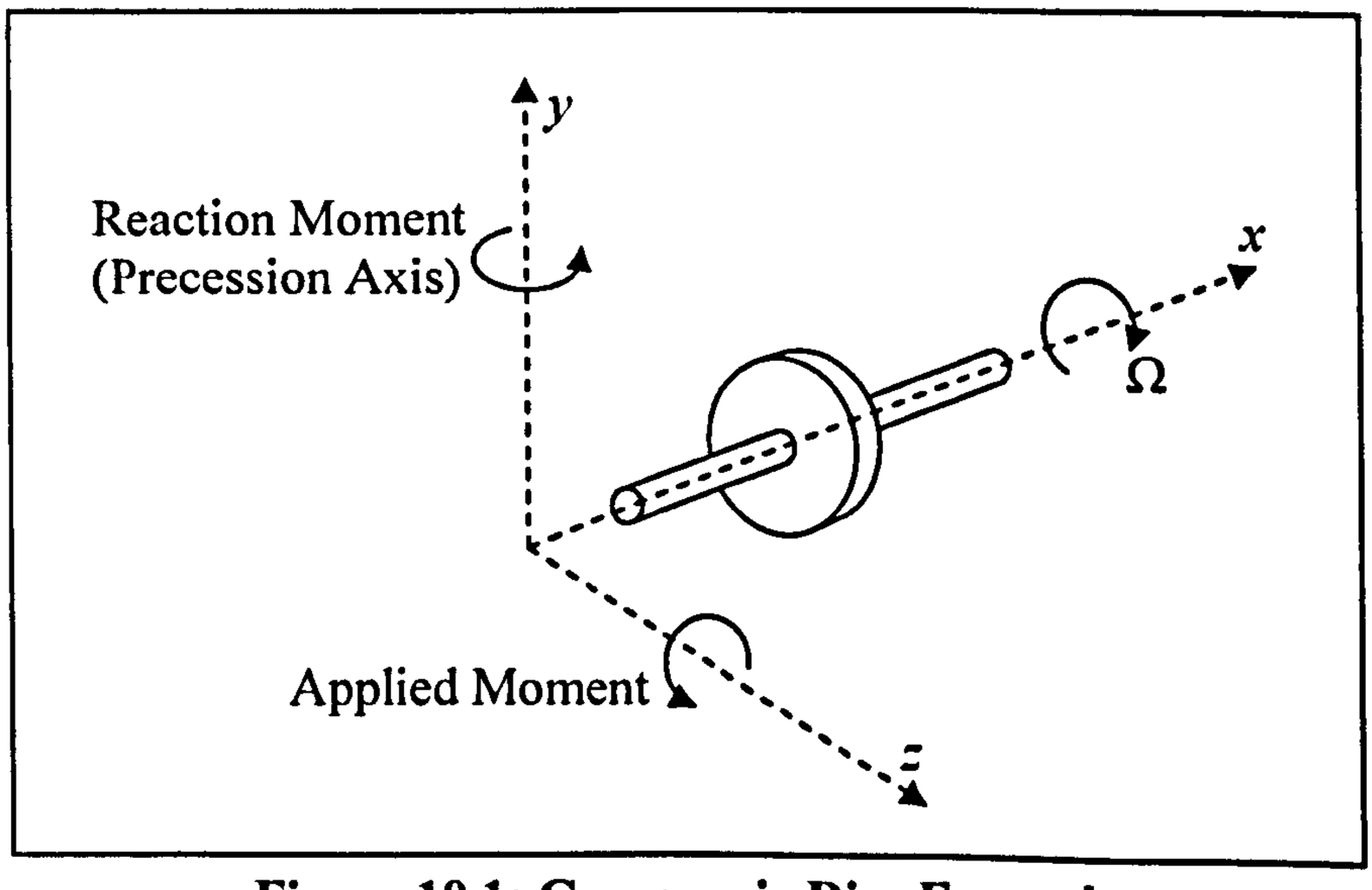

Figure 10.1: Gyroscopic Disc Example

In addition to the coupling effect described above whereby moments (or vibrations) in one axis translate to create moments in another, the gyroscopic forces have a second major effect. That is the splitting of natural frequencies. Gyroscopic forces cause a single natural frequency to split into two frequencies, for a symmetrical system these new natural frequencies tend to be either side of

the original with the spacing increasing with the rotation speed. This is of great importance in the analysis of rotor-dynamic systems as the change in natural frequencies will also change acceptable running conditions. These effects are fully shown for simple propellers in Chapter 8.

The literature survey in Chapter 2 showed there has been more research centred on the centrifugal stiffening effect of propeller elements than the gyroscopic effects. It is the considered opinion of this author that this is due to the centrifugal stiffening not only changing the natural frequencies but also increasing stresses especially at the blade's root. As such the centrifugal stiffening effect presented in this thesis is based on a paper by Hoa, S.V., [1979]. A full derivation is given in Chapter 6 both to improve understanding and because discrepancies were found in the original publication. The final stiffening effect is dependant on the square of the propeller rotation speed, however it must be noted that this stiffening effect is in addition to the static stiffness of the beam and does not replace it.

Unlike the complications involved with the gyroscopic effect, centrifugal stiffening is relatively straightforward to understand. In essence the rotation of a propeller blade creates an axial tension along the length of the blade. This will be greatest at the root and fall to zero at the propeller tip. Since the force will be proportional to the rotation speed squared multiplied by the distance from the axis of rotation. The axial force creates an axial stress which in turn increases the bending stiffness of the propeller blade. This in turn increases the natural frequencies of the system. The effect is proportionally much greater the more slender the initial propeller blade since in this type of system the static bending stiffness will be very small.

The additional bending stiffness does not have the exact same effect on all the natural frequencies, although all the bending frequencies do increase. Handelman, G., Boyce, W., and Cohen, H., [1958] and Kumar, R., [1974] stated that the increase in natural frequencies caused by the increase in stiffness, is most significant for the first mode of vibration. However this is not strictly true as the

frequency shift is approximately equal for all three of the first modes, which has not been previously reported. However it would be correct to state that the frequency shifts of the higher modes are less significant than those of lower modes in terms of percentage frequency shift.

The inclusion of gyroscopic and centrifugal stiffening terms described in this work makes the modelling of propeller blades using Euler finite beam elements a viable proposition. This is a convenient technique that allows a blade to be modelled very simply as a series of connected elements rather than using a fine mesh of elements. Since rectangular section elements can easily be derived a propeller can be modelled to include a changing cross-section size along its length and any twist along its axis of symmetry. Euler beam theory is not limited to the round or rectangular matrices used in this study (for shafts or propellers respectively). Should the analysis of a different cross section shape be required it is possible to determine the second moment of area and shear modulus without the need for major changes. Thus the modelling procedure becomes even more flexible. The associated changes in bending mode shapes and frequencies can then be accounted for.

10.2 CONCLUSIONS

The aim of the present research to develop an Euler finite beam element capable of modelling propellers with particular attention given to the gyroscopic and centrifugal stiffening effects has been achieved. The results of this work have particular applications to wind turbine blades, helicopter rotors, or other propellers. Furthermore some more research into the standard gyroscopic shaft formulation has been performed.

The findings of the research can be summarised as follows:

- For shaft analysis it has previously been published that Timoshenko theory is superior to Euler theory for thick beams, for example; Lee, C.W., [1993]. However results in Chapter 7 show that for shafts up to 0.5

metres in diameter rotating at up to 40 Hz Euler theory achieves almost identical results and is more than adequate for computational analysis. Even though at 48 metres long one may assume the shaft to be slender this is not really case since it has so many support positions along its length.

- For the Euler gyroscopic propeller element coupling is demonstrated, whereby lateral vibrations in one plane are translated creating coupled vibrations in a perpendicular plane. Also the 'splitting' of natural frequencies has been established in Chapter 8. This shows as a single natural beam frequency becoming two natural frequencies either side of the original, the separation increasing with rotation speed. Where more complex (non-symmetric) propeller blades are analysed this effect often becomes a frequency shift instead.

- Results show that for propellers lateral changes in system response due to gyroscopic forces must not be ignored due to the possibility of significant changes in system behaviour. The effect is greater the closer the width and thickness of the blade are dimensionally, since the coupled natural frequencies in both axes are then closer together. The change is also more significant for more flexible (slender) blades.

- The increase in bending stiffness due to centrifugal stiffening increases the natural frequencies of vibration. These frequencies continue to increase with rotation speed although not exponentially so since the propeller has a static bending stiffness also.

- Frequency change is most significant for slender beams where the static bending stiffness is comparatively low. As the propeller beam becomes progressively thicker and the slenderness ratio is reduced the effect becomes far less insignificant and if rotation speeds are also very low centrifugal stiffening could be ignored.

- The gyroscopic effect may increase or decrease a natural frequency, thus in some instances the combined increase from gyroscopic and centrifugal stiffening will create a dramatic frequency change from a static prediction.

- Finally it should be noted that for propeller analysis it is equally important to include gyroscopic effects and centrifugal stiffening effects since both are approximately equal in magnitude. The methods used here are considered superior to the simplistic approach at attaching a rotational point disc inertia.

10.3 FURTHER WORK

The primary aim of developing a finite element capable of simulating a propeller including gyroscopic motion due to bending and centrifugal stiffening due to centrifugal forces has been realised. However there are further refinements that could be achieved.

- Firstly the techniques described could be used to produce a Timoshenko propeller element, doing this and using the same solver would be useful to demonstrate any limitations between Timoshenko and Euler models.

- Secondly although the main gyroscopic effect due to bending has been formulated there are two more possible displacements that will induce gyroscopic moments. There is rotation of the element about its own axis of symmetry to consider. This will produce a gyroscopic moment similar in direction and derivation to that produced here. Rough calculations show that for most blades the change in inertia will be less than 5% of that due to bending for the same degree of rotation of the blade's root, thus the effect is considerably smaller than that due to bending. There is also the moment produced by an axial extension of a propeller blade. For

many blade types this will be insignificant since the axial extension will be close to zero. However a universal code should be capable of analysing all blade types including highly flexible materials which will extend, or indeed blades with exceedingly high rotation speeds.

- Finally an experimental model could be set up in order to fully validate the gyroscopic coupling effects on a propeller blade, however it is this authors belief that since the work done is analytical experimental methods are unnecessary with the modelling type of verification already performed being sufficient.

REFERENCES

Abbas, B.A.H., [1979] "Simple Finite Elements for Dynamic Analysis of Thick Pre-Twisted Blades" *Aeronautical Journal,* Vol. 83, pp 450-453

Al-Ansary, M.D., [1998] "Flexural Vibrations of Rotating Beams Considering Rotary Inertia" *Journal of Computers and Structures,* Vol. 69, pp 321-328

Aleyaasin, M., Ebrahimi, M., and Whalley, R., [2000] "Flexural Vibration of Rotating Shafts by Frequency Domain Hybrid Modelling" *Journal of Computers and Structures,* Vol. 79, pp 319-331

ANSYS Theory reference 001099 Ninth Edition 14.16.5 SAS IP, Inc.©

Bauer, H.F., and Eidel, W., [1988] "Vibration of a Rotating Uniform Beam, Part II: Orientation Perpendicular to the Axis of Rotation" *Journal of Sound and Vibration,* Vol. 122(2), pp 357-375

Bir, G., and Stol, K., [1999] "Operating Modes of a Teetered-Rotor Wind Turbine" *International Modal Analysis Conference* NREL/CP-500-25983

Carnegie, W., [1959] "Vibrations of Rotating Cantilever Blading: Theoretical Approaches to the Frequency Problem Based on Energy Methods" *Journal of Mechanical Engineering Science,* Vol. 1(3), pp 235-240

Carnegie, W., [1964] "Vibrations of Pre-Twisted Cantilever Blading Allowing for Rotary Inertia and Shear Deflection" *Journal of Mechanical Engineering Science,* Vol. 6(2), pp 105-109

Carnegie, W., Stirling, C., and Fleming, J., [1965-66] "Vibration Characteristics of Turbine Blading Under Rotation; Results of an Initial Investigation and Details of a High-Speed Test Installation" *Proceedings of the Institute of Mechanical Engineers,* Vol. 180(3), pp 124-132

Chatelet, E., D'Ambrosio, F., and Jacquet-Richardet, G., [2005] "Toward global modelling approaches for dynamic analyses of rotating assemblies of turbomachines" *Journal of Sound and Vibration,* Vol. 282(1-2), pp 163-178

Chen, C.L., and Chen, L.W., [2002] "Random Vibration of a Rotating Blade with External and Internal Damping by the Finite Element Method" *Journal of Sound and Vibration,* Vol. 252(4), pp 697-715

Chen, L.W., and Ku, D.M., [1991] "Finite Element Analysis of Natural Whirl Speeds of Rotating Shafts" *Journal of Computers and Structures,* Vol. 40, pp 741-747

Cowper, G.R., [1966] "The Shear Coefficient in Timoshenko's Beam Theory" *Journal of Applied Mechanics,* pp 335-340

Davis, R., Henshell, R.D., and Warburton, G.B., [1972] "A Timoshenko Beam Element" *Journal of Sound and Vibration,* Vol. 22(4), pp 475-487

Dokainish, M.A., and Rawtani, S., [1971] "Vibration Analysis of Rotating Cantilever Plates" *International Journal for Numerical Methods in Engineering* Vol. 3, pp 233-248

Esat, I.I., [1993] "Mathematical Modelling of Small Amplitude Oscillation of Multi-Body Systems" *Journal of machine vibration* Vol. 2, pp 30-35

Esat, I.I., et al. [1997] "Hybrid Modelling; Mixed Rigid and Flexible Systems" *ASME Journal,* 97-AA-91

Esat, I.I., [2002] Vibratio Computer Code Formulations

Esat, I.I., Banisoleiman, K., and Jones, S., [2002] "Modelling and Analysis of Stresses in a Flexible Shafting System Under Harmonic Excitations" *Integrated Design and Process Technology Conference* June 2002 Society for Design and Process Science

Gasch, R., [1976] "Vibration of Large Turbo-Rotors in Fluid-Film Bearings on an Elastic Foundation" *Journal of Sound and Vibration,* Vol. 47(1), pp 53-73

Genta, G., [1985] "Consistent Matrices in Rotor Dynamics" *Meccanica,* Vol. 20, pp 235-248

Genta, G., and Tonoli, A., [1996] "A Harmonic Finite Element for the Analysis of Flexural, Torsional and Axial Rotordynamic Behaviour of Discs" *Journal of Sound and Vibration,* Vol. 196(1), pp 19-43

Genta, G., and Tonoli, A., [1997] "A Harmonic Finite Element for the Analysis of Flexural, Torsional and Axial Rotordynamic Behaviour of Blade Arrays" *Journal of Sound and Vibration,* Vol. 207(5), pp 693-720

Gmür, T.C., and Rodrigues J.D., [1991] "Shaft Finite Elements for Rotor Dynamics Analysis" *Transactions of the ASME, Journal of Vibration and Acoustics,* Vol. 113, pp 482-493

Green, R.B., [1948] "Gyroscopic Effects on the Critical Speeds of Flexible Rotors" *Journal of Applied Mechanics,* Vol. 70, pp 369-376

Handelman, G., Boyce, W., and Cohen, H., [1958] "Vibrations of a Uniform Rotating Beam with Tip Mass" *Proceedings of the Third U.S. National Congress of Applied Mechanics,* pp 175-180

Hoa, S.V., [1978] "Vibration Frequency of a Curved Beam with Tip Mass" *Journal of Sound and Vibration,* Vol. 61(3), pp 427-436

Hoa, S.V., [1979] "Vibration of a Rotating Beam with Tip Mass" *Journal of Sound and Vibration,* Vol. 67(3), pp 369-381

Hodges, D.H., [1979] "Vibration and Response of Non-Uniform Rotating Beams with Discontinuities" *Journal of the American Helicopter Society,* Vol. 24(5), pp 43-50

Hong, S-W., and Park, J-H., [1999] "Dynamic Analysis of Multi-Stepped Distributed Parameter Rotor-Bearing Systems" *Journal of Sound and Vibration,* Vol. 227(4), pp 769-785

Huang, B.W., and Huang, J.H., [2001] "Mode Localization in a Rotating Mistuned Turbo Disk with Coriolis Effect" *International Journal of Mechanical Sciences,* Vol. 43, pp 1643-1660

Jacquet-Richardet, G., Ferraris, G., and Rieutord, P., [1996] "Frequencies and Modes of Rotating Flexible Bladed Disc-Shaft Assemblies: A Global Cyclic Symmetry Approach" *Journal of Sound and Vibration,* Vol. 191(5), pp 901-915

Jeffcott, H.H., [1919] "The Lateral Vibration of Loaded Shafts in the Neighbourhood of a Whirling Speed – The Effect of Want of Balance" *Philosophical Magazine* Series 6, Vol. 37, pp 304

Jones, L.H., [1975] "The Transverse Vibration of a Rotating Beam with Tip Mass: The Method of Integral Equations" *Quarterly of Applied Mathematics,* Vol. XXXIII(3), pp193-203

Jones, S., and Esat, I., [2003] "Gyroscopic Beam Element Matrix Derivation and Results" *Society for Design and Process Science; Integrated Design and Process Technology Conference, December 2003.*

Kapoor, K.K., and Hartz, B.J., [1966] "Stability of Plates Using the Finite Element Method" *Journal of the Engineering Mechanics Division, Proceedings of the American Society of Civil Engineers* EM2, pp 177-195

Kapur, K.K., [1966] "Vibrations of a Timoshenko Beam, Using a Finite Element Approach" *Journal of the Acoustical Society of America* Vol. 40(5) pp 1058-1063

Kim, Y.D., and Lee, C.W., [1986] "Finite Element Analysis of Rotor Bearing Systems Using a Modal Transformation Matrix" *Journal of Sound and Vibration,* Vol. 111(3), pp 441-456

Kumar, R., [1974] "Vibrations of Space Booms Under Centrifugal Force Field" *Canadian Aeronautics and Space Institute Transactions* Vol. 7(1), pp 1-5

Lamb, F.R.S., and Southwell, R.V., [1921] "The Vibrations of a Spinning Disk" pp 272-280

Lee, C.W., [1993]. "Vibration Analysis of Rotors" *Kluver Academic Publishers Dordrecht.* ISBN 0-7923-2300-9

Łuczko, J., [2002] "A Geometrically Non-Linear Model of Rotating Shafts with Internal Resonance and Self-Excited Vibration" *Journal of Sound and Vibration,* Vol. 255(3), pp 433-456

Magari, P.J., and Shultz, L.A., [1987] "Development of a Rotating Blade Finite Element with an Application to the Analysis of Helicopter Rotorsystems" *American Institute of Aeronautics and Astronautics, Inc.*, pp 17-27

Mohiuddin, M.A., and Khulief, Y.A., [1999] "Coupled Bending Torsional Vibration of Rotors Using Finite Element" *Journal of Sound and Vibration,* Vol. 223(2), pp 297-316

Morton, P.G., [1968] "Influence of Coupled Asymmetric Bearings on the Motion of a Massive Flexible Rotor" *Applied Mechanics Group. Proc. Institute of Mechanical Engineers* Vol. 182(1), pp 255

Naguleswaran, S., [1994] "Lateral Vibration of a Centrifugally Tensioned Uniform Euler-Bernoulli Beam" *Journal of Sound and Vibration,* Vol. 176(5), pp 613-624

Nelson, H.D., [1977] "A Finite Rotating Shaft Element Using Timoshenko Beam Theory" *Engineering Research Centre Report ERC-R-77023, Arizona State University*, pp 61

Nelson, H.D., [1980] "A Finite Rotating Shaft Element Using Timoshenko Beam Theory" *Journal of Mechanical Design,* Vol. 102, pp 793-803

Nelson, H.D., and McVaugh, J.M., [1976] "The Dynamics of Rotor-Bearing Systems Using Finite Elements" *Journal of Engineering for Industry,* Vol. 98, pp 593-600

Peters, D.A., [1973] "An Approximate Solution for the Free Vibrations of Rotating Uniform Cantilever Beams" *NASA Technical Memorandum,* N78-33289

Putter, S., and Manor, H., [1978] "Natural Frequencies of Radial Rotating Beams" *Journal of Sound and Vibration* Vol. 56(2), pp 175-185

Rankine, W.A., [1879] "On the Centrifugal Force of Rotating Shafts" *Engineer, London* Vol. 27, pp 249

Rao, J.S., and Carnegie, W., [1969] "Non-Linear Vibrations of Rotating Cantilever Beams" *The Aeronautical Journal of the Royal Aeronautical Society,* Vol. 74, pp 161-165

Rouch, K.E., and Kao, J.S. [1979] "A Tapered Beam Finite Element for Rotor Dynamics Analysis" *Journal of Sound and Vibration,* Vol. 66(1), pp 119-140

Ruhl, R.L., [1970] "Dynamics of Distributed Parameter Turbo-Rotor Systems: Transfer Matrix and Finite Element Techniques" *PhD Thesis, Cornell University, Ithaca, N.Y.*

Ruhl, R.L., and Booker, J.F., [1972] "A Finite Element Model for Distributed Parameter Turbo-Rotor Systems" *Transactions of the ASME, Journal of Engineering for Industry,* Vol. 94. pp 126-132

Sakata, M., Kimura, K., Park, S.K.,. and Ohnabe, H., [1989] "Vibration of Bladed Flexible Rotor Due to Gyroscopic Moment" *Journal of Sound and Vibration,* Vol. 131(3), pp 417-430

Sauer, G., and Wolf, M., [1989] "Finite Element Analysis of Gyroscopic Effects" *Finite Elements in Analysis and Design,* Vol. 5, pp 131-140

Southwell, and Gough., [1921] "The Free Transverse Vibration of Airscrew Blades" *British A.R.C. Report and Memoranda,* No. 766

Stafford, R.O., and Giurgiutiu, V., [1975] "Semi-Analytic Methods for Rotating Timoshenko Beams" *International Journal of Mechanical Science,* Vol. 17, pp 719-727

Stephen, N.G., and Wang, P.J., [1986] "Stretching and Bending of Rotating Beam" *Journal of Applied Mechanics,* Vol. 53, pp 869-872

Thomas, D.L., Wilson, J.M., and Wilson R.R., [1973] "Timoshenko Beam Finite Elements" *Journal of Sound and Vibration,* Vol. 31(3), pp 315-330

Thomas, J., and Abbas, B.A.H., [1975] "Finite Element Model for Dynamic Analysis of Timoshenko Beam" *Journal of Sound And Vibration,* Vol. 41(3), pp291-299

Thomson, W.T., [1993] "Theory of Vibration with Applications" *Fourth Edition, Published by Chapman & Hall,* ISBN 0 412 54620 5

Timoshenko, S.P., [1922] "On the Transverse Vibrations of Bars of Uniform Cross-Section" *Philosophical Magazine,* Vol. 43, pp 125-131

Wang, J.T.S., Mahrenholtz, O., and Böhm, J., [1976] "Extended Galerkin's Method for Rotating Beam Vibrations Using Legendre Polynomials" *Solid Mechanics Archives,* Vol. 1, pp341-365

Wright, A.D., Smith, C.E., Thresher, R.W., and Wang, J.L.C., [1982] "Vibration Modes of Centrifugally Stiffened Beams" *Journal of Applied Mechanics,* Vol. 49, pp 197-202

Xiong, G.L., Yi, J.M., Zeng, C., Guo, H.K., and Li, L.X., [2003] "Study of the Gyroscopic Effect of the Spindle on the Stability Characteristics of the Milling System" *Journal of Materials Processing Technology,* Vol. 138, pp 379-384

Yang, J.B., Jiang, L.J., and Chen, D.CH., [2004] "Dynamic Modelling and Control of a Rotating Euler-Bernoulli Beam" *Journal of Sound and Vibration,* Vol. 274, pp 863-875

Yigit, A., Scott, R.A., and Galip-Ulsoy, A., [1988] "Flexural Motion of a Radially Rotating Beam Attached to a Rigid Body" *Journal of Sound and Vibration,* Vol. 121(2), pp 201-210

Yoo, H.H., and Shin, S.H., [1998] "Vibration Analysis of Rotating Cantilever Beams" *Journal of Sound and Vibration,* Vol. 212(5), pp 807-828

Yoo, H.H., Park, J.H., and Park, J., [2001] "Vibration Analysis of Rotating Pre-Twisted Blades" *Journal of Computers and Structures,* Vol. 79, pp 1811-1819

Zienkiewicz, O.C., [1971] "The Finite Element Method in Engineering Science" *2nd Edition, McGraw-Hill Publishing Company Ltd.*

Zienkiewicz, O.C., and Morgan, K., [1983] "Finite Elements and Approximation" *John Wiley & Sons Inc.* 0-471-89089-8

Zienkiewicz, O.C., and Taylor, R.L., [1988] "The Finite Element Method: Basic Formulation and Linear Problems" *4th Edition, McGraw-Hill Publishing Company Ltd.* Vol. 1

Zienkiewicz, O.C., and Taylor, R.L., [2000] "The Finite Element Method: The Basics" 5th *Edition, Butterworth-Heinemann Publishing Company Ltd.* Vol. 1

Zorzi, E.S., and Nelson, H.D., [1977] "Finite Element Simulation of Rotor-Bearing Systems with Internal Damping" *Journal of Engineering for Power,* Vol. 99(1), pp 71-76

Zorzi, E.S., and Nelson, H.D., [1980] "The Dynamics of Rotor-Bearing Systems with Axial Torque; A Finite Element Approach" *Transactions of the ASME, Journal of Mechanical Design,* Vol. 102, pp 158-161

Zou, C-P., Hua, H-X., and Chen, D-S., [2002] "Modal Synthesis Method of Lateral Vibration Analysis for Rotor-Bearing System" *Journal of Computers and Structures,* Vol. 80, pp 2537-2549

APPENDIX

ELEMENT MATRICES

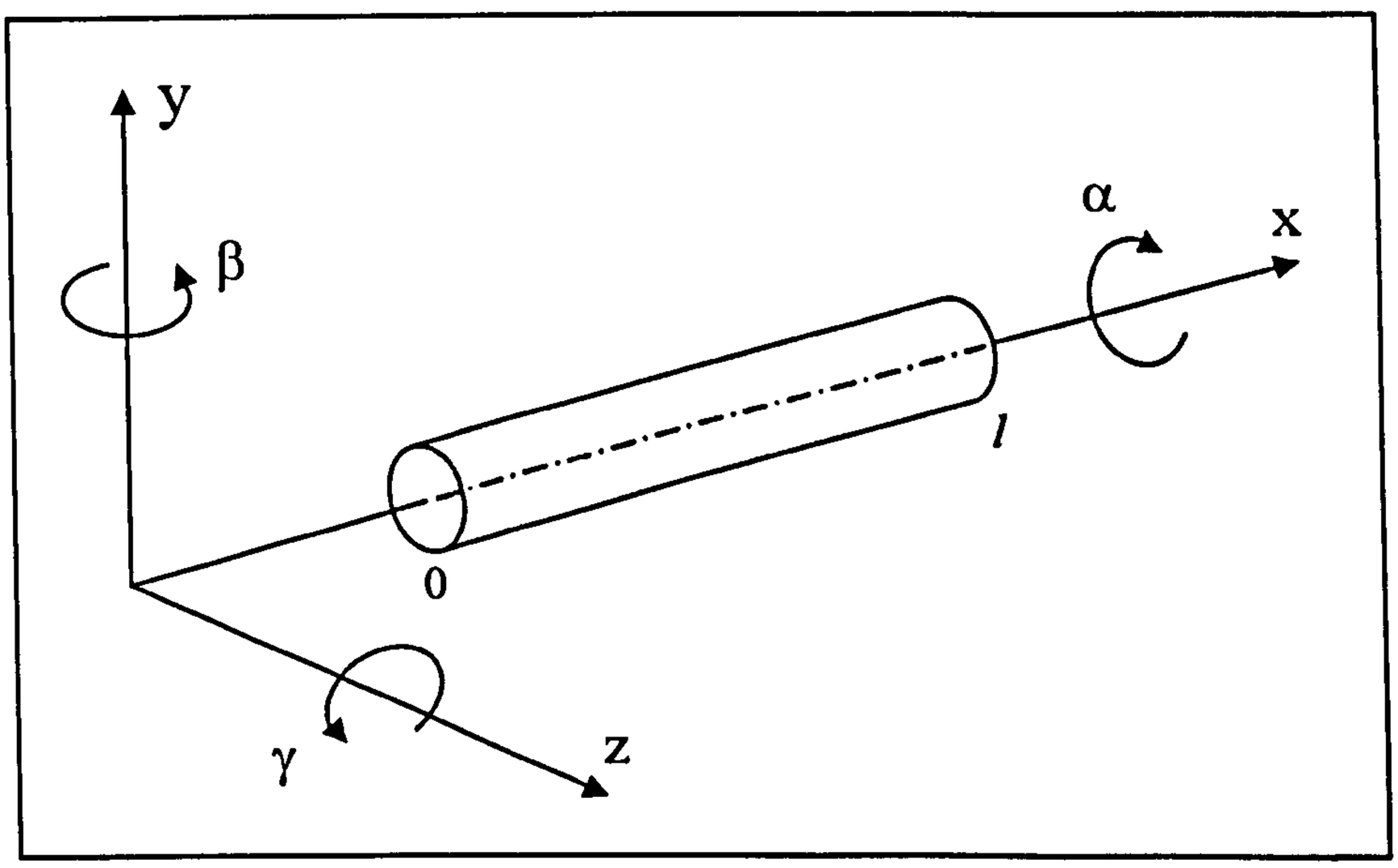

Figure A.1: Element Axis System

The displacement vector is as follows for all matrices:

$$u_k^T = (x_0 \quad y_0 \quad z_0 \quad \alpha_0 \quad \beta_0 \quad \gamma_0 \quad x_1 \quad y_1 \quad z_1 \quad \alpha_1 \quad \beta_1 \quad \gamma_1)$$

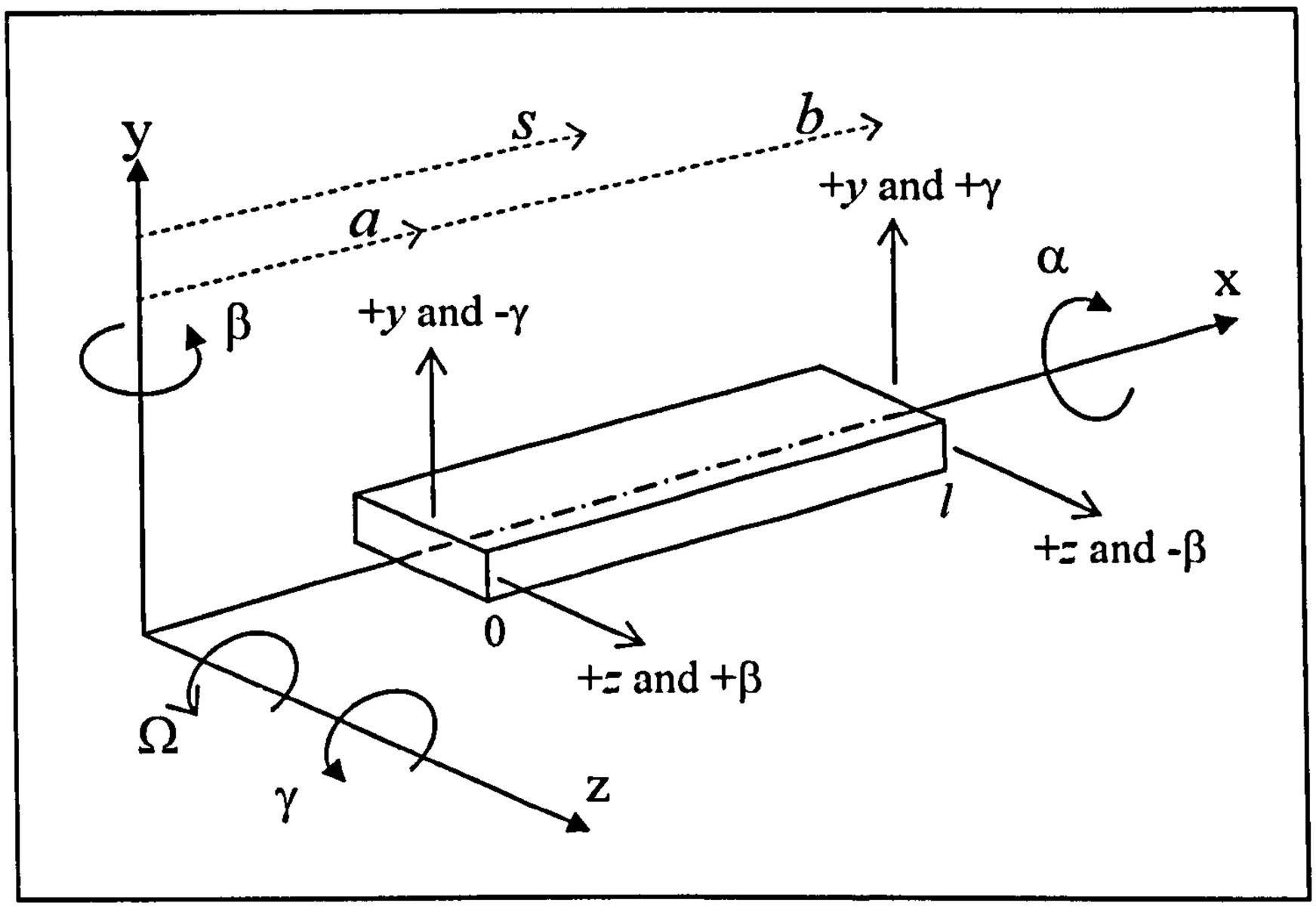

Figure A.2: Gyroscopic Propeller Definitions

Note: a, b and s are global distances from the axis of rotation

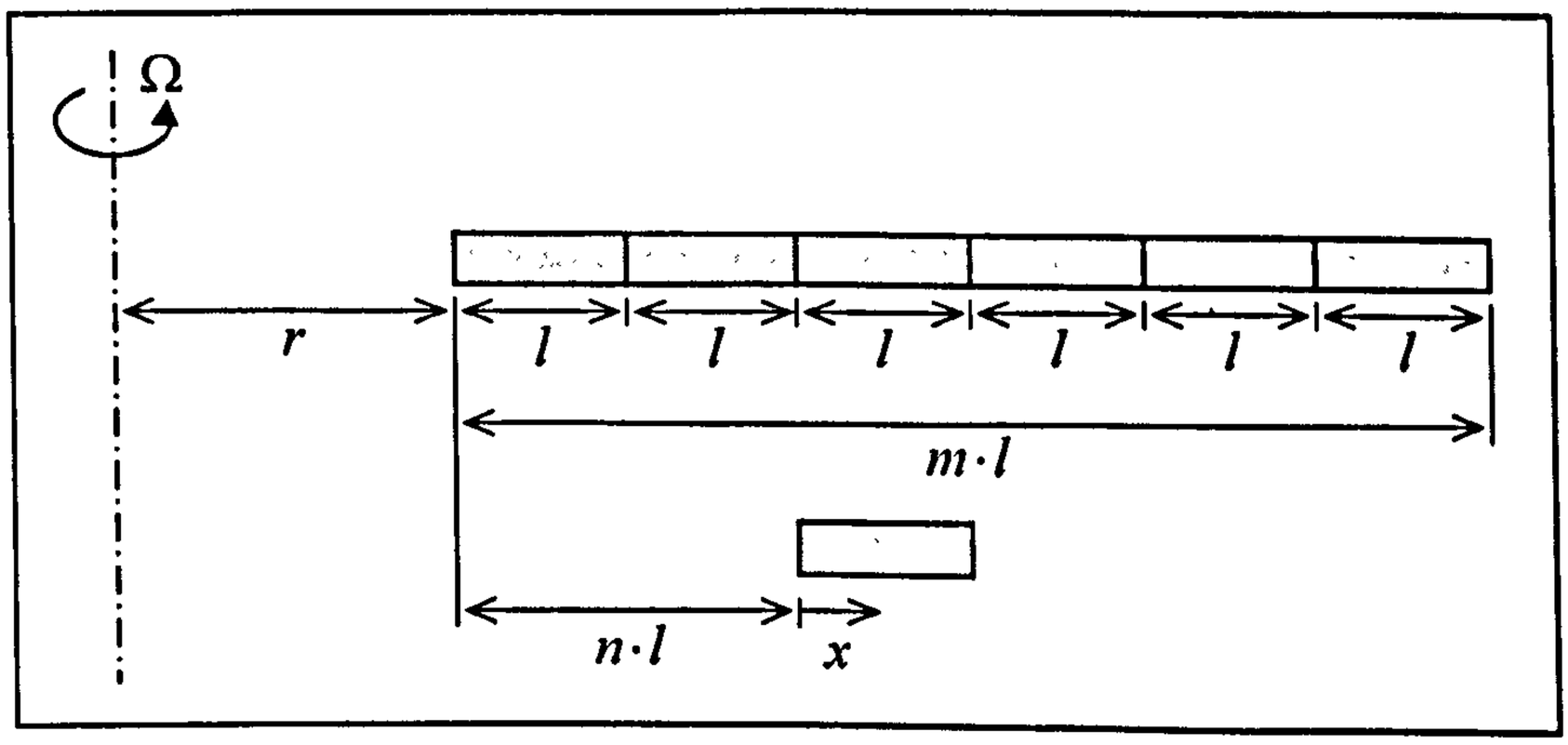

Figure A.3: Centrifugal Stiffening Propeller Definitions

A.1 Mass Element Bending Matrix

$$[M_k]=\begin{bmatrix}
0 & 0 & 0 & 0 & 0 & 0 & 0 & 0 & 0 & 0 & 0 & 0 \\
0 & \frac{13l\mu}{35} & 0 & 0 & 0 & \frac{11l^2\mu}{210} & 0 & \frac{9l\mu}{70} & 0 & 0 & 0 & -\frac{13l^2\mu}{420} \\
0 & 0 & \frac{13l\mu}{35} & 0 & -\frac{11l^2\mu}{210} & 0 & 0 & 0 & \frac{9l\mu}{70} & 0 & \frac{13l^2\mu}{420} & 0 \\
0 & 0 & 0 & 0 & 0 & 0 & 0 & 0 & 0 & 0 & 0 & 0 \\
0 & 0 & -\frac{11l^2\mu}{210} & 0 & \frac{l^3\mu}{105} & 0 & 0 & 0 & -\frac{13l^2\mu}{420} & 0 & -\frac{l^3\mu}{140} & 0 \\
0 & \frac{11l^2\mu}{210} & 0 & 0 & 0 & \frac{l^3\mu}{105} & 0 & \frac{13l^2\mu}{420} & 0 & 0 & 0 & -\frac{l^3\mu}{140} \\
0 & 0 & 0 & 0 & 0 & 0 & 0 & 0 & 0 & 0 & 0 & 0 \\
0 & \frac{9l\mu}{70} & 0 & 0 & 0 & \frac{13l^2\mu}{420} & 0 & \frac{13l\mu}{35} & 0 & 0 & 0 & -\frac{11l^2\mu}{210} \\
0 & 0 & \frac{9l\mu}{70} & 0 & -\frac{13l^2\mu}{420} & 0 & 0 & 0 & \frac{13l\mu}{35} & 0 & \frac{11l^2\mu}{210} & 0 \\
0 & 0 & 0 & 0 & 0 & 0 & 0 & 0 & 0 & 0 & 0 & 0 \\
0 & 0 & \frac{13l^2\mu}{420} & 0 & -\frac{l^3\mu}{140} & 0 & 0 & 0 & \frac{11l^2\mu}{210} & 0 & \frac{l^3\mu}{105} & 0 \\
0 & -\frac{13l^2\mu}{420} & 0 & 0 & 0 & -\frac{l^3\mu}{140} & 0 & -\frac{11l^2\mu}{210} & 0 & 0 & 0 & \frac{l^3\mu}{105}
\end{bmatrix}$$

A.2 Mass Element Axial Deformation Matrix

$$[M_k]=\begin{bmatrix}
\frac{\mu l}{3} & 0 & 0 & 0 & 0 & 0 & \frac{\mu l}{6} & 0 & 0 & 0 & 0 & 0 \\
0 & 0 & 0 & 0 & 0 & 0 & 0 & 0 & 0 & 0 & 0 & 0 \\
0 & 0 & 0 & 0 & 0 & 0 & 0 & 0 & 0 & 0 & 0 & 0 \\
0 & 0 & 0 & 0 & 0 & 0 & 0 & 0 & 0 & 0 & 0 & 0 \\
0 & 0 & 0 & 0 & 0 & 0 & 0 & 0 & 0 & 0 & 0 & 0 \\
0 & 0 & 0 & 0 & 0 & 0 & 0 & 0 & 0 & 0 & 0 & 0 \\
\frac{\mu l}{6} & 0 & 0 & 0 & 0 & 0 & \frac{\mu l}{3} & 0 & 0 & 0 & 0 & 0 \\
0 & 0 & 0 & 0 & 0 & 0 & 0 & 0 & 0 & 0 & 0 & 0 \\
0 & 0 & 0 & 0 & 0 & 0 & 0 & 0 & 0 & 0 & 0 & 0 \\
0 & 0 & 0 & 0 & 0 & 0 & 0 & 0 & 0 & 0 & 0 & 0 \\
0 & 0 & 0 & 0 & 0 & 0 & 0 & 0 & 0 & 0 & 0 & 0
\end{bmatrix}$$

A.3 Mass Element Torsional Deformation Matrix

$$[M_k]=\begin{bmatrix}
0 & 0 & 0 & 0 & 0 & 0 & 0 & 0 & 0 & 0 & 0 & 0 \\
0 & 0 & 0 & 0 & 0 & 0 & 0 & 0 & 0 & 0 & 0 & 0 \\
0 & 0 & 0 & 0 & 0 & 0 & 0 & 0 & 0 & 0 & 0 & 0 \\
0 & 0 & 0 & \frac{\mu r^2 l}{6} & 0 & 0 & 0 & 0 & 0 & \frac{\mu r^2 l}{12} & 0 & 0 \\
0 & 0 & 0 & 0 & 0 & 0 & 0 & 0 & 0 & 0 & 0 & 0 \\
0 & 0 & 0 & 0 & 0 & 0 & 0 & 0 & 0 & 0 & 0 & 0 \\
0 & 0 & 0 & 0 & 0 & 0 & 0 & 0 & 0 & 0 & 0 & 0 \\
0 & 0 & 0 & 0 & 0 & 0 & 0 & 0 & 0 & 0 & 0 & 0 \\
0 & 0 & 0 & \frac{\mu r^2 l}{12} & 0 & 0 & 0 & 0 & 0 & \frac{\mu r^2 l}{6} & 0 & 0 \\
0 & 0 & 0 & 0 & 0 & 0 & 0 & 0 & 0 & 0 & 0 & 0 \\
0 & 0 & 0 & 0 & 0 & 0 & 0 & 0 & 0 & 0 & 0 & 0
\end{bmatrix}$$

A.4 Stiffness Element Bending Matrix

$$[K_k]=\begin{bmatrix}
0 & 0 & 0 & 0 & 0 & 0 & 0 & 0 & 0 & 0 & 0 & 0 \\
0 & \frac{12EI}{l^3} & 0 & 0 & 0 & \frac{6EI}{l^2} & 0 & -\frac{12EI}{l^3} & 0 & 0 & 0 & \frac{6EI}{l^2} \\
0 & 0 & \frac{12EI}{l^3} & 0 & -\frac{6EI}{l^2} & 0 & 0 & 0 & -\frac{12EI}{l^3} & 0 & -\frac{6EI}{l^2} & 0 \\
0 & 0 & 0 & 0 & 0 & 0 & 0 & 0 & 0 & 0 & 0 & 0 \\
0 & 0 & -\frac{6EI}{l^2} & 0 & \frac{4EI}{l} & 0 & 0 & 0 & \frac{6EI}{l^2} & 0 & \frac{2EI}{l} & 0 \\
0 & \frac{6EI}{l^2} & 0 & 0 & 0 & \frac{4EI}{l} & 0 & -\frac{6EI}{l^2} & 0 & 0 & 0 & \frac{2EI}{l} \\
0 & 0 & 0 & 0 & 0 & 0 & 0 & 0 & 0 & 0 & 0 & 0 \\
0 & -\frac{12EI}{l^3} & 0 & 0 & 0 & -\frac{6EI}{l^2} & 0 & \frac{12EI}{l^3} & 0 & 0 & 0 & -\frac{6EI}{l^2} \\
0 & 0 & -\frac{12EI}{l^3} & 0 & \frac{6EI}{l^2} & 0 & 0 & 0 & \frac{12EI}{l^3} & 0 & \frac{6EI}{l^2} & 0 \\
0 & 0 & 0 & 0 & 0 & 0 & 0 & 0 & 0 & 0 & 0 & 0 \\
0 & 0 & -\frac{6EI}{l^2} & 0 & \frac{2EI}{l} & 0 & 0 & 0 & \frac{6EI}{l^2} & 0 & \frac{4EI}{l} & 0 \\
0 & \frac{6EI}{l^2} & 0 & 0 & 0 & \frac{2EI}{l} & 0 & -\frac{6EI}{l^2} & 0 & 0 & 0 & \frac{4EI}{l}
\end{bmatrix}$$

A.5 Stiffness Element Axial Deformation Matrix

$$[K_k]=\begin{bmatrix}
\frac{EA}{l} & 0 & 0 & 0 & 0 & 0 & -\frac{EA}{l} & 0 & 0 & 0 & 0 & 0 \\
0 & 0 & 0 & 0 & 0 & 0 & 0 & 0 & 0 & 0 & 0 & 0 \\
0 & 0 & 0 & 0 & 0 & 0 & 0 & 0 & 0 & 0 & 0 & 0 \\
0 & 0 & 0 & 0 & 0 & 0 & 0 & 0 & 0 & 0 & 0 & 0 \\
0 & 0 & 0 & 0 & 0 & 0 & 0 & 0 & 0 & 0 & 0 & 0 \\
0 & 0 & 0 & 0 & 0 & 0 & 0 & 0 & 0 & 0 & 0 & 0 \\
-\frac{EA}{l} & 0 & 0 & 0 & 0 & 0 & \frac{EA}{l} & 0 & 0 & 0 & 0 & 0 \\
0 & 0 & 0 & 0 & 0 & 0 & 0 & 0 & 0 & 0 & 0 & 0 \\
0 & 0 & 0 & 0 & 0 & 0 & 0 & 0 & 0 & 0 & 0 & 0 \\
0 & 0 & 0 & 0 & 0 & 0 & 0 & 0 & 0 & 0 & 0 & 0 \\
0 & 0 & 0 & 0 & 0 & 0 & 0 & 0 & 0 & 0 & 0 & 0 \\
0 & 0 & 0 & 0 & 0 & 0 & 0 & 0 & 0 & 0 & 0 & 0
\end{bmatrix}$$

A.6 Stiffness Element Torsional Deformation Matrix

$$[K_k]=\begin{bmatrix}
0 & 0 & 0 & 0 & 0 & 0 & 0 & 0 & 0 & 0 & 0 & 0 \\
0 & 0 & 0 & 0 & 0 & 0 & 0 & 0 & 0 & 0 & 0 & 0 \\
0 & 0 & 0 & 0 & 0 & 0 & 0 & 0 & 0 & 0 & 0 & 0 \\
0 & 0 & 0 & \frac{GJ}{l} & 0 & 0 & 0 & 0 & 0 & -\frac{GJ}{l} & 0 & 0 \\
0 & 0 & 0 & 0 & 0 & 0 & 0 & 0 & 0 & 0 & 0 & 0 \\
0 & 0 & 0 & 0 & 0 & 0 & 0 & 0 & 0 & 0 & 0 & 0 \\
0 & 0 & 0 & 0 & 0 & 0 & 0 & 0 & 0 & 0 & 0 & 0 \\
0 & 0 & 0 & 0 & 0 & 0 & 0 & 0 & 0 & 0 & 0 & 0 \\
0 & 0 & 0 & -\frac{GJ}{l} & 0 & 0 & 0 & 0 & 0 & \frac{GJ}{l} & 0 & 0 \\
0 & 0 & 0 & 0 & 0 & 0 & 0 & 0 & 0 & 0 & 0 & 0 \\
0 & 0 & 0 & 0 & 0 & 0 & 0 & 0 & 0 & 0 & 0 & 0
\end{bmatrix}$$

A.7 Gyroscopic Element Bending Matrix for Shaft

$$[G_k]=\frac{\Omega\mu r^2}{60l}\begin{pmatrix}
0 & 0 & 0 & 0 & 0 & 0 & 0 & 0 & 0 & 0 & 0 & 0\\
0 & 0 & 36 & 0 & -3l & 0 & 0 & 0 & -36 & 0 & -3l & 0\\
0 & -36 & 0 & 0 & 0 & -3l & 0 & 36 & 0 & 0 & 0 & -3l\\
0 & 0 & 0 & 0 & 0 & 0 & 0 & 0 & 0 & 0 & 0 & 0\\
0 & 3l & 0 & 0 & 0 & 4l^2 & 0 & -3l & 0 & 0 & 0 & -l^2\\
0 & 0 & 3l & 0 & -4l^2 & 0 & 0 & 0 & -3l & 0 & l^2 & 0\\
0 & 0 & 0 & 0 & 0 & 0 & 0 & 0 & 0 & 0 & 0 & 0\\
0 & 0 & -36 & 0 & 3l & 0 & 0 & 0 & 36 & 0 & 3l & 0\\
0 & 36 & 0 & 0 & 0 & 3l & 0 & -36 & 0 & 0 & 0 & 3l\\
0 & 0 & 0 & 0 & 0 & 0 & 0 & 0 & 0 & 0 & 0 & 0\\
0 & 3l & 0 & 0 & 0 & -l^2 & 0 & -3l & 0 & 0 & 0 & 4l^2\\
0 & 0 & 3l & 0 & l^2 & 0 & 0 & 0 & -3l & 0 & -4l^2 & 0
\end{pmatrix}$$

A.8 Gyroscopic Element Bending Matrix for Propeller

$$\mathbf{G}_{e_p}=\frac{\mu\Omega}{210}\begin{pmatrix}
0 & 0 & 0 & 0 & 0 & 0 & 0 & 0 & 0 & 0 & 0 & 0\\
0 & 0 & 36(2a^2+3ab+2b^2) & 0 & -3l(-2a^2+4ab+5b^2) & 0 & 0 & 0 & -36(2a^2+3ab+2b^2) & 0 & 3l(-5a^2-4ab+2b^2) & 0\\
0 & -36(2a^2+3ab+2b^2) & 0 & 0 & 0 & -3l(-2a^2+4ab+5b^2) & 0 & 36(2a^2+3ab+2b^2) & 0 & 0 & 0 & 3l(-5a^2-4ab+2b^2)\\
0 & 0 & 0 & 0 & 0 & 0 & 0 & 0 & 0 & 0 & 0 & 0\\
0 & 3l(-2a^2+4ab+5b^2) & 0 & 0 & 0 & 2l^2(9a^2+3ab+2b^2) & 0 & 3l(2a^2-4ab-5b^2) & 0 & 0 & 0 & -l^2(3a^2+ab+3b^2)\\
0 & 0 & 3l(-2a^2+4ab+5b^2) & 0 & 2l^2(9a^2+3ab+2b^2) & 0 & 0 & 0 & 3l(2a^2-4ab-5b^2) & 0 & l^2(3a^2+ab+3b^2) & 0\\
0 & 0 & 0 & 0 & 0 & 0 & 0 & 0 & 0 & 0 & 0 & 0\\
0 & 0 & -36(2a^2+3ab+2b^2) & 0 & -3l(2a^2-4ab-5b^2) & 0 & 0 & 0 & 36(2a^2+3ab+2b^2) & 0 & 3l(5a^2+4ab-2b^2) & 0\\
0 & 36(2a^2+3ab+2b^2) & 0 & 0 & 0 & -3l(2a^2-4ab-5b^2) & 0 & -36(2a^2+3ab+2b^2) & 0 & 0 & 0 & 3l(5a^2+4ab-2b^2)\\
0 & 0 & 0 & 0 & 0 & 0 & 0 & 0 & 0 & 0 & 0 & 0\\
0 & -3l(-5a^2-4ab+2b^2) & 0 & 0 & 0 & -l^2(3a^2+ab+3b^2) & 0 & -3l(5a^2+4ab-2b^2) & 0 & 0 & 0 & 2l^2(2a^2+3ab+9b^2)\\
0 & 0 & -3l(-5a^2-4ab+2b^2) & 0 & l^2(3a^2+ab+3b^2) & 0 & 0 & 0 & -3l(5a^2+4ab-2b^2) & 0 & -2l^2(2a^2+3ab+9b^2) & 0
\end{pmatrix}$$

A.9 Centrifugal Stiffening Element Matrix for Propeller

$$\mathbf{K}_{e_{cs}} = \mu\Omega^2 \begin{bmatrix}
0 & 0 & 0 & 0 & 0 & 0 & 0 & 0 & 0 & 0 & 0 & 0 \\
0 & A & 0 & 0 & 0 & -D & 0 & -A & 0 & 0 & 0 & -E \\
0 & 0 & A & 0 & D & 0 & 0 & 0 & -A & 0 & E & 0 \\
0 & 0 & 0 & 0 & 0 & 0 & 0 & 0 & 0 & 0 & 0 & 0 \\
0 & 0 & D & 0 & B & 0 & 0 & 0 & -D & 0 & F & 0 \\
0 & -D & 0 & 0 & 0 & B & 0 & D & 0 & 0 & 0 & F \\
0 & 0 & 0 & 0 & 0 & 0 & 0 & 0 & 0 & 0 & 0 & 0 \\
0 & -A & 0 & 0 & 0 & D & 0 & A & 0 & 0 & 0 & E \\
0 & 0 & -A & 0 & -D & 0 & 0 & 0 & A & 0 & -E & 0 \\
0 & 0 & 0 & 0 & 0 & 0 & 0 & 0 & 0 & 0 & 0 & 0 \\
0 & 0 & E & 0 & F & 0 & 0 & 0 & -E & 0 & C & 0 \\
0 & -E & 0 & 0 & 0 & F & 0 & E & 0 & 0 & 0 & C
\end{bmatrix}$$

Where:

$$A=\frac{3[l(7\mathrm{m}^2-7n^2-7n-2)+7r(2m-2n-1)]}{35}$$

$$B=\frac{l^2[l(14m^2-14n^2-7n-2)+7r(4m-4n-1)]}{210}$$

$$C=\frac{l^2[l(14m^2-14n^2-21n-9)+7r(4m-4n-3)]}{210}$$

$$D=-\frac{l[l(7m^2-7n^2-14n-5)+14r(m-n-1)]}{140}$$

$$E=-\frac{l[l(7m^2-7n^2+2)+14r(m-n)]}{140}$$

$$F=-\frac{l^2[l(7m^2-7n^2-7n-3)+7r(2m-2n-1)]}{420}$$